

**ALMA MATER STUDIORUM-UNIVERSITA' DI BOLOGNA**

**SCUOLA DI FARMACIA, BIOTECNOLOGIE E SCIENZE  
MOTORIE**

**CORSO DI STUDIO IN BIOTECNOLOGIE MOLECOLARI E  
INDUSTRIALI**

***Sea organisms as a source of collagen-derived  
polymers for skin tissue engineering  
applications***

**Tesi di laurea in Cellule staminali**

**Presentata da:  
Modena Silvia**

**Relatori:  
Motta Antonella  
Migliaresi Claudio  
Bonsi Laura**

**Matricola n°  
0000708507**

**Anno accademico 2016/2017**

... to my beloved grandfather and brother,

Bruno and Davide

# Table of contents

## ABSTRACT

### 1. INTRODUCTION

1.1. Skin anatomy and physiology .....	7
1.2. Wound healing .....	9
1.2.1. Adult wound healing .....	11
1.2.2. Fetal wound healing .....	16
1.2.3. Assisted wound healing .....	18
1.3. Tissue Engineering: definition and approaches for skin replacement .....	
1.4. Scaffold for skin tissue engineering: strategies for matrix design and fabrication .....	20
1.5. Polymers for skin replacement in Tissue Engineering .....	
1.6. Cell sources .....	35
1.7. Open questions with commercially available skin substitutes .....	

### 2. RESEARCH STRATEGIES AND OBJECTIVES

2.1. Aims of the thesis .....	37
2.2. Strategies: polymer selection and processing definition .....	

### 3. MATERIALS AND METHODS

3.1. Jellyfish collagen extraction .....	
3.2. Jellyfish isolated collagen characterization .....	
3.2.1. Molecular weight evaluation by SDS-polyacrylamide gel electrophoresis .....	
3.2.2. Collagen tertiary conformation analysis by circular dichroism spectroscopy .....	
3.2.3. Secondary structure evaluation by Fourier transform infrared spectroscopy .....	
3.2.4. Collagen thermal behaviour analysis by differential scanning calorimetry .....	
3.2.5. Collagen amino acid composition measurements by high performance liquid chromatography .....	
3.3. Silk fibroin water solution processing .....	
3.4. Scaffold fabrication .....	
3.4.1. Tissue Culture Plate-well coating .....	
3.4.2. Films .....	
3.4.3. 3D sponges .....	
3.5. Scaffold characterization .....	
3.5.1. Morphological analysis by scanning electron microscopy .....	
3.5.2. Secondary structure evaluation by Fourier transform infrared spectroscopy .....	
3.5.3. Thermal behaviour by differential scanning calorimetry .....	
3.6. Preliminary biocompatibility evaluation: <i>in vitro</i> testing .....	
3.6.1. Cell lines: MRC-5, NIH 3T3 .....	
3.6.2 Design of cell culture .....	
3.6.3 Cytotoxicity: LDH-based assay .....	

3.6.4 Confocal laser scanning microscopy (image acquisition) .....  
3.6.5. Cell viability: Live/Dead .....  
3.6.6 Metabolic activity: Alamar blue® assay .....  
3.6.7 Cell proliferation: PicoGreen assay.....  
3.6.8 Collagen synthesis: Immunocytochemistry.....  
3.6.9 Specific markers expression: Reverse transcription quantitative PCR in real  
time .....  
3.6.10 Statistical analysis .....

**4. RESULTS AND DISCUSSION**

4.1. Optimization of jellyfish collagen extraction.....  
4.2. Material evaluation on MRC-5 cell culture .....  
4.2. Material evaluation on NIH 3T3 cell culture.....  
4.3. Collagen expression and assembly .....

**5. CONCLUSIONS AND FUTURE PERSPECTIVES**

**BIBLIOGRAPHY .....**

**ACKNOWLEDGMENTS .....**

# Abstract

Advanced therapies combating acute and chronic skin wounds are likely to be brought about using our knowledge of regenerative medicine coupled with appropriately tissue engineered skin substitutes. At the present time, there are no models of an artificial skin that completely replicate normal uninjured skin and they are usually accompanied by fibrotic reactions that result in the production of a scar. Natural biopolymers such as collagen have been a lot investigated as potential source of biomaterial for skin replacement in Tissue Engineering.

Collagens are the most abundant high molecular weight proteins in both invertebrate and vertebrate organisms, including mammals, and possess mainly a structural role in connective tissues. From this, they have been elected as one of the key biological materials in tissue regeneration approaches, as skin tissue engineering. In addition, industry is constantly searching for new natural sources of collagen and upgraded methodologies for their production. The most common sources are skin and bone from bovine and porcine origin. However, these last carry high risk of bovine spongiform encephalopathy or transmissible spongiform encephalopathy and immunogenic responses. On the other hand, the increase of jellyfish has led us to consider this marine organism as potential collagen source for tissue engineering applications.

In the present study, novel form of acid and pepsin soluble collagen were extracted from dried *Rhopilema hispidum* jellyfish species in an effort to obtain an alternative and safer collagen. We studied different methods of collagen purification (tissues and experimental procedures). The best collagen yield was obtained using pepsin extraction method (34.16 mg collagen/g of tissue). The isolated collagen was characterized by SDS-polyacrylamide gel electrophoresis and circular dichroism spectroscopy. The results revealed the existence of triple helical arrangements of collagen and its fair closeness in molecular weight with mammalian collagen. The structural properties were analyzed by using Fourier transform infra-red spectrum, the stability of collagen was given the single transition peak in differential scanning calorimetry and the amino acid analysis emphasized a possible presence of like-type I collagen. Tissue Culture Plate-well coating by using jellyfish collagen was compared with standard Tissue Culture Plate and commercially available bovine type I collagen in terms of cell viability (Live/Dead analysis) and proliferation (AlamarBlue<sup>®</sup> assay). The *in vitro* results show that jellyfish collagen exhibited higher cell viability than the other samples. Film-like scaffolds and porous three-dimensional scaffolds composed of jellyfish collagen and a water-stable natural

polymer, silk fibroin, presented smooth surface with micro roughness and highly porous and interconnected pore structure, respectively. The latter appeared to be useful for an high-density cell seeding and an efficient nutrient supply. Adhesion, spreading and proliferation of MRC-5 and NIH 3T3 fibroblasts on silk fibroin, silk fibroin/collagen blend and jellyfish coated fibroin scaffolds were also observed to investigate the biocompatibility and a potential bioactive role of collagen. The biological evaluations suggested that the adding of collagen, as bioabsorbable coating containing RGD sequence, could facilitates fibroblasts attachment and proliferation *in vitro*. Additionally, a preliminary study was made in order to determine the potential of collagen-based scaffold in promoting wound healing biomarkers by fibroblasts. The secretion of type I and III collagens in collagen coated fibroin scaffolds was assessed by immunocytochemistry and reverse transcription quantitative PCR in real time. Our data confirmed the broad biocompatibility of jellyfish collagen, its biological effects on mammalian cells and its important role in promoting cell adhesion and proliferation. Given the bioavailability of jellyfish collagen and its biological properties, this marine material is thus a good candidate for replacing bovine or human collagens in selected biomedical applications.

# 1 1. Introduction

## 1.1 Skin anatomy and physiology

The skin is the largest organ of the body in vertebrates, accounting for approximately 16% of the total body weight of an adult and covering its entire surface. It performs many vital functions, including protection against external physical, chemical, and biologic assailants like ultra-violet radiation and pathogens, as well as prevention of excess water loss from the body, regulation of electrolyte balance, thermos- and immunoregulation. It plays a central role as a sensory organ due to a widespread system of sweat glands and cells sensitive to touch, pain, pressure, itching, and temperature changes [1]. When this barrier is disrupted due to any cause—surgery, ulcers, burns, neoplasms or traumas, the functions of the skin are no longer adequately performed. It is therefore vital to restore the integrity of the skin as soon as possible [2]. In order to understand skin functioning, it is necessary to focus on this integumentary system organization, formed by the skin and its derivative structures.

The skin is composed of three layers, the epidermis and dermis with a complex nerve and blood supply. A third subcutaneous layer, the hypodermis, is composed mainly of fat and a layer of loose connective tissue.

The outermost level of the cutis, the epidermis, is thin and highly cellular, but has sufficient thickness to provide vital barrier function. The epidermis is a stratified, squamous epithelium layer and consists of a specific constellation of cells known as keratinocytes, which function to synthesize keratin, a long, threadlike protein with a protective role. The keratinocytes, which represent the majority of the cells, differ from the “clear” dendritic cells by possessing intercellular bridges and ample amounts of stainable cytoplasm. This layer harbours a number of other cell populations, such as melanocytes, responsible for producing the pigment melanin, Langerhans cells and Merkel cells, involved in the immune response and in the sensation of touch, respectively. The epidermis commonly is divided into four layers according to keratinocyte morphology, position and maturation as they differentiate into horny cells, including the basal cell layer (stratum basale or germinativum, the deepest layer adjacent to the basal lamina), the squamous cell layer (stratum spinosum), the granular cell layer (stratum granulosum), and the cornified or horny cell layer (stratum corneum) (Figure 1.1). The epidermis renews itself continually and gives rise to derivative structures, such as pilosebaceous apparatuses, nails, and sweat glands. The basal layer, in fact, is the primary location of mitotically active cells in the epidermis, the basal cells, which undergo

proliferation cycles that provide for the renewal of the outer epidermis. However, not all basal cells have the potential to divide. Epidermal stem cells in the basal layer are clonogenic cells with a long lifespan that progress through the cell cycle very slowly under normal conditions. Moreover, in healthy skin, a balance between the formation of new keratinocytes in the stratum basale and the shedding of dead keratinocytes from the stratum corneum is maintained. Hyperplasiogenic conditions, such as wounding, can instead increase the number of cycling cells in the epidermis by stimulating division of stem cells. The epidermis is a dynamic tissue in which cells are constantly in unsynchronized motion, as differing individual cell populations pass not only one another but also melanocytes and Langerhans cells as they move toward the surface of the skin [1]. This level is avascular (without blood vessels) and is dependent on blood vessels of the underlying dermis for oxygenation, metabolite provision and removal of metabolic waste products [3].

The dermis, lied below the epidermis, is an integrated system of fibrous, filamentous, and amorphous connective tissue that accommodates stimulus-induced entry by nerve and vascular networks, epidermally derived appendages, fibroblasts, macrophages, and mast cells. Other blood-borne cells, including lymphocytes, plasma cells, and other leukocytes, enter the dermis in response to various stimuli as well. The dermis comprises the bulk of the skin and is composed of two layers: the reticular and papillary layers. The papillary layer contains the nerves and capillaries that nourish the epidermis, whereas the reticular layer is made up of strong connective woven network of fibres containing collagen with some elastic fibres and glycosaminoglycans (GAGs), which provide physical support, pliability, elasticity and tensile strength to the epidermis. The dermis, in fact, interacts with the epidermis in maintaining the properties of both tissues. These matrix components also vary in a depth-dependent manner and undergo turnover and remodelling in normal skin, in pathologic processes, and in response to external stimuli [1]. The major cell type present in the dermis is fibroblast (mesenchymal cell), which is responsible for collagen and elastin synthesis and is capable of producing remodelling enzymes such as proteases and collagenases, which play an important role in the wound healing process [4]. The dermal vasculature is made up of endothelial cells forming two intercommunicating *plexuses*: the *subpapillary* or *superficial plexus* and *lower plexus* at the dermal-subcutaneous interface. This thick connective tissue is separated from the dermis by a multi-layered membrane, the basement membrane, it is an extremely complex and dynamic structure, which is responsible of the tight junction of the upper epidermis and underlying connective tissue.



The dermis lies on the subcutaneous tissue, the hypodermis, which contains small lobes of adipose tissue (fat cells known as lipocytes) that is well vascularized and contributes to both the mechanical and the thermoregulatory properties of the skin [4]. Considered an endocrine organ, the subcutaneous tissue provides the body with buoyancy, hormone synthesis and functions as a storehouse of energy.

The thickness of these layers varies considerably, depending on the geographic location on the anatomy of the body; however, they form an effective barrier to the external environment, allow the transmission of sensory information, and serve a significant role in maintaining homeostasis [1]. Intact, healthy skin is essential for patient wellbeing. In fact, because the skin serves as a protective barrier against the outside world, any break in it must be rapidly and efficiently mended.

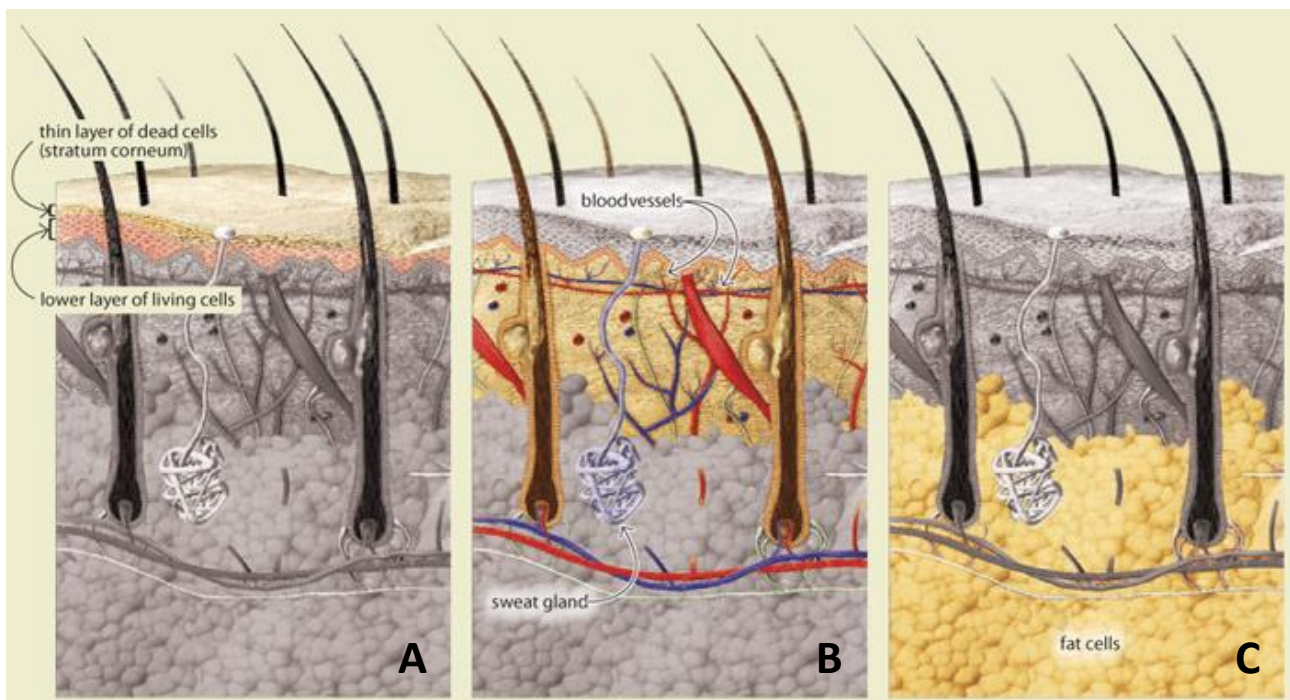


Figure 1.1: A schematic of the structure of skin. A) epidermis; B) dermis; C) hypodermis.  
(<https://answersingenesis.org/human-body/skin/>)

## 1.2 Wound healing

A wound is a disruption in the epithelial integrity of the skin and may be accompanied by breakdown of the structure and function of underlying normal tissue. Wounds can also occur as a part of a disease process (ex. diabetic ulcers) or have an accidental or intentional etiology

[5]. There are multiple reasons for skin damage, including genetic disorders (bullous conditions), acute trauma, chronic wounds or even surgical interventions. One of the most common reasons for major skin loss is thermal trauma, where substantial areas of skin can be damaged, often without the possibility of skin regeneration.

Wounds can be divided into epidermal, superficial partial-thickness, and deep partial-thickness and full-thickness with increasing depth of the injury. Treatment approaches differ accordingly.

Epidermal injuries, typical of sunburns, light scalds or grazing, do not require specific surgical treatment as only the epidermis is affected and this regenerates rapidly without scarring, as no extracellular matrix (ECM) deposition occurs to contribute towards the scar tissue.

Superficial partial-thickness wounds affect the epidermis and superficial parts of the dermis and heal by epithelialization from the margins of the wound, where basal keratinocytes change into a proliferating migratory cell type and cover the damaged area. Cells migrate either from the wound edge, hair follicle or from sweat gland remnants that lie in the deeper dermis, which has been preserved in this depth of injury. Each hair follicle and sweat gland is lined with epithelial cells capable of contributing to epithelial regeneration across the wounded surface and contains a reserve of self-renewal stem cells, located in the bulge region of the follicle.

Deep partial-thickness injuries involve greater dermal damage that results in fewer skin appendages. Remaining and pronounced scarring as fibroplasia is more intensive when compared with superficial partial-thickness wounds.

Full-thickness injuries are characterized by the complete destruction of epithelial-regenerative elements. This type of injury heals by contraction, with epithelialization from only the edge of the wound, leading to cosmetic and functional defects and extensive scarring [6].

The continuity of the skin must be restored expeditiously because it plays a crucial role in maintaining homeostasis. Tissue repair is normally a rapid process that has been devised through evolution to allow animals to escape danger and rapidly recover tissue integrity using scarring to join the wound edges or to fill tissue voids. Wound healing has often been described as a sequential natural restorative response to tissue injury and it is more specifically an event-driven process, whereby signals from one cell typeset off cascades in other cell types, which propel the wound through the phases of healing.

In order to fully understand the differences between regeneration and the normal outcome of tissue repair, namely fibrosis and scarring, it is useful at this point to briefly review the processes of normal wound repair or adult wound healing, the scarring process and to consider early fetal tissues, which undergo scar-free healing. In designing a smart skin replacement for grafting, it is obvious that the mechanisms of both wound healing and regeneration must be at the forefront of the tissue engineers' mind [4].

### 1.2.1 Adult wound healing

Adult wound healing is essentially a repair process, which normally exhibits scarring [4].

Regardless of the aetiology of the wound, the repair processes are similar. A wound results in tissue damage, which stimulates a coordinated physiological response or cellular events to provide homeostasis and restoration of the tensile strength of injured skin. Acute wounds, including surgical incisions, usually pass through the wound healing phases relatively quickly. Wounds that demonstrate delayed healing 12 weeks after the initial insult are termed chronic wounds, often because of prolonged pathological inflammation. Surgical incisions are usually clean and cause minimal tissue loss and disruption. These wounds can be closed immediately with sutures and tend to heal rapidly. As a result, epithelial regeneration predominates over fibrosis. This is termed closure by primary intention or healing. When the tissue loss, in particular soft tissue, has been more extensive, the edges cannot be approximated, or the wound must be left open due to sepsis, the reparative process is prolonged, as the defect must fill with extensive granulation tissue. This process is termed as closure by secondary intention and involves wound contraction and epithelialization [6, 7].

At the time of insult, healing occurs as a carefully regulated, systemic cascade of overlapping processes that require the coordinated completion of a variety of cellular and extracellular activities, with the aim of restoring tissue integrity. These activities occur in a cascade that correlates with the appearance of different cell types in the wound during various stages of the healing process. These processes (triggered by tissue injury) involve four overlapping but well-defined phases of hemostasis, inflammation, proliferation, and tissue remodeling. The regulation of these events is multifactorial (Figure 1.2, 1.3) [5].

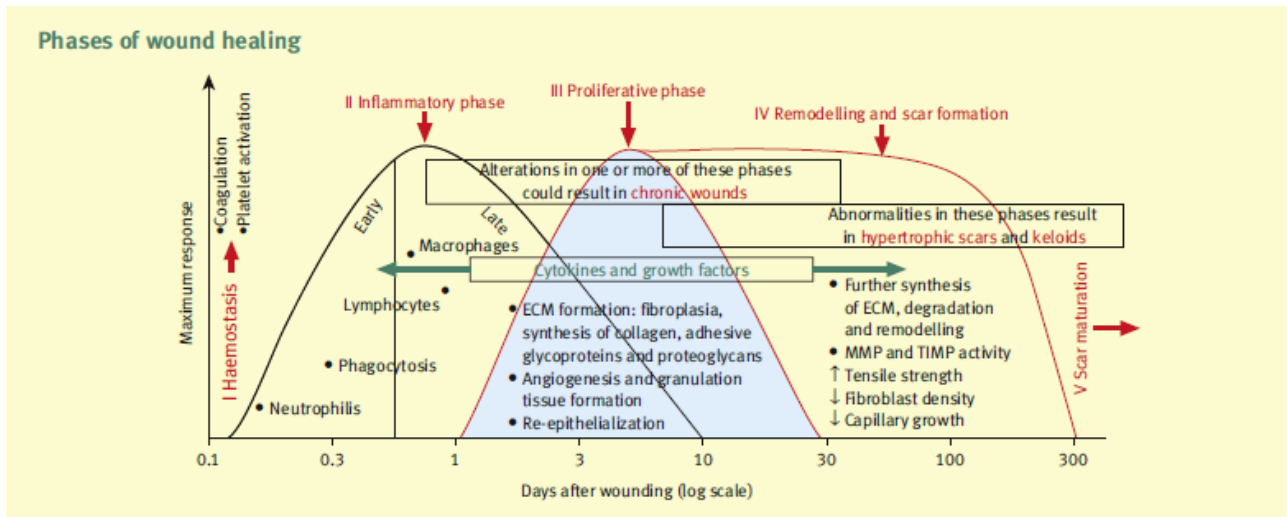


Figure 1.2: Major cells and their effects on wound during various stages of the normal healing process.

## The vascular response and hemostasis

Bleeding occurs immediately after tissue injuries as a result of the disruption of blood vessels on a macro- or micro vascular scale. The immediate response of the body is to prevent exsanguination and promote hemostasis. Damaged arterial vessels rapidly constrict through the contraction of smooth muscle in the circular layer of the vessel wall, mediated by increasing cytoplasmic calcium levels. Within a few minutes, the reduced blood flow mediated by arteriole constriction leads to tissue hypoxia and acidosis. This promotes the production of vasoactive metabolites to cause a reflex vasodilatation and to increase vascular permeability, facilitating the entry of platelets and inflammatory cells into the extra-cellular space around the wound [7]. Upon activation, platelets, which represent the first cells to appear after injury, undergo adhesion as well as aggregation and at the same time release many mediators (e.g. serotonin) and adhesive proteins (e.g. fibrinogen, fibronectin). With the conversion by thrombin of fibrinogen to fibrins during platelet aggregation, a fibrin clot is formed to stop the bleeding [8]. The clot consists of platelets embedded in a mesh of cross-linked fibrin fibers, provides the provisional matrix for cellular migration and serves as a reservoir of cytokines and growth factors [9]. The second component of hemostasis is coagulation achieved via intrinsic and extrinsic coagulation pathways.

## The cellular response and inflammation

The cellular response of the inflammatory phase takes place 24-72 hours after wounding and is characterized by the influx of leukocytes into the area of injury, whose activity is to

minimize bacterial contamination of the wound, thus preventing infection. Neutrophils and monocytes are recruited to the wound by chemotactic factors released during hemostasis by platelets, such as transforming growth factor- $\beta$  (TGF-  $\beta$ ) and platelet-derived growth factor (PDGF), which leads to them passing down a chemical gradient towards the wound.

In the early inflammatory state, neutrophils (polymorphonuclear leukocytes), once in the wound environment, can perform their function of killing and phagocytizing bacteria and damaged matrix proteins within the wound bed by releasing degrading enzymes and free radicals derived from oxygen. Within 24–48 hours, epithelial cells from both edges begin to migrate and proliferate along the dermis, depositing components of basement membrane as they progress [5]. Later in inflammation, the number of neutrophils declines and macrophages (tissue-derived monocytes) predominate. They appear to act as the key regulatory cells for repair. They function as phagocytic cells as well as being the primary producer of growth factors, such as epidermal growth factor (EGF) and vascular endothelial growth factors (VEGF), which are important in regulating the inflammatory response, stimulating angiogenesis and enhancing matrix production. During this late phase, collagen fibers are evident at the incision margins of the wound and epithelial cell proliferation continues, yielding a thickened epidermal-covering layer [7, 8].

## Proliferative phase

The initial inflammatory responses to injury provide the necessary framework to the subsequent production of a new functional barrier. In this phase of healing, cellular activity predominates. The major events during this phase are reinforcement of the injured dermal tissue (i.e. fibroplasia), the establishment of appropriate blood supply (i.e. angiogenesis), the creation of a permeability barrier (i.e. reepithelialization), and wound contraction, which occur simultaneously [7].

Fibroplasia describes a process in which fibroblasts are stimulated to proliferate by growth factors, released from the hemostatic clot, and then migrate into the provisional matrix of wound fibrin clot, where they lay down a collagen-rich matrix (proteoglycans and elastin) and subsequently produce collagen and fibronectin. The resulting vascular, fibrous tissue, which replaces the clot at the wound site, is termed as granulation tissue. It represents a scaffold for contact guidance, a reservoir for growth factors and is composed of a different range of collagens (a higher proportion of type III collagen). Once sufficient matrix has been laid down, fibroblasts change to a myofibroblast phenotype and participate in wound contraction, by

connecting to the surrounding proteins like collagen. Collagens synthesized by fibroblasts are the key component in providing strength to tissue [7, 8]. Crucial interaction exists between the fibroblasts and the extracellular matrix, which helps to regulate further synthesis of the ECM and subsequent remodeling [5].

Angiogenesis refers to new blood vessel growth by the sprouting of preexisting vessels adjacent to the wound (neovascularization). As in most normal adult tissues, dermal blood vasculatures remain quiescent. In response to the injury, microvascular endothelial cells initiate an angiogenic process consisting of activation of endothelial cells, local degradation of their basement membrane, sprouting into the wound clot, cell proliferation, tubule structure formation, reconstruction of the basement membrane, and, eventually, regression and involution of the newly formed vasculature as tissue remodeling [8]. Those processes are triggered and guided by molecules that act as angiogenic factors, including fibroblast growth factors (ex. FGF), VEGF, which are secreted by fibroblasts and platelets at the healing site [10]. Angiogenic capillary sprouts invade the fibronectin-rich wound clot and organize into a microvascular network throughout the granulation tissue, providing nutrition and oxygen to growing tissues. During angiogenesis, endothelial cells also produce and secrete biologically active substances or cytokines, such as vascular endothelial growth factor and angiopoietins. Development of new capillary vessels is dependent on not only the cells and cytokines present but also the production and organization of extracellular matrix components, such as laminin [8].

Re-epithelialization is the process of restoring an intact epidermis after cutaneous injury. It generally involves several processes. The epidermal keratinocytes initially respond to an epidermal defect by migrating from the edges of the wound within 24 hours, thanks to several elements, including the extracellular matrix, integrin receptors and matrix metalloproteinases (MMPs). Reepithelialization also involves increased proliferation of keratinocytes located near the cells of the migrating front tongue. This proliferating source of keratinocytes ensures an adequate supply of cells to form a delicate covering over the exposed raw area. Further growth and differentiation of these epithelial cells restore an intact basement membrane that connects the epidermis and the underlying dermis, re-establishing the stratified epidermis [8].

Contraction of the wound begins about 7 days after injury, mediated mainly by myofibroblasts. Interactions between actin and myosin pull the cell bodies closer together decreasing the area of tissue needing to heal [7].

## Remodeling and scar formation

The final stage of adult wound healing is the remodelling of the extracellular matrix and its subsequent changes over time, which results in the development of normal epithelium and, in the adult, maturation of the scar tissue. This phase involves a balance between synthesis and degradation of collagen and other ECM components, through mechanisms of proteolysis (metalloproteinases) and new matrix secretion (tissue inhibitors of metalloproteinases) [7]. It occurs throughout the entire wound repair process as fibrin clot formed in the early inflammatory phase is replaced by the granulation tissue that is rich, similar to the case in the fetal dermis, in immature type III collagen and blood vessels. During the proliferative phase, it is subsequently substituted by a collagenous scar predominantly of type I collagen with much less mature blood vessels [8]. As the scar, the end point of the normal mammalian tissue repair, matures, collagen bundles increase in diameter, corresponding with increasing tensile strength of the wound. However, these collagen fibers never regain the original strength of unwounded skin, and a maximum of 80% strength of unwounded skin can be achieved [5].

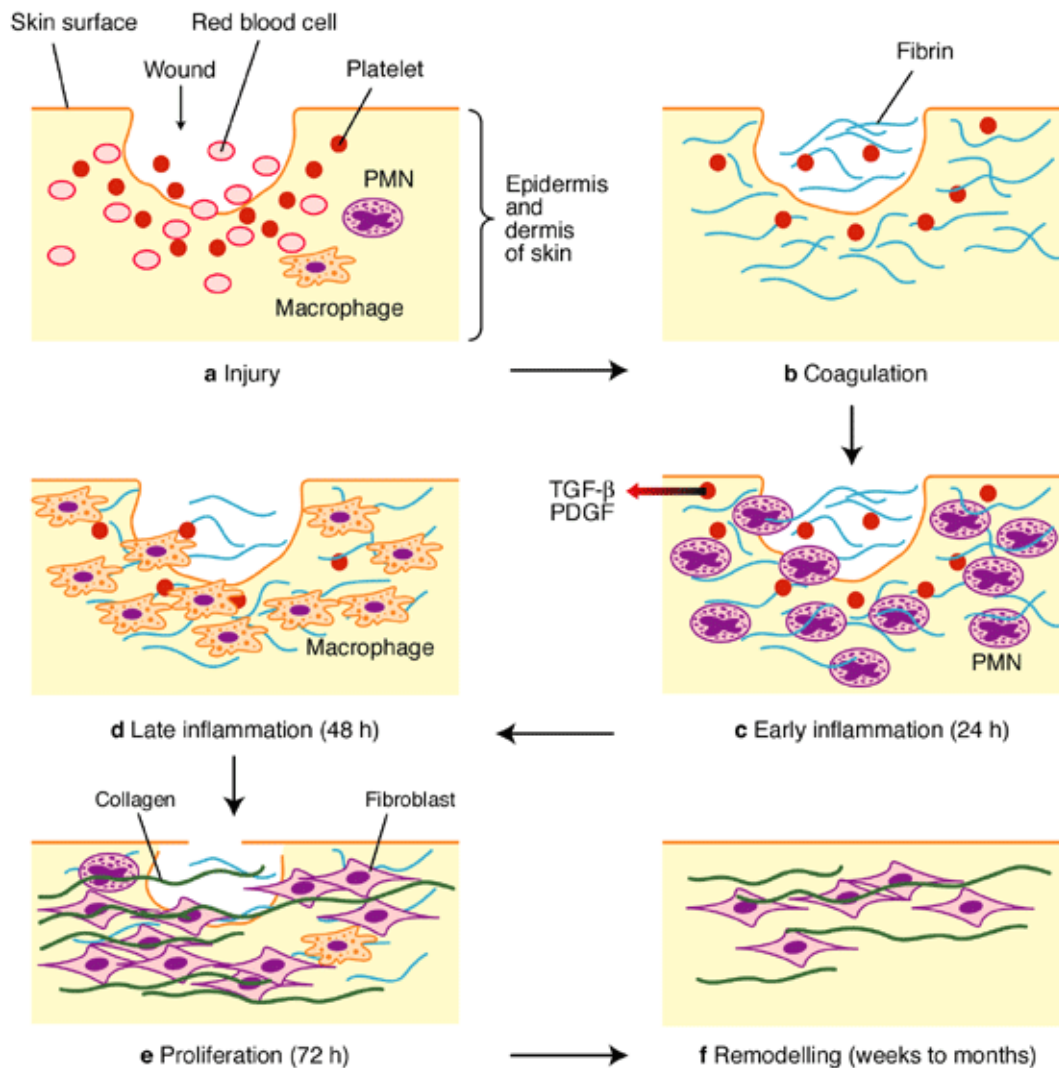


Figure 1.3: Principal events that occurs after a cutaneous injury.  
([http://www.pilonidal.org/\\_assets/pdf/phase\\_healing.pdf](http://www.pilonidal.org/_assets/pdf/phase_healing.pdf))

Certain mammalian tissues, in human in specific stage of development, have a capacity for complete regeneration without scarring. Good example include embryonic or fetal skin, which might be useful to further clarify the regenerative process, identify the factors expressed during regeneration with the aim to incorporate them to produce novel replacement skin [11].

## 1.2.2 Fetal regeneration

Fetal wound repair is essentially a regenerative process, characterized by an absence of scarring and fibrosis. These differences in the healing processes have sparked great interest



and have lead to the development of several animal models in which fetal scarless healing has been described.

Wound on early fetal mammalian tissues heal via different mechanisms with no sign of scarring and complete restitution of the normal skin architecture or result in much less scarring than an equivalent wound in adult tissues. Such healing is believed only to occur through a gestational age equivalent to the first third of human development; after that time, normal scarring as evident in the adult occurs.

The transition from scar-free embryonic wound healing to scar-forming adult wound healing is a gradual one. It is characterized by the abnormal organization of the neo-dermis, predominantly the abnormal deposition of small parallel bundles of extracellular matrix (consisting largely of collagen types I and III and fibronectin) to form the scar in the adult. This process is opposed to minimal inflammation and complete restoration of normal skin structure, with the correct deposition of large bundles of extracellular matrix and regularly distributed hair follicles, capillaries and glands in the neo-dermis of an embryonic wound. Scarring is therefore a morphogenetic problem, i.e. a failure of the regeneration of the normal skin structure as opposed to a biochemical problem, e.g. abnormal composition of the scar tissue [12].

There are a large number of differences between the healing of embryonic and adult wounds. Many of these differences are epiphenomenon, i.e. not causative of the scar-free healing phenotype because, of course, embryos are still developing and do not have the same stable phenotype as the adult. Consequently, many obvious differences between embryonic and adult wounds have been shown to be irrelevant to scar formation or the lack of it. Originally, it was thought that the sterile aqueous environment provided by the amniotic fluid was important in fetal scar-free healing, whereas adult wounds are exposed to air and numerous potential contaminating agents, e.g. bacteria, viruses, foreign bodies, etc. A particularly elegant demonstration of the irrelevance of the sterile, fluid, embryonic environment to scar-free healing was an ontological investigation of wound healing and scarring in the pouch young of the marsupial *Monodelphis domestica* (Armstrong & Ferguson 1995, 1997), whose skin wounds heal perfectly with no scars. Moreover, it point out that repair and regeneration of the skin appear to be correlated with the degree of skin differentiation and the inflammatory response to wounding [13].

Many other differences between embryonic scar-free healing wounds and adult scar-forming wounds have been shown, but only a few of the myriad of cellular and molecular differences

between embryonic and adult healing remain as potential mechanisms and therapeutic targets involved in skin scarring, including:

- Lack of fibrin clots and platelet degranulation,
- Markedly reduced inflammatory response, consisting of small numbers of poorly differentiated inflammatory cells,
- Markedly elevated levels of molecules involved in skin growth, remodeling and morphogenesis.

As a consequence of these principal variables the growth factor profile at a healing embryonic wound is very different qualitatively (i.e. the types of growth factor present), quantitatively (i.e. the amounts of such growth factors present) and temporally (i.e. the length of time the growth factors are present) compared with an adult wound. Thus, for example, there are major differences in the TGF $\beta$  isoforms present in embryonic and adult wounds. Embryonic wounds express very high levels of TGF $\beta$ 3, a skin morphogenetic factor predominantly synthesized by keratinocytes and fibroblasts and very low levels of TGF $\beta$ 1, TGF $\beta$ 2 and PDGF, which is virtually absent in embryonic wounds (owing to the lack of platelet degranulation). By contrast, adult wounds contain predominantly TGF $\beta$ 1, TGF $\beta$ 2 and large quantities of PDGF. Experimental manipulation of the growth factor profile of adult wounds by exogenous addition of TGF $\beta$ 3 or neutralization of TGF $\beta$ 1, TGF $\beta$ 2, PDGF, etc., results in markedly reduced or absent scarring [12]. Such implications may be very important in artificial skin substitutes or grafts to enhance host take and minimize scarring at the perimeter and base of the graft.

### 1.2.3 Strategies for guided wound healing: state of the art

Serious injury to the skin, such as burns, trauma or chronic ulcers, requires immediate coverage to facilitate repair and restore skin function and so to fulfill the wound healing process.

In the field of skin repair, the clinical 'gold standard' for skin replacement is the autologous skin graft in which an area of suitable skin is separated from the tissue bed and transplanted to the recipient area on the same individual from which it must receive a new blood supply. Grafts may be full thickness in which a complete section of epidermis and dermis is transplanted, or split thickness that includes only part of the dermis. After application of a graft to a full-thickness wound, its capillaries merge with the capillary network in the excise

wound. This “graft take” is essential for a proper supply of nutrients and ensures graft survival. The split skin donor site heals within one week and can be used for skin graft harvesting up to 4 times; however, repeated harvesting is associated with scarring at the donor sites as well as lengthy hospital stays. Moreover, in the case of a more extensive injury, donor sites are extremely limited and might leave the patient with too little undamaged skin to harvest enough autologous split skin grafts (SSGs). To address the problem of limited SSG harvesting sites, a meshing technique is used that stretches the graft and therefore can cover a larger wounded area at the expense of cosmetic and functional outcome [14].

Another possibility is the use of allografts or allogeneic transplantation (from a non-genetically identical individual of the same species), which include syngeneic grafts, performed between genetically identical individuals such as monozygotic twins, xenogeneic skin grafting that involves the transfer of tissue between species. Allografts of cadaver skin are also used as a temporary cover for full thickness burns but all these methodologies are subject to rejection, because antigens present in the donor tissue may elicit an immune reaction in the recipient [4]. These allografts can be obtained for example from non-profit European skin banks; however, there is not enough tissue available to meet the current demand and only a few of these tissue banks exist worldwide. Allografts incorporate into deep wounds and provide pain relief; however, ethical as well as safety issues remain, as the rigorous screening for viral diseases and standardized sterilization techniques cannot completely eliminate the possibility of infective agent transmission. In comparison to autologous SSGs, a major disadvantage of allografts is that they leave the patients for weeks with wounds prone to complications. Eventually, allografts undergo immunogenic rejection and the site of injury needs to be covered with an autologous SSG. Delayed rejection can occur in patients with extensive burns due to their pathologically suppressed immune response, but eventually can be triggered by the highly immunogenic epithelial cells of the allograft during its vascularization [14]. Accordingly, there is a great need for an alternative that can provide a more permanent solution, like tissue-engineered skin substitutes, which aim for skin regeneration.

## 1.3 Tissue engineering: definition and approaches for skin replacement

The definition of Tissue Engineering (TE) was first established in 1988, during a conference organized by the National Science Foundation in Lake Tahoe (California). It was defined as the “application of principles and methods of engineering and life sciences toward fundamental understanding of structure–function relationship in normal and pathological mammalian tissues and the development of biological substitutes to restore, maintain, or improve functions” [15]. TE refers to an interdisciplinary field of therapeutic or diagnostic products and processes, which are based upon the combination of three different components that is living cells, engineering biomaterials and suitable biochemical factors. The aim of Tissue Engineering is therefore to replace or regenerate structures and tissues in the organism, which have been compromised by traumas or pathologies implanting in the damaged site new artificially produced tissue that allows cell growth and thus restoring the original tissue.

The term regenerative medicine is often used synonymously with tissue engineering, although it is a broad field that includes tissue engineering but also incorporates research on self-healing, where the body uses its own systems, sometimes with help foreign biological material to recreate cells and rebuild tissues and organs [16].

The paradigm of TE is schematically shown in Figure 1.4. Functional tissue can be fabricated starting from a scaffold that is a tridimensional structure able to guide tissue development, eventually combined with a cells and/or growth factors able to regenerate tissues in a critical size defect. Several cell sources can be employed, from cells extracted from the patient in the damaged tissue to stem cells of different origin, cultured so that they express the suitable phenotype.

From the previous considerations, it becomes evident how the approach of Tissue Engineering implies the transfer of the medical treatment to a cellular level: the resources needed for tissue regeneration are introduced in the pathologic environment in a suitable configuration to optimize their activity and help the natural processes of self-repair. The main challenge of this strategy is to control the 3D new tissue development in a functional way. The achievement of this goal is highly dependent on many variables: the use of a cell-free or a pre-seeded scaffold, the choice of the most appropriate cell source, the material of the scaffold, the

design of the morphological, chemical and physical properties of the scaffold, the parameters of the preliminary *in vitro* culture, the concentration of growth factors, and so on [17].

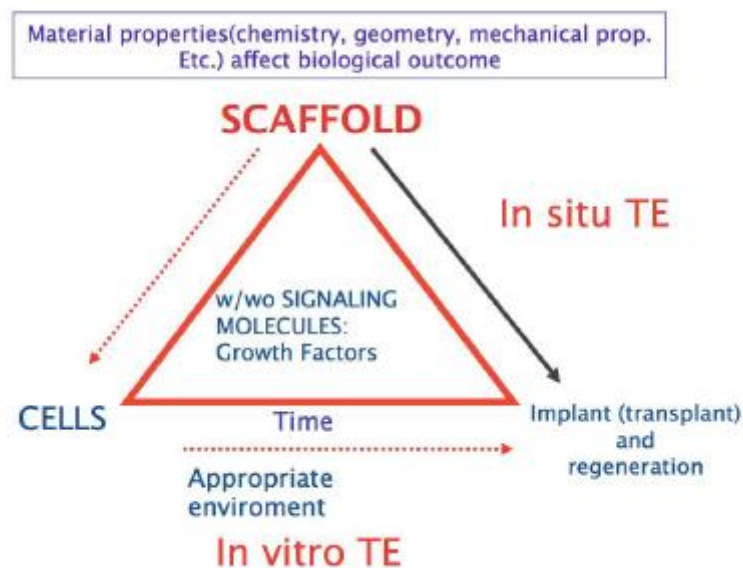


Fig. 1.4: The paradigm of tissue engineering [15].

The strategy generally followed consists in combining these components, in order to mimic characteristics and properties of the biological system to be regenerated. This principle is well known as biomimetic. It implies that the cellular behavior has to be known in detail, both during normal tissue morphogenesis and during the repair and regeneration phases when damage or pathology is present. In fact, only in this case we will be able to evaluate how cells can be guided towards tissue regeneration, that is, which signals have to be provided, both *in vitro* and *in vivo* [18].

Many challenges have to be handled to reach its final aim, i.e. to gradually substitute organ transplantation. However, efforts have been done towards this objective and several tissue engineered applications are today commercially available, for instance for skin regeneration to heal burns or diabetic ulcers.

Alternative life-saving approaches in the treatment of extensive full-thickness wounds, where donor sites for SSG harvesting are not available, in fact, include the use of cultured autologous fibroblasts and/or keratinocytes and bioengineered skin substitutes. 'Off-the-shelf' availability or the possibility of producing, in a relatively short period of time, sufficient quantities of epithelium capable of permanent wound closure sometimes make these approaches the treatments available in extensive deep injuries.

Because of the great importance and demand for skin-replacement products, there is a long history of material development, and many research groups worldwide have focused on creating biomaterials for skin substitution [6].

On the other hand, these skin substitutes can be utilized as complex human-based organ-like test systems for basic or pharmaceutical research. In skin TE, various biological and synthetic materials are combined with *in vitro*-cultured cells to generate functional tissues (Figure 1.5). A critical issue is the *ex vivo* expansion that is required to obtain sufficient numbers of the needed cells, while preserving the cells' normal phenotype and functionality. Only then, these cells can be used for either the generation of skin substitutes that are suitable for transplantation or as *in vitro* test systems [14].

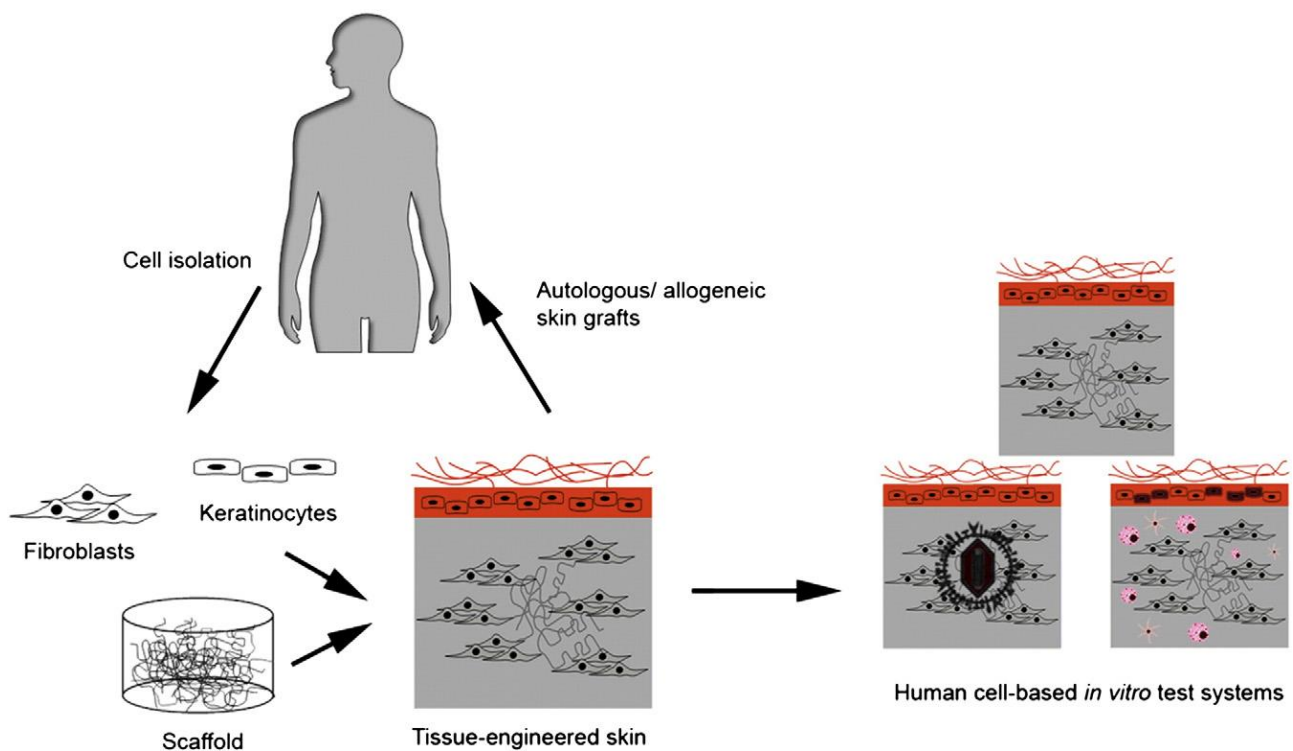


Figure 1.4: Scheme of principles of skin tissue engineering. Primary keratinocytes and fibroblasts are isolated from human donor tissues, which are then *in vitro* expanded prior seeding onto suitable scaffold materials/matrices. For a full-thickness skin equivalent, the fibroblasts and the matrix are initially used to establish the dermal part. The keratinocytes are seeded afterwards on the top of the dermis to ultimately form the epidermal part of the skin substitute. The *in vitro*-engineered skin can serve as skin graft or can be used as human-cell based *in vitro* test system [14].

Promising results have been obtained in these fields thanks to the development of bioreactors, i.e. systems able to provide suitable cell culture conditions in terms of nutrient flow and mechanical stimulation.

Skin formation *in vitro* has been improved, but many difficulties has still to be ridden out: stimuli have to be designed specifically according to the application and the mechanisms underlying the integration of a graft after implantation *in vivo* need to be understood [19].

Finally, a crucial remark has to be done about the economical, social and ethical impact that a clinical application of skin tissue engineering will have. Many issues need to be solved, such as the debate about the use of embryonic stem cells or the necessary requirements to start a clinical trial on humans. However, results remain promising and more and more benefits will soon be available for patients.

## 1.4 Scaffold for skin tissue engineering: strategies for matrix design and fabrication

Nowadays the importance of the extracellular matrix structure is well known, especially for connective tissues like skin. For this reason, the main approach of Tissue Engineering consists in producing a functional tissue starting from a scaffold. Scaffolds are three dimensional structures or matrices made of natural and/or artificial materials and populated by cells, before or after implantation. The chemical, physical and biological properties of the scaffold have to be designed carefully, to guide the tissue regeneration in a functional way. To improve tissue restoration, specific chemical (i.e. growth factors) or mechanical (i.e. hydrostatic pressure or compressive stimulation) signals can be conjugated to the material in order to help, in the damaged site, tissue morphogenesis, ECM functional distribution throughout the scaffold and cell differentiation [15].

Scaffolds have mainly a structural role, supporting cell growth and allowing a certain integrity during tissue regeneration [21]. On these bases, the ideal properties of a scaffold can be outlined: a high tridimensional and interconnected porosity to allow cell migration, waste removal and nutrient diffusion; morphology and elasticity have to be designed according to the physiological properties of the damaged tissue; its surface has to be chemically suitable to induce cell adhesion, proliferation and differentiation. The biodegradability of the material has to be carefully evaluated: the scaffold has to degrade in a controlled fashion, so that its 3D structure can be gradually substituted with new tissue and the loss of mechanical stability is compensated by the formation of fresh ECM. Finally, a scaffold needs to be implanted easily;

its production should be reproducible also on a large scale for a clinical application and has to be sterilized to avoid any contaminations which may cause the failure of an implant [20, 21]. To fabricate a scaffold, several so-called biomaterials have been proposed and used: polymers, metals, ceramics and composites. The action of a biomaterial, which is treating, augmenting or replacing any tissue or function in the body, is governed by the interaction between material and organism, that is, by the reciprocal effect of the biological environment on the material and vice versa. The property, which describes this interaction, is called biocompatibility and it is a fundamental requirement of a scaffold for TE. This term was defined exhaustively by Williams as: “the ability of a biomaterial to perform its desired function with respect to a medical therapy, without eliciting any undesirable local or systemic effects in the recipient or beneficiary of that therapy, but generating the most appropriate beneficial cellular or tissue response in that specific situation, and optimizing the clinically relevant performance of that therapy” [22].

With the aim of skin regeneration, the current focus of research is towards developing a tissue-engineered skin equivalent that combines living cells with natural or synthetic cellular components. An engineered skin substitute bioconstruct would need to comply with major requirements and specific criteria. They must be safe for the patient, be clinically effective and be convenient in handling and application [4]. Properties of the ‘ideal’ skin substitute for *in vivo* use have been described elsewhere and recently reviewed by MacNeil (2007). In general, such biomaterials must not be toxic, immunogenic or cause excessive inflammation, and should also have no or low level of transmissible disease risk. The biomaterial for skin reconstruction should be biodegradable, repairable and able to support the reconstruction of normal tissue, with similar physical and mechanical properties to the skin it replaces. It should provide pain relief, prevent fluid and heat loss from the wound surface and protect the wound from infection. It is also of great advantage if the skin substitute bioconstruct is cost-effective, readily available, user-friendly and possesses a long shelf life.

Shakespeare (2005) outlines four groups of functions which bioengineered skin-replacement products can offer: *protection*—by establishing a mechanical barrier to micro-organisms and vapour loss; *procrastination*—following early wound debridement some wound cover is needed until permanent wound closure can be achieved with serial skin grafts or cultured autologous cell applications; *promotion*—delivery to the wound bed of dermal matrix components, cytokines and growth factors, which can promote and enhance natural host wound-healing responses; *provision*—of new structures, such as dermal collagen or cultured



cells, which are incorporated into the wound and persist during wound healing and/or thereafter. There are many different classifications of currently available skin-substitute products and they can be summarized as follows:

- (i) Anatomical structure:
  - dermo-epidermal (composite),
  - epidermal,
  - dermal.
- (ii) Duration of the cover:
  - permanent,
  - semi-permanent,
  - temporary.
- (iii) Type of the biomaterial:
  - biological: autologous, allogeneic, xenogeneic,
  - synthetic: biodegradable, non-biodegradable.
- (iv) Skin substitute composition regarding cellular component:
  - cellular,
  - acellular.
- (v) Primary biomaterial loading with cellular component occurs:
  - *in vitro*,
  - *in vivo*.

However, the anatomical structure classification is the most commonly used, also if many more are still in the process of investigation and are not reported in this context (Table 1.1) [6].



- Dermo-epidermal or composite skin substitutes aim to mimic the histological structure of normal skin where both epidermal and dermal layers are present. This similarity also provides some functional resemblance to the normal skin. Most of these products are based on allogeneic skin cells (keratinocytes and fibroblasts), incorporated into a scaffold. Although mimicking the functional architecture of normal skin, the epidermal/dermal skin substitutes should be considered as temporary biologically active wound dressings, providing growth factors, cytokines and ECM for host cells while initiating and regulating wound healing. Major pitfalls are the high manufacturing costs and their failure to close the wound permanently due to tissue rejection.
- Epidermal substitutes. A key step in the designing and production of epidermal substitutes is the isolation of keratinocytes from a donor and the subsequent *in vitro* culture of these cells, to obtain the necessary number of keratinocytes for therapeutic needs. To initiate a culture of autologous cells, a skin biopsy of 2–5 cm<sup>2</sup> is usually taken along with initial wound debridement of the patient. Subsequently, the epidermis is separated from the

dermis and single keratinocytes are enzymatically released and cultured on mitotically inactivated mouse fibroblasts or also in xenogeneic-free conditions [14]. Allogeneic products have the advantage of reduced manufacturing costs compared to autologous products. Nevertheless, a shortcoming of both products is that they show poor attachment rates that can lead to the formation of blisters [23].

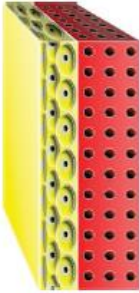

- Dermal substitutes. For the treatment of full-thickness burns, both the epidermal and the dermal layers of the skin need to be replaced, as the treatment with cultured epidermal (keratinocyte) sheets alone would result in an inferior outcome [14]. In contrast to cultured epidermal sheets, engineered dermal constructs can prevent wound contraction and they provide a greater mechanical stability. The dermal and epidermal equivalents must be applied consecutively, as good dermal vascularization by the debrided wound bed needs to be achieved prior to application of the epidermal layer [24].

Despite all efforts, an off-the-shelf, full-thickness skin replacement is not yet available. A future prospective is to incorporate cellular growth-enhancing substances or additional cell types, besides keratinocytes and fibroblasts, in the bioengineered skin substitutes to obtain constructs with improved function and higher resemblance to native skin. Since poor vascularization of skin grafts is still an unsolved problem, many attempts have been made to improve the angiogenesis in transplanted grafts. A common approach is to stimulate the formation of capillary network by applying growth factors such as vascular endothelial growth factor (VEGF) [25].

a)

brand name/manufacturer	schematic representation	incorporated human cells	primary cellular loading occurs	cell source	scaffold source	scaffold material	duration of the cover
Apligraf Organogenesis Inc., Canton, Massachusetts, CA, USA		cultured keratinocytes and fibroblasts	<i>in vitro</i>	allo	xeno	bovine collagen	temporary
OrCel Ortec International, Inc., New York, NY, USA		cultured keratinocytes and fibroblasts	<i>in vitro</i>	allo	xeno	bovine collagen sponge	temporary

b)

brand name/manufacturer	schematic representation	incorporated human cells	primary cellular loading occurs	cell source	scaffold source	scaffold material	duration of the cover
Laserskin or Vivoderm Fidia Advanced Biopolymers, Padua, Italy		cultured keratinocytes (confluent cell sheet)	<i>in vitro</i>	auto	recomb	HAM	permanent
Bioseed-S BioTissue Technologies GmbH, Freiburg, Germany		cultured keratinocytes (subconfluent cell suspension)	<i>in vitro</i>	auto	allo	fibrin sealant	permanent

27

c)



brand name/manufacturer	schematic representation	incorporated human cells	primary cellular loading occurs	cell source	scaffold source	scaffold material	duration of the cover
GraftJacket Wright Medical Technology, Inc., Arlington, TN, USA		—	<i>in vivo</i>	—	allo	human acellular pre-meshed dermis	permanent
Matrigel Dr Suwelack Skin and HealthCare AG, Billerbeck, Germany		—	<i>in vivo</i>	—	xeno	bovine non-cross-linked lyophilized dermis, coated with $\alpha$ -elastin hydrolysate	permanent

Table 1.1: Examples of currently commercially available or marketed dermo-epidermal (a), epidermal (b) and dermal (c) skin constructs, with their specific characteristics. [6]

## 1.5 Polymers for skin replacement in Tissue Engineering

The individual cells of the skin are orchestrated to behave in such a way that skin integrity is re-established in an evolutionarily proven, most robust way. It is highly challenging to design experiments capturing how this orchestration actually takes place. Although 2D monolayer experiments are ideal for analyzing individual cellular functions such as migration mechanistically on the single cell level, wound healing cannot be reduced merely to cell migration [27]. Thus, for understanding wound healing, the analysis of the orchestration of the individual processes taking part in wound healing has to be performed. This can only be undertaken in 3D wound-healing models, which include the use of a proper scaffold, which have to be systematically and quantitatively characterized.

In this context, materials used to fabricate specific constructs play a critical role for example in providing for epidermal cover, dermal and epidermal/dermal replacement, through different interactions that can establish with cells.

Synthetic polymers, such as polycaprolactone (PCL), poly(lactic acid) (PLA), polyglycolic acid (PGA), or blends are generally less biocompatible than natural polymers and it is necessary to evaluate the possible toxicity of the released monomers. On the other hand they have high and tunable properties and are easily processed and adapted to the final purpose.

A number of natural derived polymers have excellent properties that have led to their use in skin tissue engineering because of similar cellular properties to human skin tissue, including those pertaining to adhesion and infiltration. The most common used materials in this field are represented by collagen, silk fibroin, gelatin et al. [28, 29, 42], which are obtained by extraction from living organisms. They are closer in composition and structure with the ECM, possess usually a good interaction cell-material, low toxicity, and an ideal environment for cell growth and activity but exhibit poor engineering properties, and are characterized by a certain variability.

Collagen is the most abundant family of proteins constituting the extracellular matrix in animals and it represents one third of the total protein in humans [30, 31, 32].

Collagens are the major structural and biologically active components of all connective tissues including skin where provide proper stability and structural integrity of tissues and organs [33].

These molecules are ubiquitously found in living beings, in quite conserved forms, both in terms of gene and amino acid sequences, especially in the triple helix structure. They have a complex structural and hierarchical organization, with 28 genetically distinct collagen types reported up to now in vertebrates [29, 35, 36]. The different collagen types are characterized by considerable complexity and diversity in their structure, their splice variants, the presence of additional, non-helical domains, their assembly, distribution and their function. Based on their structure and supramolecular organization, they can be grouped in different families. Collagen Type I and Type III represent essential components of skin during human development and the Type I is the most abundant and best known among the wide types [64, 65, 66].

Generally, collagens are formed by polypeptide chains constituted by repeating triplets Gly-X-Y of Glycine and two other amino acids, where proline and hydroxyproline (Hyp) are the most common, of about 1000 total amino acids.

Collagen, as other secreted protein, follows a standard biosynthesis pathway. Collagen chains are synthesized as longer precursors called procollagens, delivered and packaged within the Golgi apparatus into secretory vesicles and released into the extracellular space, where they are finally assembled and cross-linked. The resultant protein structurally consists almost completely of three  $\alpha$ -helices forming its secondary structure, a triple-stranded helix, which is 1.5 nm in diameter and 300 nm long [29, 34]. This is called tropocollagen, a protein consisting of three polypeptide units. Mammal collagen I typically results of the association of two identical  $\alpha 1(I)$  chains and one  $\alpha 2(I)$  chain, slightly different in chemical composition. In other collagen types the three  $\alpha$ -helices are distinct or can be all the same such as in collagen III. The polypeptide chains wrap around one another forming a characteristic triple helix-tertiary structure. As in all protein complexes, the organization of several protein molecules – quaternary structure – is determinant of protein function and in collagen, in proper condition of temperature and pH, the triple helices self-assemble and cross link in staggered formation to form collagen fibrils, ranging from 10 to 300 nm in diameter. Those fibrils are also packed together to form collagen fibers between 0.5 to 3.0  $\mu\text{m}$  diameter (Figure 1.5) [44].

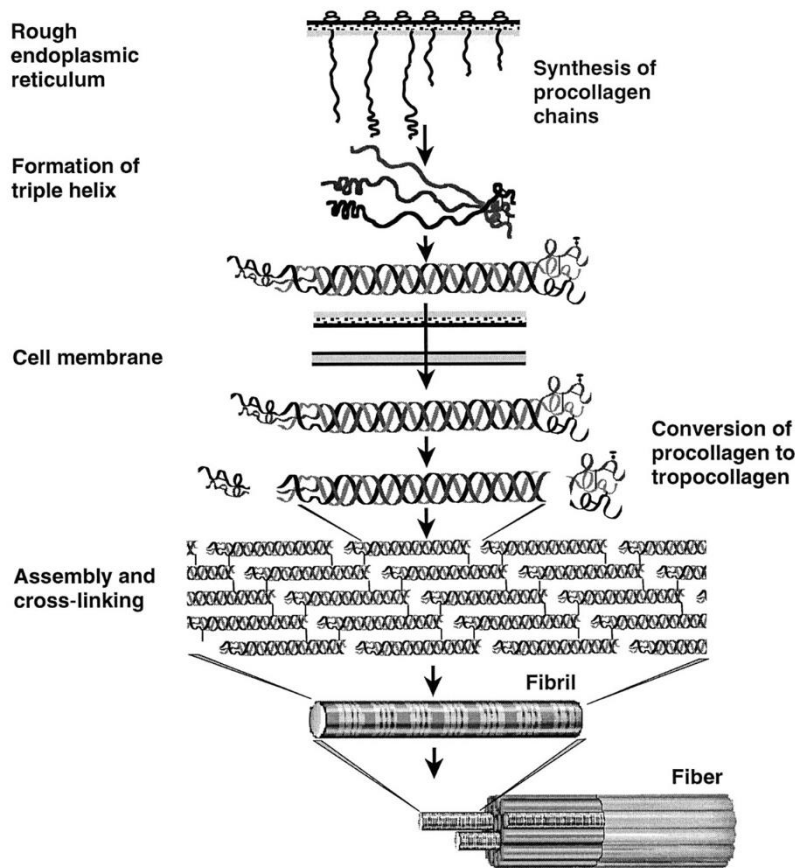


Figure 1.5: Representation of collagen synthesis, secretion and assembly [22].

Characteristic fibrillar and micro-fibrillar networks, formed by collagen types I, II, III, V and XI that represent about 90% of the total collagen, contribute to the basement membrane structure as well as other structures of the extracellular matrix.

The importance of collagen is attributed to many of its essential characteristics, including thermal stability, mechanical strength and the ability to interact with other biomolecules and cells. These properties are derived from the triple-helix structure with its interstrand hydrogen bonds, hydroxylation of Proline residues in the Y position and covalent crosslinking within the triple helices. The hierarchical nature of collagen organization permits the assessment of its mechanical properties of tissues like skin, at different levels of structural complexity, including the tropocollagen monomer, individual collagen fibrils, and collagen fibres [32].

In addition to these characteristics, its biodegradability and its poor immunogenicity explain that collagen has a wide range of applications in the health-related sectors, namely in cosmetics, pharmaceutical industries and tissue engineering field.

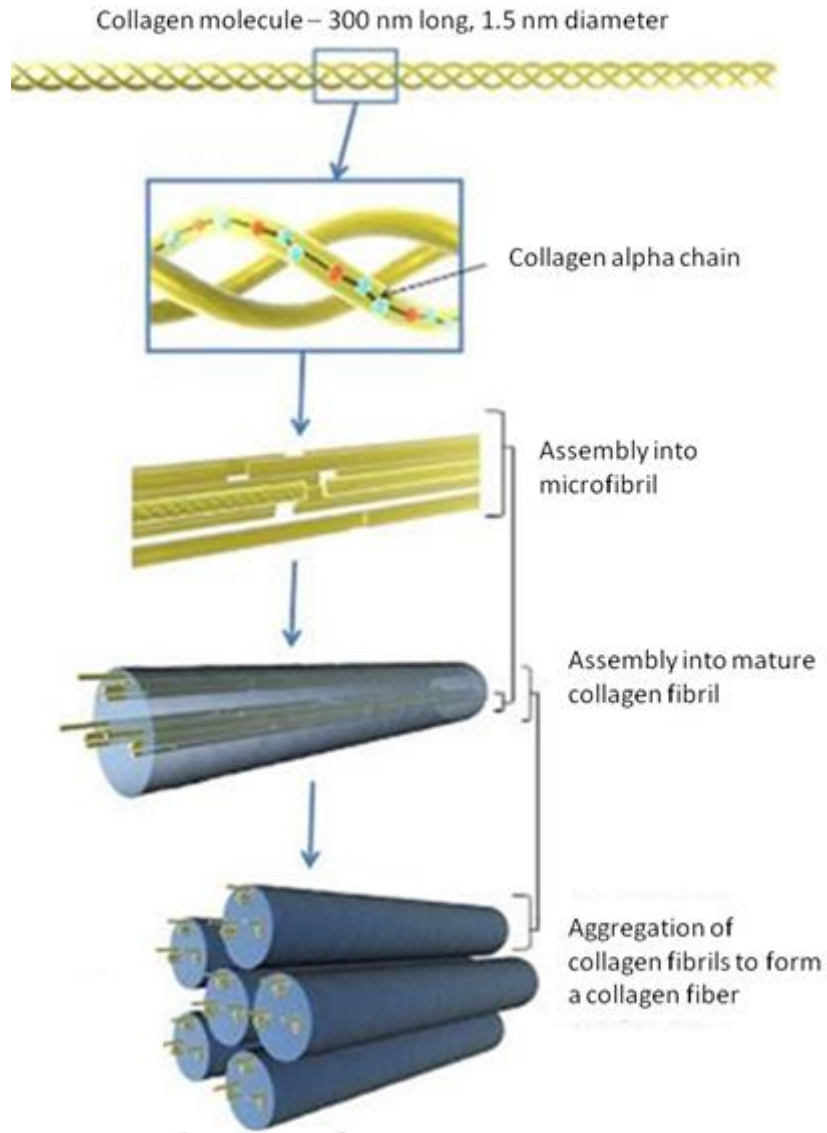


Figure 1.6: Representation of collagen assembly.

The high potential of collagen use has been the rational for intense research on collagen applications over the years. On Figure 1.7, it is possible to observe the impressive and continuous increase in the number of papers on collagen published in this 21st century (data collected from search in ISI Web of Knowledge™ using the terms “collagen” and “marine collagen”, the total number of papers, taking 2001 as reference), from about 15 thousand in 2001 to more than 26 thousand in 2013, experiencing the same increment rate of the total number of papers [37].

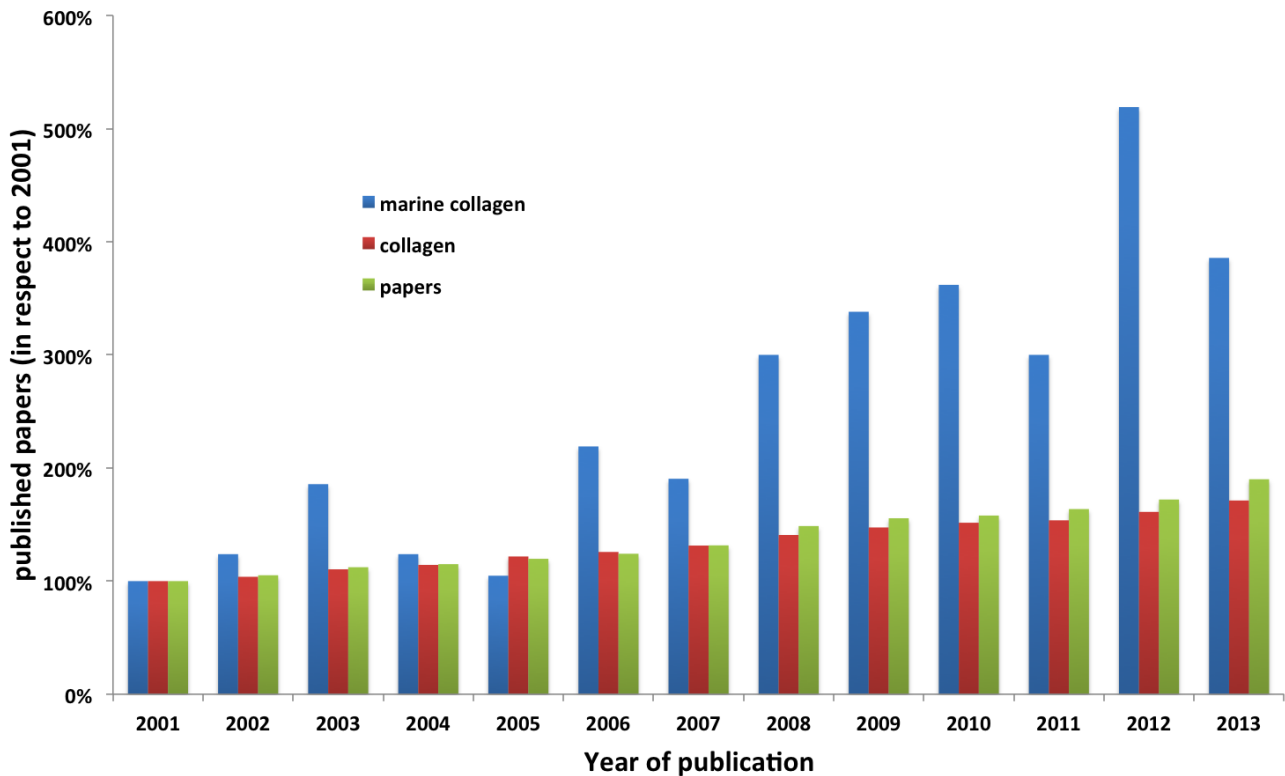


Figure 1.7: Increment on the number of papers on collagen, marine collagen and in total, published in the last 13 years (XXI century), taking 2001 as reference.

Regarding its industrial exploitation, collagen has mainly bovine and porcine origins, which have been a matter of concern in the last years. In fact, due to religious constraints related with avoidance of porcine and bovine products and to the recent episode of the wide scale bovine spongiform encephalopathy (BSE) outbreak in bovines, other collagen sources are being debated. In this regard, besides the use of recombinant technology (more expensive and not always effective), the use of collagen with marine origin is being considered highly attractive by the industry as an important alternative source. There is also significant research on marine origin collagens, as can be seen by the number of papers published in the last years on this subject depicted in Figure 1.7, indicating the growing attraction of such material in the last years [37].

Marine collagens can be obtained from different sources, such as fishes, or invertebrate marine animals, such as jellyfish. The latter is often considered as gelatinous animals (mostly water and a developed collagen-rich mesoglea), and their increasingly frequent outbreaks generate ecological and economic consequences from the formation of ocean jellyfish to beach closures. In this way, this alternative source takes into account the management of natural wastes and/or ecological problems and its by-products could acquire an important increase of the economic value [37]. Additionally, from genomic programs, molecular cloning,



biochemical and/or ultrastructural studies, it has been demonstrated that invertebrate fibrillary collagens would share the same characteristics than their human counterparts [38]. Under these conditions, jellyfish might be a model of great interest.

Silk is a typical fibrous protein produced by epithelial cells of a variety of insects including *Bombyx mori* silkworm. The raw silk thread presents two inner fibroin filaments (75-80 wt %) embedded into a sericin matrix (20-25 wt %), which acts as a glue (Figure 1.8) [39].

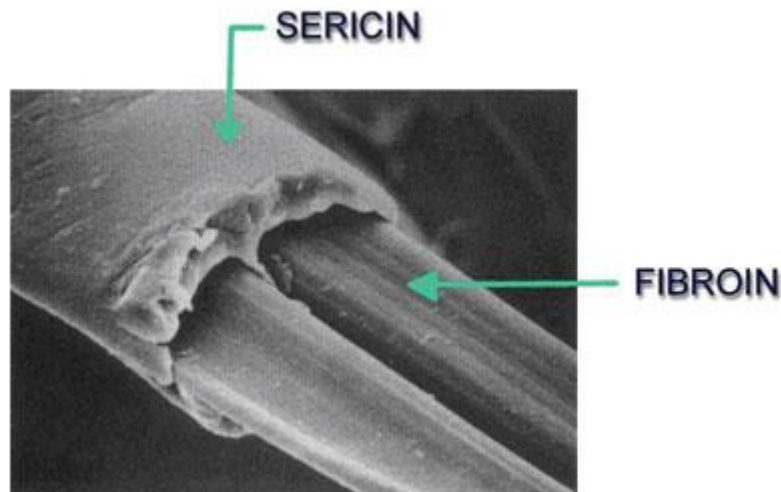


Figure 1.8: The structure of a silk filament.  
([www.dermasilk.com.au/content.php?view=HEALTHCARE\\_PROFESSIONALS](http://www.dermasilk.com.au/content.php?view=HEALTHCARE_PROFESSIONALS))

Silk fibroin is a natural fibrous polymer that forms the filaments of *Bombyx mori* cocoons and has been used in clinic as biomedical sutures for decades. Because of its impressive biological compatibility, non-immunogenic and mechanical properties, and good elasticity, silk fibroin have also been explored for many other biomedical applications including fibroblast and osteoblast cell support matrixes [41]. It is a protein mainly comprising of glycine, alanine, serine and tyrosine amino acids that form a crystalline  $\beta$ -sheets silk fibres, leading to its unique mechanical properties and hydrophobic domain structure [42]. When properly degummed – sericin removal – and sterilized, silk fibroin products have good biocompatibility, comparable with other biomaterials like collagen, good oxygen and water vapor permeability, biodegradability and minimal inflammatory reaction [43]. Host immune system plays a key role in degradation of silk fibroin mediated by macrophages, proving that silk is not only biodegradable but also bio-resorbable [44]. In addition, this protein is able to support endothelial cells attachment and growth to improve the formation of microcapillary

structures *in vitro* [45]. All these properties make silk fibroin suitable for the production of scaffolds especially for skin tissue engineering purpose.

Not only the material choice has to be considered, but also the different types of structures that material(s) can acquire, after fabrication, may influence significantly cells adhesion, proliferation and differentiation.

In this study, an initial simplified 2D model has been favoured to move later into a more complex 3D environment. Firstly, water-insoluble silk films, jellyfish collagen/fibroin blend and jellyfish collagen coated fibroin films have been prepared with a low  $\beta$ -sheet content, by using an all aqueous process. This type of constructs allows to evaluate some properties not directly linked with scaffold geometry. In fact, while the bulk structure and properties of these cast fibroin and collagen/fibroin blend films are of significant importance, the surface characteristics appear to be equally important, especially in connection with the growing interest in biomedical applications of the films. The surface properties of a material are the key factors controlling the interactions that occur when it is exposed to biological environments. Understanding of the surface features of these films could therefore provide new opportunities for these materials in biomedical fields.

Additionally, scaffold 3D geometry should define the space and the outer shape of the defect or lack to finally be properly adapted, also matching the healthy tissue stiffness and strength while maintaining an interconnected pore network for cell migration and nutrient transportation. It must also provide an environment in which cells can maintain their phenotype and synthesize proteins and molecules. The structure of the tissue scaffolds should be designed to have high macro- and micro-porosity, high surface area, fully interconnected geometry, structural strength and a specific three-dimensional shape [15]. For these reasons, three-dimensional (3D) jellyfish collagen/fibroin scaffolds and jellyfish collagen coated bioabsorbable fibroin scaffold using a freeze drying technique without methanol treatment were reported in this study. Especially, collagen in the form of sponge is useful in the treatment of different wounds, such as pressure sores, donor sites, leg ulcers and decubitus ulcers, as it adheres well to wet wounds, absorbs large quantities of tissue exudates, preserve a moist environment, and encourages the formation of new granulation tissue and epithelium on the wound.

## 1.6 Cell sources

One of the postulates tissue engineering is to combine scaffold with cells to produce new-engineered tissue. For this purpose, it is essential to understand cell behaviour in two situations: the normal morphogenesis and repair/regeneration phase in case of tissue damage. In both cases, cells create and/or recreate functional structures using signal molecules and the information encoded in the genome, synthesizing proteins according to a precise pattern. If we acquire knowledge of these processes, both in the case of healthy tissue and in the case of pathological tissue, it is possible to use them to design a functional instructive scaffold for new tissue formation.

In skin tissue engineering, scaffolds can be populated by cells before or after implantation. In the first approach, cells are an integral part of the graft and it involves a time of pre-culture *in vitro*. In the latter case, cells available in the implantation site are supposed to migrate inside the 3D structure and synthesize new extracellular matrix.

In this context, pre-seeded scaffolds were used in combination with fibroblast cells, which represent a primary cell component in the inflammatory phase of wound healing process and the cell type able to produce certain type of collagen, such as collagen I and III essential for skin regeneration.

Additionally, there are many reports of host immunogenic tolerance to allogeneic fibroblasts (Coulomb et al 1998) and their survival in the host up to more than three weeks. Long-term preservation of allogeneic fibroblasts and their proliferation up to two months in the host without signs of immune rejection have also been reported. On the contrary, allogeneic keratinocytes provide effective pain relief and accelerate wound healing, but they do not survive longer than a few weeks when applied to the wound because they are rejected by the host.

Therefore, in order to produce permanent dermo/epidermal skin substitutes, it appears that either allogeneic or autologous fibroblasts can be used. In particular, two different fibroblast cells of different origin were chosen: NIH 3T3 and MRC-5 cell lines (Paragraph 3.6.1).

## 1.7 Open questions with commercially available skin substitutes

In this context, we highlighted the most important principles that submit to tissue engineering of skin and reported some skin substitutes available in the treatment of skin injuries in humans along with the advantages and disadvantages associated with their use. At present, no manufactured skin substitute has provided an outcome consistently comparable to an autograft because no currently skin replacement biomaterials possess all the above-mentioned properties nor can they fully replace the functional and anatomical properties of the native skin [6]. One of the most important problems of skin constructs concern with reduced vascularization when a skin graft is placed on a recipient wound bed. Presently available skin substitutes that integrate well often suffer from scarring problems at the graft margins and absence of differentiated structures, with regard to lack of temperature control provided by sweat and sebaceous glands, as well as hair follicles. Additionally, in skin substitutes an adequate vascular supply from adipose tissue and nerve supply do not exist; critically these constructs have no resident Langerhans cells, which play an important function in immune regulation in the skin. At the last, understanding the mechanisms by which foetal wounds heal together with new skin substitute biomaterials could result in a real breakthrough in adult wound healing with the possibility of real skin regeneration rather than defective and inferior scar-like skin repair.

The goal is hereby to combine jellyfish collagen and silk fibroin with fibroblast cells to produce a novel prospective skin equivalent, which is both functional and durable, and allows the integration and manipulation of the cell biology of host cells and the multitude of signals that control their behavior. Conventionally in fact, tissue-engineered skin exists as cells grown *in vitro* and subsequently seeded onto a scaffold or some porous material, which is then placed *in vivo* at the site of injury.

## 2. Research strategies and objectives

### 2.1 Aims of the thesis

In the previous chapter there was introduced molecular details of wound healing and concept of skin replacement in Tissue Engineering, its main approaches, advantages, polymers used in this field and open questions. Special attention is paid to collagen, which has been finding application in a myriad of fields, in particular as part of scaffold in the skin tissue engineering context. In recent years, great interest was shown toward new sources of this material, such as marine organisms, being considered as harmless to humans and being an abundant source of material with economic potential.

The objective of the presented research work was collagen extraction optimization from dried jellyfish, *Rhopilema hispidum*, in order to obtain good yields required for scaffold fabrication in Tissue Engineering. One of possible applications, to which such work refers, is the use of this material for skin tissue engineering, in order to support wound healing process. Aimed to this, the jellyfish collagen was characterized to evaluate the specific collagen type isolated, its specific structure by comparing to a commercial type I collagen, its biocompatibility and potential use to prepare implantable biomaterials for humans. Different types of scaffolds morphologies were produced, in particular, Tissue Culture Plate-well coating, film and 3D sponge, in order to find suitable structures for the above mentioned purpose.

After chemical-physical characterization of the constructs, preliminary biological *in vitro* evaluations were performed, using two different fibroblast cell lines, with the aim of assessing viability, adhesion and proliferation of cells grown on jellyfish collagen scaffolds, respect to other commercial biomaterials. The bioactivity of jellyfish collagen like coating was also assessed based on its ability to induce the main wound healing biomarkers synthesis by fibroblasts.

My research project was carried out in the BIOtech – Center for Biomedical Technologies, Department of Industrial Engineering, University of Trento.

## 2.2. Strategies: polymer selection and processing definition

Collagens are the major structural and biologically active components of all connective tissues including skin where provide proper stability and structural integrity of tissues and organs. The high potential of collagen use, especially from marine origin, has been the rational for intense research on collagen applications over the years.

Silk fibroin, a natural fibrous biopolymer, known for its favorable properties in the Tissue Engineering field, and whose extraction method results already optimized, was used in this specific work with the final objective of skin replacement fabrication.

Instead of introducing a chemical or physical crosslink, jellyfish collagen coated silk fibroin construct and marine collagen/silk fibroin blend were used in order to produce water-stable scaffolds. These latter combine their promising properties for wound healing purpose, such as impressive biocompatibility, biodegradability, minimal inflammatory response, favourable mechanical properties, and the reported ability of collagen to help and promote cell adhesion and proliferation. Chemically and morphologically different types of scaffolds were produced in order to discriminate which factors affected adhesion and growth of cells. Films produced by solvent-casting technique, and sponges, produced by freeze-drying technique without introducing a chemical crosslink, were characterized by high porosity and an interconnected pore structure.

# 3. Materials and Methods

## 3.1 Jellyfish collagen extraction

Collagen has been finding application in a myriad of fields and depending on the specific application and the desired formulation, different strategies can be followed to process collagen from marine origin. In principle, processing methodologies similar to the ones used with mammal collagens can be used with marine collagens, but due to specific characteristics of the latter, tuning of those methodologies may be needed and none should be taken for granted.

As raw material, *Rhopilema hispidum* jellyfish specie was investigated as possible source of collagen for the next 2D-well coating, film and sponge production (Figure 3.1). *Rhopilema hispidum* was dried, salted with NaCl and then transported from Thailand to the laboratory in Trento. The sample presented the typical structure of jellyfish, composed by umbrella and oral arms.



Figure 3.1: From dried jellyfish to lyophilized collagen (PSC).

It is possible to define a general methodology to isolate collagen from jellyfish, composed by three fundamental phases: pre-treatment or preparation, extraction and recovery. To reach the final optimized protocol, different procedures have been tested in our laboratory starting from an experimental method found in literature, which lead to low yields [53].

### Protocol 1 (starting protocol)

#### *Pre-treatment phase (at room temperature)*

- **8.45 g** of sample were weighed and cut into small pieces;
- the tissue was cleaned using bidistilled water in a solid-solvent ratio of 1:10 (w/v) for 1 day;

- the cleaned tissue was separated from bidistilled water through sieve filtration, for subsequent collagen extraction.

*Extraction phase (at 4 °C)*

- the pieces of jellyfish were extracted with 0.5 M acetic acid for 3 days with stirring;
- the extract was centrifuged at 15000 g for 30 min;
- the supernatant (ASC) was collected for the next phase;
- the insoluble components were solubilized with 10 v of 0.5 M acetic acid containing 0.05 % (w/v) pepsin for 2 days under continuous stirring;
- the solution was centrifuged at 15000 g for 30 min and the supernatant (PSC) was collected for the next phase;

*Recovery phase (at room temperature)*

- both the supernatants (ASC and PSC) were salted-out by adding NaCl at a final concentration of 0.9 M;
- the resulting precipitates were collected by centrifugation at 15000 g for 30 min;
- the pellets were dissolved and resuspended in 0.5 M acetic acid;
- then, dialyzed against 0.1 M acetic acid against distilled water for 2 days, by using two dialysis cassettes (3500 MW). The dialysis solutions were changed three times every day;
- in the end, the solutions were stored at -80 °C and then freeze-dried to obtain dry weight collagen.

From the above starting procedure, several modifications were made by BIOtech research group until to achieve a better protocol in terms of yield (protocol 6).

Protocol 6

*Pre-treatment phase (at room temperature)*

- **11.12 g** of sample were weighed and cut into small pieces;
- the tissue was cleaned using **bidistilled water** in a solid-solvent ratio of 1:10 (w/v) for 1 day and using **0.1 M NaOH solution (1:10 w/v)** for another day;
- after 1 day the tissue was separated from bidistilled water through sieve filtration, and after second day the sample was **centrifuged at 10000 g for 10 min** to separate the tissue from NaOH solution for subsequent collagen extraction.

*Extraction phase (at 4 °C)*



- the pieces of jellyfish were extracted with 0.5 M acetic acid for 3 days with stirring;
- the extract was centrifuged at 15000 g for 30 min;
- the supernatant (ASC) was collected for the next phase;
- the insoluble components were solubilized with 10 v of 0.5 M acetic acid containing **0.2 % (w/v) pepsin** for **3 days** under continuous stirring;
- the solution was centrifuged at 15000 g for 30 min and the supernatant (PSC) was collected for the next phase;

#### *Recovery phase (at 4 °C)*

- both the supernatants (ASC and PSC) were salted-out by adding **NaCl** at a final concentration of **2 M**;
- the resulting precipitates were collected by centrifugation at 15000 g for 30 min;
- the pellets were dissolved and resuspended in 0.5 M acetic acid;
- then, dialyzed against 0.1 M acetic acid against distilled water for 3 days, by using two dialysis cassettes (3500 MW). The dialysis solutions were changed three times every day;
- in the end, the solutions were stored at -80 °C and then freeze-dried to obtain dry weight collagen.

Starting from Protocol 6, my thesis project aimed to optimize the collagen isolation procedure, leading to increased yields with the final protocol (Protocol 9).

#### Protocol 7

##### *Pre-treatment phase (at room temperature)*

- **10.16 g** of sample were weighed and **mincing with a mixer** into small pieces;
- the tissue was cleaned using bidistilled water in a solid-solvent ratio of 1:10 (w/v) for 1 day and using 0.1 M NaOH solution (1:10 w/v) for another day;
- after 1 day the tissue was separated from bidistilled water through sieve filtration, and after second day the sample was centrifuged at 10000 g for 10 min to separate the tissue from NaOH solution for subsequent collagen extraction.

##### *Extraction phase (at 4 °C)*

- the pieces of jellyfish were extracted with 0.5 M acetic acid for 3 days with stirring;
- the extract was **centrifuged** at 15000 g **for 1 h**;
- the supernatant (ASC) **was discarded** (due to the low yield);

- the insoluble components were solubilized with 10 v of 0.5 M acetic acid containing 0.2 % (w/v) pepsin for 3 days under continuous stirring;
- the solution was **centrifuged** at 15000 g **for 1 h** and the supernatant (PSC) was collected for the next phase;

*Recovery phase (at 4 °C)*

- the supernatant (PSC) was salted-out by adding NaCl at a final concentration of 2 M;
- the resulting precipitate was collected by **centrifugation** at 15000 g **for 1 h**;
- the pellet was dissolved and resuspended in 0.5 M acetic acid;
- then, dialyzed against 0.1 M acetic acid against distilled water for 3 days, by using one dialysis cassette (3500 MW). The dialysis solution was changed three times every day;
- in the end, the solution was stored at -80 °C and then freeze-dried to obtain dry weight collagen.

Protocol 8

*Pre-treatment phase (at room temperature)*

- **9.75 g** of sample were weighed and mincing with a mixer into small pieces;
- the tissue was cleaned using bidistilled water in a solid-solvent ratio of 1:10 (w/v) for 1 day and using 0.1 M NaOH solution (1:10 w/v) for another day;
- after 1 day the tissue was separated from bidistilled water through sieve filtration, and after second day the sample was centrifuged at 10000 g for 10 min to separate the tissue from NaOH solution for subsequent collagen extraction.

*Extraction phase (at 4 °C)*

- the pieces of jellyfish were extracted with 0.5 M acetic acid for 3 days with stirring;
- the extract was **ultra-centrifuged at 20000 g** for 1 h;
- the supernatant (ASC) was discarded (due to the low yield);
- the insoluble components were solubilized with 10 v of 0.5 M acetic acid containing **0.5 % (w/v) pepsin** for 3 days under continuous stirring;
- the solution was **ultra-centrifuged at 20000 g** for 1 h and the supernatant (PSC) was collected for the next phase;

*Recovery phase (at 4 °C)*

- the supernatant (PSC) was salted-out by adding **NaCl** at a final concentration of **2.5 M**;
- the resulting precipitate was collected by **ultra-centrifugation at 15000 g** for 1 h;
- the pellet was dissolved and resuspended in 0.5 M acetic acid;

- then, dialyzed against 0.1 M acetic acid against distilled water for 3 days, by using one dialysis cassette (3500 MW). The dialysis solution was changed three times every day;
- in the end, the solution was stored at  $-80\text{ }^{\circ}\text{C}$  and then freeze-dried to obtain dry weight collagen.

#### Protocol 9 (final protocol)

- **All collagen purification steps were carried out at  $4\text{ }^{\circ}\text{C}$ .**

##### *Pre-treatment phase*

- **10.13 g** and **20.15 g** of sample were weighed and mincing with a mixer into small pieces;
- the tissues were cleaned using bidistilled water in a solid-solvent ratio of 1:10 (w/v) for 1 day, using 0.1 M NaOH solution (1:10 w/v) for 1 day and **using 70 % Ethanol solution for another day**;
- after 1 day the tissues were separated from bidistilled water through sieve filtration, after second day the samples were centrifuged at 10000 g for 10 min to separate the tissue from NaOH solution, and **after third day the samples were centrifuged at 10000 g for 10 min to separate the tissue from 70 % Ethanol solution**, for subsequent collagen extraction.

##### *Extraction phase*

- the pieces of jellyfish were directly solubilized with 10 v of 0.5 M acetic acid containing **0.2 % (w/v) pepsin** for 3 days under continuous stirring (**no ASC extraction**);
- the solutions were ultra-centrifuged at 20000 g for 1 h and the supernatants (PSC) were collected for the next phase;

##### *Recovery phase*

- the supernatants (PSC) were salted-out by adding **NaCl** at a final concentration of **2 M**;
- the resulting precipitates were collected by ultra-centrifugation at 15000 g for 1 h;
- the pellets were dissolved and resuspended in 0.5 M acetic acid;
- then, dialyzed against 0.1 M acetic acid against distilled water for 3 days, by using two dialysis cassettes (3500 MW). The dialysis solutions were changed three times every day;
- in the end, the solutions were stored at  $-80\text{ }^{\circ}\text{C}$  and then freeze-dried to obtain dry weight collagen.

## 3.2 Jellyfish isolated collagen characterization

The characteristics of collagen *in vivo* are unique and when the goal is to mimic the collagen role in extracellular matrix, as is the case of skin tissue engineering approaches producing collagen-based matrices for cell culture, it is of extremely importance the evaluation of processed collagen properties. Since there are so many sources from where collagens can be extracted, and so many types, it is crucial to study its characteristics with particular care and accuracy.

There are several techniques that can be used to characterize collagen samples (in solution or in solid state), addressing structural, chemical and morphological features. With a good characterization and, consequently, a better knowledge of the sample, it is easier to have a desired biological response or to establish a relationship between results and features of the produced structure [29].

### 3.2.1 Molecular weight evaluation by SDS-polyacrylamide gel electrophoresis

One of the methods that was used to characterize collagen purity and breakdown was the sodium dodecyl sulfate polyacrylamide gel electrophoresis (SDS-PAGE). With gel electrophoresis, proteins and their fragments can be separated, based on their size. It was possible to observe the protein fragments by loading protein samples in the small wells of the gel, which, under an applied electrical field, travel through the gel matrix depending on their size: the smallest go further than the large ones, which stay trapped in the gel net. From this, it was possible to compare with collagens obtained from other sources, taken as reference, and propose an identification of the collagen type (I, II, ...) when the collagen bands are similar. In the case of collagens from the same type but from different species, where the amino acid sequence was changed although the same chain types were present (for instance,  $\alpha_1$ ,  $\alpha_2$  and  $\beta$  chains in type I collagen), slightly shifts in the position of the bands may be observed. This was most probably caused by small differences in the molecular weight as a consequence of different amino acid sequences [29].

SDS-PAGE buffers composition were reported in the following table (Table 2):

<i>SDS PAGE Resolving gel</i>	0.37 M Tris-HCl pH 8.8 (Resolving Buffer), 12 % (w/v) Acrylamide, 0.1 % (w/v) SDS (sodium dodecyl sulfate), 0.5 % (w/v) APS (ammonium persulfate), 1 % (w/v) TEMED (N,N,N',N'-Tetramethylethylenediamine) added to initiate the polymerization reaction just before pouring the solution.
<i>SDS PAGE Stacking gel</i>	0.08 M Tris-HCl pH 6.8 (Stacking Buffer), 4.2 % (w/v) Acrylamide, 2 % (w/v) SDS, 1 % (w/v) APS, 2 % (w/v) TEMED added to initiate the polymerization reaction just before pouring the solution.
<i>3X SDS PAGE gel Loading Buffer</i>	240 mM Tris-HCl, 30% (w/v) glycerol, 6% (w/v) SDS, 1.6% (w/v) $\beta$ -mercaptoethanol, 0.9 mM Bromophenol Blue
<i>SDS gel Running Buffer</i>	25 mM Tris-HCl, 200 mM Glycine, 0.1% (w/v) SDS, pH 8.3
<i>Staining solution</i>	0.001 g/mL Coomassie, 40% (v/v) methanol, 10% (v/v) acetic acid, 50% (v/v) water
<i>Destainig solution</i>	40% (v/v) methanol, 10% (v/v) acetic acid, 50% (v/v) water

Table 3.1: Buffer composition for SDS-PAGE electrophoresis.

As soon as 5 mL volume resolving gel was moved into the gel chamber, it was covered with 2 mM of n-butanol to exclude O<sub>2</sub> and ensure a gel flat interface. After 15 min polymerization, n-butanol was removed and the stacking gel was poured with a comb inserted to form the wells and define the lanes and allowed to polymerize for 10 min. The samples that were loaded onto the SDS-PAGE gel were prepared as follows: each sample was dissolved in 0.6 M Tris-HCl buffer (pH 6.8) which contained 25% (v/v) glycerine, 2% (w/v) SDS and 5% (v/v)  $\beta$ -mercaptoethanol. All samples were heated for 5 min at 94 °C. While the soluble fraction was ready to be loaded, the insoluble fraction and the pre induction sample were centrifuged. 13  $\mu$ L from each sample were loaded on a SDS-PAGE gel lanes. The ladder used was a volume of 8  $\mu$ L Precision Plus Protein™ Unstained Standards from BioRad. The gel was run at 130 V for 1.5 h. Staining was performed with Coomassie Staining solution and was allowed to continue overnight with mild shaking. De-staining was performed for 3 h with de-staining solution with mild shaking.

### 3.2.2 Collagen tertiary conformation analysis by circular dichroism spectroscopy

Another method used to characterize collagen purity and structure was the CD spectroscopy. Circular dichroism (CD) is an excellent method for rapidly evaluating the secondary structure, folding and binding properties of proteins. Briefly, circular dichroism is defined as the unequal absorption of left-handed and right-handed circularly polarized light. A beam of light has time dependent electric and magnetic fields associated with it. If the light is polarized by passing through suitable prisms or filters its electric field,  $E$ , will oscillate sinusoidally in a single plane. When viewed from the front, the sinusoidal wave can be visualized as the resultant of two vectors of equal length, which trace out circles, one which rotates clockwise ( $ER$ ) and the other which rotates counterclockwise ( $EL$ ). The two circularly polarized waves have physical existence. The waves are 90 degrees out of phase with each other and can be separated using a variety of prisms or electronic. When asymmetric molecules interact with light, they may absorb right and left handed circularly polarized light to different extents (hence the term circular dichroism) and also have different indices of refraction for the two waves. The result is that the plane of the light wave is rotated and that the addition of the  $ER$  and  $EL$  vectors results in a vector that traces out an ellipse and the light is said to be elliptically polarized. CD is reported either in units of  $\Delta E$ , the difference in absorbance of  $ER$  and  $EL$  by an asymmetric molecule, or in degrees ellipticity, which is defined as the angle whose tangent is the ratio of the minor to the major axis of the ellipse [46].

Circular dichroism (CD) spectra were applied to assess the secondary structure of pepsin-solubilized collagen isolated from *Rhopilema hispidum* jellyfish sample, with a Jasco J-715 spectropolarimeter (Figure 3.2). In particular, this test has been performed for observe whether the extracted collagen was denatured or not. Each collagen was diluted using 0.1 M acetic acid at 5 different concentrations (0.05, 0.1, 0.2, 0.25 and 0.3 mg/ml) and then the solutions were placed into a quartz cell with a path length of 1 mm. CD spectra measurements were performed at a wavelengths range of 350-180 nm with a scan speed of 500 nm/min at an interval of 0.5 nm. A reference spectrum containing 0.1 M acetic acid was also recorded. The CD spectra of the samples were obtained after subtracting the reference spectrum. The data were accumulated three times.



Figure 3.2: JASCO J-715 Circular Dichroism (CD) Spectropolarimeter.

### 3.2.3 Secondary structure evaluation by Fourier transform infrared spectroscopy

IR radiation excites molecules into higher energy state. As IR is passed through a sample, some of the IR is absorbed by the sample and some passes through it. As a result, the IR patterns of molecular absorption and transmission unique to the tested sample are generated. IR is like a fingerprint for every particular type of material. The chemical bonds oscillations can be in any of the forms such as vibration, stretching, bending, rocking, wagging. The vibration occurs at a specific frequency according to bonds present between atoms. According to the molecular structure, the IR radiation wavelength is absorbed. The wavelength absorbed by a particular molecule is decided by the energy difference between rest and excited vibrational states.

The absorption wavelength is proportional to initiate intra molecular oscillations. There are different regions allotted to IR waves.  $14000\text{ cm}^{-1}$  to  $4000\text{ cm}^{-1}$  for near infrared (NIR),  $4000\text{ cm}^{-1}$  to  $400\text{ cm}^{-1}$  for mid infrared (MIR) and  $400\text{ cm}^{-1}$  to  $10\text{ cm}^{-1}$  for far infrared (FIR). FTIR is the data processing technique for infrared raw data converted to understandable data/graphs. FTIR is useful for identifying any organic or inorganic chemicals in solid, liquid or gas form. It is useful to identify functional groups in chemical bonds [47, 48].

The molecular motions can be associated with functional group oscillations, which are always at the same location of the IR spectra irrespective of the substance. Any IR absorption pattern

can be easily differentiated for each compounds and can be used as a fingerprint for that specific substance [48, 49].

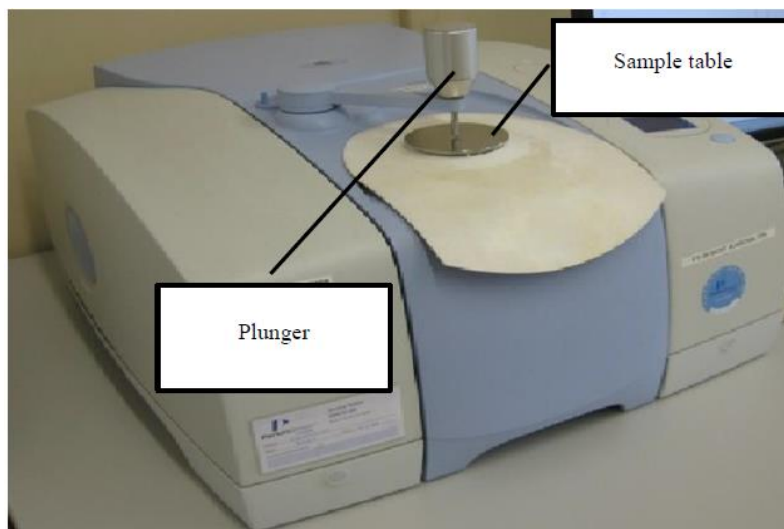


Figure 3.3: ATR-FTIR Perkin-Elmer Spectrum 100 FT-IR.

On the lower end of the visible range the infrared zone starts. Infrared waves have lower frequency and longer wavelength compared to visible range electromagnetic waves.

IR spectra can be used for compound specific detection and identification.

The FTIR is an analytical technique for IR spectroscopy and it converts IR data into useful quantitative as well as qualitative form. The mathematical technique, called Fourier transformation, is used to decode IR data.

The FTIR spectroscopy plots a graph of absorbance (or % transmittance) vs energy in the form of wavenumber  $\text{cm}^{-1}$ . The IR wavenumber range depends upon the detector but usually the  $500\text{-}4000\text{ cm}^{-1}$  range is studied. The FTIR spectrometer can be divided in to two regions.  $1600\text{-}4000\text{ cm}^{-1}$  is called “functional group region” and  $500\text{-}1600\text{ cm}^{-1}$  is called “fingerprint region”. The functional group region shows peaks related to stretching motions of the functional groups. The peaks are easily identifiable for groups such as alcohols, amines, aromatics, aliphatic, acids, esters and so on. In the fingerprint region the peaks are complex and overlap with each other. The pattern of peak in this region is very important; it can be used as fingerprint for a particular compound [49].

Sample preparation is a very important part of conventional FTIR. In conventional FTIR the solid sample has to be in a thin film form. The process of making film is time consuming. A new technique called “Attenuated total Reflection” with nil or very small sample proportion is now used. In ATR, the IR beam is passed through an optically dense crystal with higher reflective index at a certain angle. The fraction of the incident beam reflected and the wave



extends beyond the crystal surface into sample held on the crystal. The wave only penetrates 0.5  $\mu\text{m}$  to 5  $\mu\text{m}$  beyond the crystal into the sample. Therefore, the sample and crystal must be in good contact. The ATR method is a versatile method for any shape, configuration, thickness; liquids, solids and powders can be analysed [49].

Infrared spectra were obtained on the Perkin-Elmer Spectrum 100 FT-IR (Figure 3.3). The universal ATR sampling accessory, deposited neatly onto a diamond/ZnSe plate. The scans were carried out between 650 and 4000  $\text{cm}^{-1}$  at the resolution of 4  $\text{cm}^{-1}$ .

### 3.2.4 Collagen thermal behavior analysis by differential scanning calorimetry

Differential scanning calorimetry (DSC) is a thermo-analytical technique for measuring the energy necessary to establish a nearly zero temperature difference between a substance and an inert reference material, as the two specimens are subjected to identical temperature regimes in an environment heated or cooled at a controlled rate. In this way, DSC monitors heat effects associated with phase transitions and chemical reactions as a function of temperature in a controlled atmosphere. These measurements provide quantitative and qualitative information about physical and chemical changes that involve endothermic or exothermic processes or changes in heat capacity [50].

In a DSC the difference in heat flow to the sample and a reference at the same temperature, is recorded as a function of temperature. The reference is an inert material such as alumina, or just an empty aluminum pan. The temperature of both the sample and reference are increased at a constant rate. Since the DSC is at constant pressure, heat flow is equivalent to enthalpy changes:

$$\left(\frac{dq}{dt}\right)_p = \frac{dH}{dt}$$

Here  $dH/dt$  is the heat flow measured in  $\text{mcal sec}^{-1}$ . The heat flow difference between the sample and the reference is:

$$\Delta \frac{dH}{dt} = \left(\frac{dH}{dt}\right)_{\text{sample}} - \left(\frac{dH}{dt}\right)_{\text{reference}}$$

and can be either positive or negative. In an endothermic process, such as most phase transitions, heat is absorbed and, therefore, heat flow to the sample is higher than that to the reference. Hence,  $\Delta dH/dt$  is positive. Other endothermic processes include helix-coil transitions in DNA, protein denaturation, dehydrations, reduction reactions, and some decomposition reactions. In an exothermic process, such as crystallization, some cross-linking processes, oxidation reactions, and some decomposition reactions, the opposite is true and  $\Delta dH/dt$  is negative [51].

There are two types of DSC systems in common use. In power-compensation DSC, the temperatures of the sample and reference are controlled independently using separate, identical furnaces. The temperatures of the sample and reference are made identical by varying the power input to the two furnaces; the energy required to do this is a measure of the enthalpy or heat capacity changes in the sample relative to the reference.

In heat-flux DSC, which was used in this context, the sample and reference are connected by a low-resistance heat-flow path (a metal disc). The assembly is enclosed in a single furnace. Enthalpy or heat capacity changes in the sample cause a difference in its temperature relative to the reference; the resulting heat flow is small compared with that in differential thermal analysis (DTA) because the sample and reference are in good thermal contact. The temperature difference is recorded and related to enthalpy change in the sample using calibration experiments [52].

The DSC set-up is composed of a measurement chamber and a computer. The chamber consists of a sample holder and a reference holder as shown in Figure 3.4. Both are constructed of platinum to allow high temperature operation. Under each holder is a resistance heater and a temperature sensor. Currents are applied to the two heaters to increase the temperature at the selected rate. The difference in the power to the two holders, necessary to maintain the holders at the same temperature, is used to calculate  $\Delta dH/dt$ . A schematic diagram of a DSC is shown in Figure 3.5. A flow of nitrogen gas is maintained over the samples to create a reproducible and dry atmosphere. The nitrogen atmosphere also eliminates air oxidation of the samples at high temperatures. The sample is sealed into a small aluminum pan. The reference is usually an empty pan and cover, as already said. The pans hold up to about 10 mg of material [51].

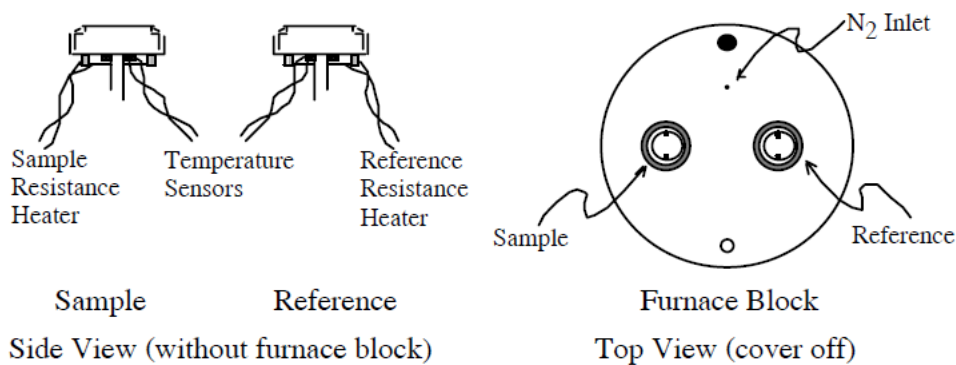


Figure 3.4: Differential scanning calorimeter sample and reference holder [51].

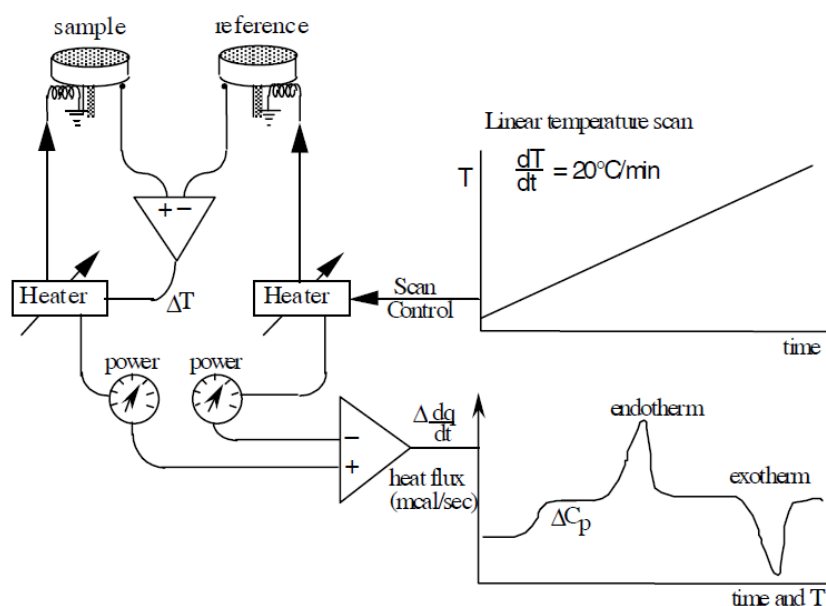


Figure 3.5: Schematic of a DSC. You choose the linear temperature scan rate. The triangles are amplifiers that determine the difference in the two input signals. The sample heater power is adjusted to keep the sample and reference at the same temperature during the scan [51].

The computer is used to monitor the temperature and regulate the rate at which the temperature of the pans changes. A typical heating rate (or temperature scan rate =  $dT/dt$ ) is around  $10^\circ\text{C}/\text{min}$ .

In a heat flux DSC system, the sample and reference are heated at the same rate from a single heating source as shown in Figure 3.6. [51].

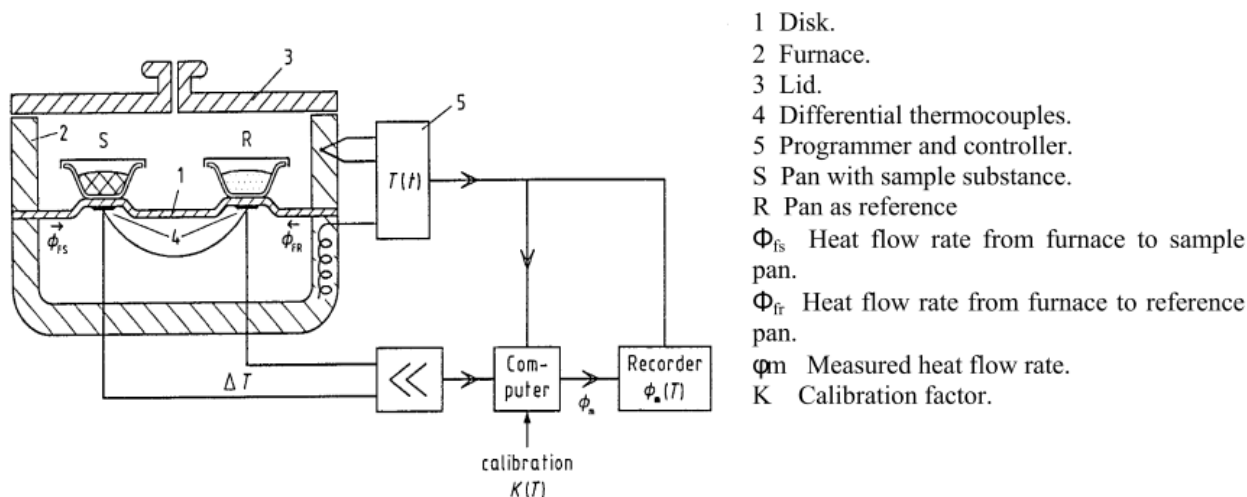


Figure 3.6: Schematic diagram of a heat flux DSC system. The sample and reference are heated at the same rate and the temperature difference is measured [51].

The rate of temperature change for a given amount of heat will differ between the two pans. This difference in the amount of heat required to increase the temperature of a sample compared to reference is measured as a function of temperature and depends on the composition of the pan contents as well as physical changes such as phase changes: the pan with sample in it heat up at different temperature than the empty pan, in spite of the same heat rate applied to both. Because the heat capacity of any material is different than air, the system varies the heat provided to one of the pans in order to keep the temperature of both pans the same; in other words higher/less heat flow will need to be supplied at the same heat rate. The difference in heat output of the two heaters is recorded and can be measured as an endothermic or exothermic peak, which is caused by transformations in the material. The result is a plot of the difference in heat ( $q$ ) versus temperature ( $T$ ). By analyzing the thermogram shape (and knowing the possible transitions, which can occur in the material), it is possible to infer which transformation happen at each temperature (e.g. glass transition is a flex, melting is an endothermic peak, crystallization is an exothermic peak).

Thermal analysis of different types of samples were done by a METTLER-TA instrument DSC12E. TOLEDO-TA89 E software was used to obtain DSC curves. Weigh the sample pan and lid if the heat capacity and latent heats were to be calculated. The sample was placed in the pan and the lid, with some small holes on the top to allow air to enter, was fixed on. It was necessary to weigh the pan with encapsulated sample to determine the sample weight for quantitative measurements. The sample pans carefully positioned on the raised platform in the front of the heating chamber and the empty non hermetic pan with lid, used as a

reference, on the platform in the rear. It was important to centre to the pans to the grid to ensure they were centered on the platform.

Several factors such as scan rate, pan type, gas type, heating rate and sample weight (in this context  $\approx 10$  mg) can affected DSC results. According to other's research, the measurement were carried out in the range of 30-330 °C under nitrogen ( $100 \text{ cm}^3/\text{min}$ ) at a scanning rate of 10 °C/min.

### 3.2.5. Collagen amino acid composition by high performance liquid chromatography

A complete analysis of the canonical protein amino acids has been established as a standard study, allowing to evaluate the typical content of each amino acids. It is composed by a protein hydrolysis followed by amino acid separation, identification and quantification using High Performance Liquid Chromatography (HPLC) [29]. Briefly, 4 mg freeze dried pepsin soluble collagen were hydrolyzed in inert atmosphere with 3 M HCl at 114 °C in oil bath heater for 20-24 hours, the hydrolysates were dried under vacuum and 0.22  $\mu\text{m}$  filtered. The hydrolysates, like standard (waters amino acid Hydrolysate in Milli-Q water) and blank samples, were derivatized, dried and diluted with sample diluents. The amino acids derivative samples were analyzed by AccQ.Tag Amino Acid Analysis Column (Waters Corporation, Milford, MA) and compared against the standard bovine type I collagen amino acids content. The area under the peak of each amino acid in chromatogram was calculated and reported as number of moles of each amino acid in the sample.

The Hydroxyproline Assay Kit (Sigma-Aldrich) was then used to quantify the content of hydroxyproline, since it is a major component of collagen, where it serves to stabilize the helical structure. Because hydroxyproline is largely restricted to collagen, the measurement of hydroxyproline levels can be used as an indicator of collagen content. Hydroxyproline concentration is determined by the reaction of oxidized hydroxyproline with 4-(Dimethylamino)benzaldehyde (DMAB), which results in a colorimetric (560 nm) product, proportional to the hydroxyproline present. This kit is suitable for hydroxyproline detection in cell and tissue culture supernatants, and other biological samples.

### 3.3 Silk fibroin water solution processing

Scaffolds were prepared starting from silkworm *Bombyx mori* polyGhybrids cocoons, kindly provided by Dr. Giovanna Salice, Cassina Rizzardi, Como, Italy. Silk fibroin aqueous solution was prepared using a specific procedure, well defined along the year:

- silkworm *Bombyx mori* cocoon were open to remove the larvae, whose life cycle was interrupted earlier by heating, and raw silk filament, discontinuous thread often full of impurities.
- Sericin was removed through a degumming process that consist in treatment of the cocoons (1L/10 g of silk) in alkaline bath of distilled water and Na<sub>2</sub>CO<sub>3</sub> (Sigma, USA, CAS: 497-19-8) (1.1 g/L of water) for 45 minutes at 98°C. After that, the silk was transferred to a second bath, similar to the first for timing and temperature, but with a lower concentration of salt (0.4 g/L of distilled water). The resulting fibers were rinsed with distilled water, in order to eliminate the sericin and any salt residues, and cooled from a temperature of 80°C to room temperature, through several baths in distilled water.
- Fibroin fibers were placed to dry under the hood at room temperature (Figure 3.7). The efficiency of the degumming process was then evaluated, which should lead to a weight loss of 25% - 30% if compared to the initial weight.

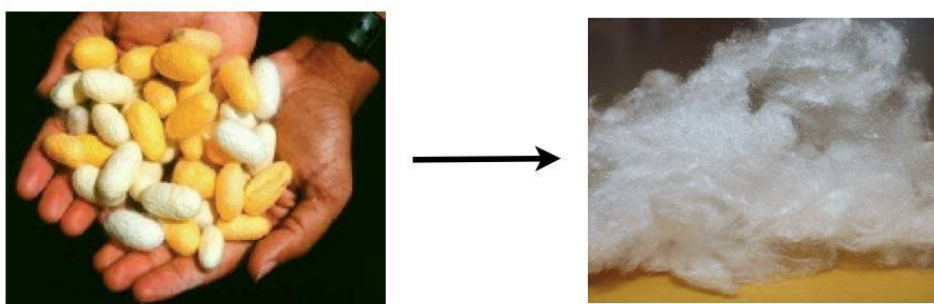


Figure 3.7: From silk cocoons to degummed fibroin.

- After obtaining degummed and dried silk, the dissolution of the silk fibroin at specific concentration was done. A specific amount of fibroin was placed into aqueous solution of LiBr 9.3 M in a concentration of 20% (2 g in 10 mL) for 4 h at 65 °C.
- The viscous LiBr/fibroin solution was placed into a dialysis cassette with a cellulose membrane (3500 MW). The cassette was then immersed in distilled water for 4 days at room temperature, under stirring conditions, and water changing were performed at

regular intervals of time with less and less frequency along the days. The process of dialysis allowed to remove LiBr from the fibroin solution through the principle of osmosis.

- The final solution was filtered, using a porous glass filter of 10  $\mu\text{m}$ , to remove further unwanted residues, so obtaining a pure fibroin water solution.
- To check the properties of this regenerated (denatured) fibroin, pH and concentration were evaluated using pH-meter and UV-VIS Nanodrop spectrophotometer (100  $\mu\text{L}$  of fibroin solution + 900  $\mu\text{L}$  dH<sub>2</sub>O), respectively.
- To sterilize the final silk product a 0.22  $\mu\text{m}$  filter was used (Sigma, USA), and the resulting silk were placed in sterile condition to be used for film and sponge scaffolds. It was necessary to vary the concentration according to the material and to the desired geometry for the specific purpose: optimal values of fibroin concentration were close to 4% with a pH  $\approx$  5-6, which suitable value for cell survival.

## 3.4 Scaffold fabrication

In this study, scaffolds and coating directly on well plates were produced using three different polymers: jellyfish collagen, silk fibroin and bovine type I collagen.

### 3.4.1 Tissue Culture Plate-well coating

The following protocol was used only for 96-well plate coating, so the volumes indicated must be scaled up for 48-well plate.

Collagen coating solutions ([c] = 1 mg/mL) were prepared by re-suspending freeze-dried jellyfish collagen in 0.02 M acetic acid in a glass tube through continuous stirring at 4 °C for 2 days. As control material, bovine type I collagen solutions were also prepared in 0.02 M acetic acid to reach a final concentration of 1 mg/mL. Under a biological hood, 200  $\mu\text{L}$  of collagen coating solution and 200  $\mu\text{L}$  of bovine type I collagen coating solution were added to each well of 96-well plate. As negative control, only DMEM was used. The well plate was placed in a culture incubator set to 37°C overnight, in order to allow complete collagen polymerization. Then, it was carefully transferred into the culture hood and left uncovered overnight, so that collagen dried down into a thin uniform layer on the well plate's bottom. After that, collagen-

coated wells were washed by adding sterile distilled water (200  $\mu$ L/well) and the plates were allowed to dry further down under the hood at room temperature for 30 min.

### 3.4.2 Films

Pepsin soluble collagen and silk fibroin were obtained through the above procedures.

1% w/v pepsin soluble collagen solutions were prepared by dissolving collagen in 0.1 M acetic acid for 24 hours with continuous stirring at 4 °C. Silk fibroin aqueous solutions (4% w/v) were obtained by dissolving degummed silk fibers from *Bombyx mori*, followed by dialysis against water (Milli-Q quality) for 3 days.

The solutions were sterilized through filtration using a 0.22  $\mu$ m filter and kept in sterile conditions.

Silk fibroin films (Figure 3.9), jellyfish collagen/fibroin blend (weight ratio, 80:20), and jellyfish collagen coated fibroin films about 1 mm thick were cast on 35 mm polystyrene Petri dishes in the following way.

The 4% silk fibroin solution in the amount of 4 mL was poured on the bottom of dish and forced to spread uniformly over the whole surface area by gently shaking and tilting the dish. For fibroin/collagen films, 4 mL silk fibroin at 4% and 4 mL collagen at 1% were mixed together to achieve 80:20 blending ratio and cast on dish.

All the films were semi-covered to ensure slow evaporation and dried overnight under the hood. After that, the samples were peeled off from the plates and carefully detached from the Petri dishes with the aid of tweezers. When without lids the silk and collagen/silk solutions generally dried within 20 h, forming water-soluble films at room temperature. Water-insoluble films were obtained by the water annealing: the soluble fibroin and collagen/fibroin films were turned, covered with parafilm and placed in a water vapour dryer with a 25 in. Hg vacuum for at least 4 hours and for a maximum of 5 hours to make them water-stability. Finally, discs having the same size of the 96- and 48-well plate's bottom were obtained with a rounded punch cutter.

When some of silk fibroin films were dried, they were coated with pepsin soluble collagen by dipping in 1 mg/mL PSC in 0.02 M acetic acid solution for 1 hour at room temperature.



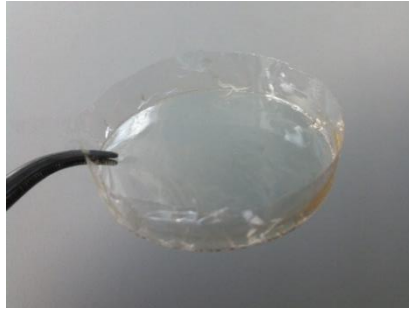


Figure 3.9: Silk fibroin film.

### 3.4.3 3D sponges

Three-dimensional (3D) silk fibroin scaffolds (Figure 3.8), jellyfish collagen/fibroin blend (weight ratio, 80:20) in water, and jellyfish collagen coated fibroin scaffolds with good porous structure were prepared in this study, using a freeze drying technique without methanol treatment.

Jellyfish pepsin soluble collagen extraction process led to freeze-dried material. From that, 1% w/v pepsin soluble collagen solution was prepared by dissolving collagen in 0.1 M acetic acid for 24 hours at 4 °C with continuous stirring.

Silk fibroin aqueous solution at a concentration of 4% was already obtained after dialysis against bidistilled water for 3 days, and transferred into sterile polystyrene Petri dishes.

To make the final solutions sterile, they were filtered through a 0.2 µm filter under a biological hood, using a syringe pump (Aladdin-1000, WPI). Rate = 50 µl/min.

To form the blending solution, the resulting collagen and fibroin solutions were mixed with mild stirring for 10 min and poured into polystyrene Petri dishes of 35 mm of diameter. The samples were covered with parafilm, perforated and kept at -80 °C for one day prior to lyophilisation, obtaining porous scaffolds with a thickness of about 2 mm. The dry porous sponges were carefully detached and removed from the dishes with the aid of tweezers, turned, covered with parafilm and placed into water vapour dryer for at least 4 hours and for a maximum of 5 hours to assure scaffolds stabilization but at the same time to prevent the material withdraws too.

Some of porous silk fibroin scaffolds were used to prepare silk fibroin scaffolds coated with pepsin soluble collagen: silk fibroin sponges were immersed in 1 mg/mL PSC in 0.02 M acetic acid solution for 1 hour at room temperature.

The fibroin, collagen/fibroin and collagen coated fibroin sponges were punched to obtain scaffolds with 6 mm (96-well plate) and 10 mm (48 well plate) of diameter.



Figure 3.8: 3D silk fibroin sponge.

## 3.5 Scaffold characterization

### 3.5.1 Morphological analysis by scanning electron microscopy

The scanning electron microscopy (SEM) is a technique of image acquisition, based on the interaction of the electrons with the tested material (Figure 3.10). Unlike the optical microscopy, which uses visible light as radiation source, the SEM exploits the small length of the electrons (variable between 0.1 and 0.005 Å), allowing the detection of morphological characteristics and composition of the substrate, with a resolving power equal up to 5 Å and with considerably higher magnifications.

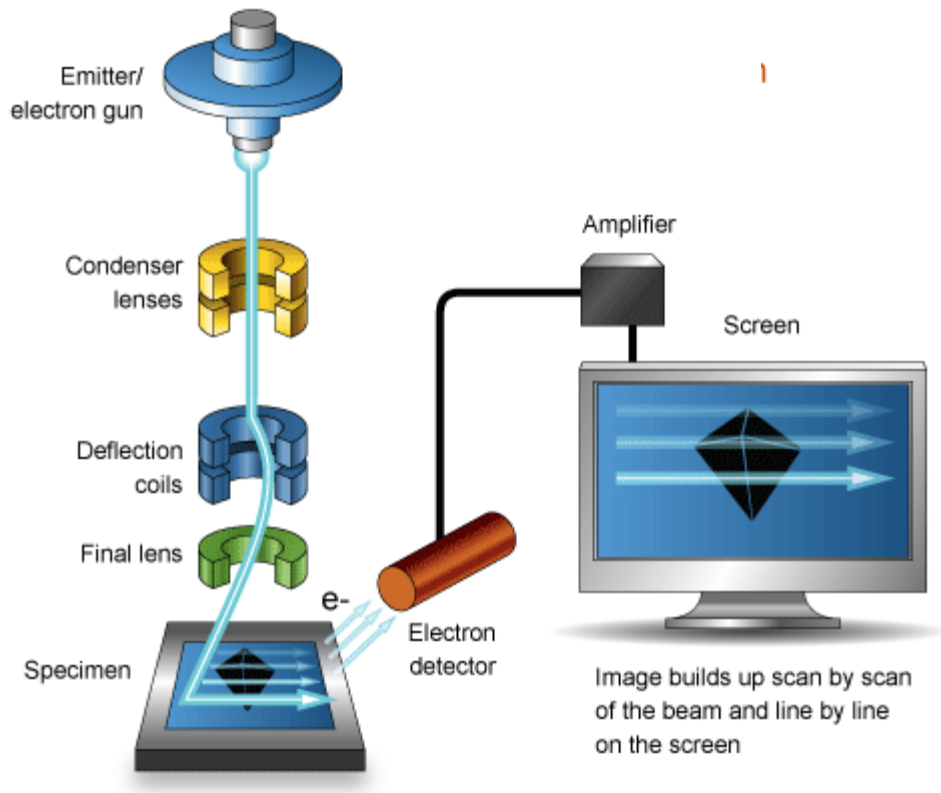


Figure 3.10: SEM layout and function.

<http://www.ammrf.org.au/myscope/sem/practice/principles/layout.php>

The scanning electron microscope consists of several components: a cylindrical column equipped with condenser, systems of electromagnetic coils and a tungsten filament coated with zirconium. The latter, when temperature increases due to current flow, generates the electrons beam, which is essential for the morphological analysis of the material.

The system provides a holder for the samples placement and a series of sensors able to detect the deflected electrons by the collision with the atoms of the sample. The emitted electrons are then subjected to acceleration, by electrostatic or magnetic condenser, and when the voltage changes (0.3 kV - 3 kV), electrons speed can be varied. Through the system of lenses and magnetic fields, generated by the circulating current in the electromagnetic coils, the electron beam can be focused and directed on the sample surface where interactions between electrons and the material occur.

These interactions cause energy emissions of various types, in particular, consist of Back-Scattered electrons (BSE), secondary electrons, Auger electrons and variable energy photons. Back-Scattered electrons are electrons with energy higher than 50 eV and arise from the elastic scattering interactions of the primary beam with the nuclei of the atoms constituting the sample. This emission provides information on the average atomic number of the affected

area, the topography and the crystal structure of the sample. The secondary electrons, electrons emerging from the sample, possess a lower energy of 50 eV and are produced as a result of the interaction of inelastic scattering between the backscattered electrons and the valence electrons of the atoms. Their recognition provides information about the topography of the material. Finally, the Auger electrons are electrons of atom core, that are expelled giving rise to electronic holes, which are occupied by the outer electrons resulting in a radiation release.

The emissions, generated by the interaction electron-matter, are then detected by suitable sensors, which transfer the converted signals to a computer that can reproduce the images for visual analysis of the sample. In the image, the lightest areas correspond to high emission of secondary electrons on the part of that region, while the darker areas are equivalent to regions with lower emission. It is clear, therefore, that the light intensity of the pixels on the screen is proportional to the intensity of the secondary electrons flow, which depends on the surface topology of the analyzed material.

In order to use this method of investigation, the samples (sponges and films) should be conductors or alternatively treated by a metallization process, called sputtering. For this purpose, in this study, the surface of the samples, previously cut using a punch, has been coated by a thin layer of gold, in order to make it conductive and able to absorb and transmit the beam of electrons, preventing accumulation of charge. Processed samples were fixed to an adhesive carbon stub and placed on a platform in the vacuum chamber, which is essential to prevent the spread of the electron beam by residual gas. At this point, it was possible to scan the sample at preferred magnifications and captured interest images.

Images were acquired using a scanning electron microscope (SEM), (Zeiss, Supra 40) by using the following main instrumental parameters: Voltage for the electrons acceleration of 4.00 kV and Working Distance equal to 4.5 mm.

This technique was also used to investigate the samples after AlamarBlue® assay, in order to observe how cells were able to adhere to the scaffolds. In this case, sponges and films were previously fixed with 2.5 % gluteraldehyde in 0.1 M cacodylic buffer at 4 °C for 20 min. After fixation solution removal, samples were washed in 0.1 M cacodylic buffer for three times and dehydrated in ascending ethanol concentrations (70%, 80%, 90%, 95% and 2 x 100%) for 10 min (each concentration). Then, the ethanol was removed and the samples were dried keep the plate open overnight. At the end of the process, scaffolds were coated with gold before SEM observation.

### 3.5.2 Secondary structure evaluation by Fourier transform infrared spectroscopy

The principles of the technique was explained in the previous section (3.2.3).

FT-IR spectroscopy of collagen and silk fibroin films and freeze-dried sponges was relied on the Perkin-Elmer Spectrum 100 FT-IR (Figure 3.2). The universal ATR sampling accessory, deposited neatly onto a diamond/ZnSe plate. Spectra were collected between wave numbers of 4000 and 650  $\text{cm}^{-1}$  at the resolution of 4  $\text{cm}^{-1}$  and additionally compared with not-stabilized silk fibroin films and 3D sponges.

### 3.5.3 Thermal behaviour by differential scanning calorimetry

The thermal behaviour of each scaffold was determined by means of differential scanning calorimetry (DSC) using a METTLER-TA instrument DSC12E and according to the method described in the paragraph 3.2.4.

## 3.6 Preliminary biocompatibility evaluation: *in vitro* testing

The aim of these evaluations was to evaluate the influence of the marine collagen-fibroin scaffolds over the proliferation and the metabolic activity of MRC-5 and NIH 3T3 cells considering different ratio of the biopolymers, in particular the bioactivity of marine collagen. Qualitative analysis of cells viability and migration were evaluated considering differences in chemical composition and morphologies of scaffolds.

### 3.6.1 Cell lines: MRC-5, NIH 3T3

MRC-5

Human fetal lung fibroblast cells (MRC-5) are derived from the normal human lung tissue of a 14-week-old male fetus. They carry a normal diploid karyotype ( $2n = 46, XY$ ). The cell line was established in the 1960s [54].

MRC-5 cells (ATCC) were cultured in MEM medium, supplemented with 10% fetal bovine serum, 1 mM sodium pyruvate, 2mM L-glutamine, 1% non-essential amino acid solution 100X (Sigma-Aldrich M7145). They grow adherently in culture, are capable of 42 to 46 population doublings before the onset of senescence and exhibit fibroblast morphology. When confluent, MRC-5 cells are very elongated and show a characteristic alignment which is not found in other types of fibroblasts such as NIH 3T3 cells (Figure 3.11).

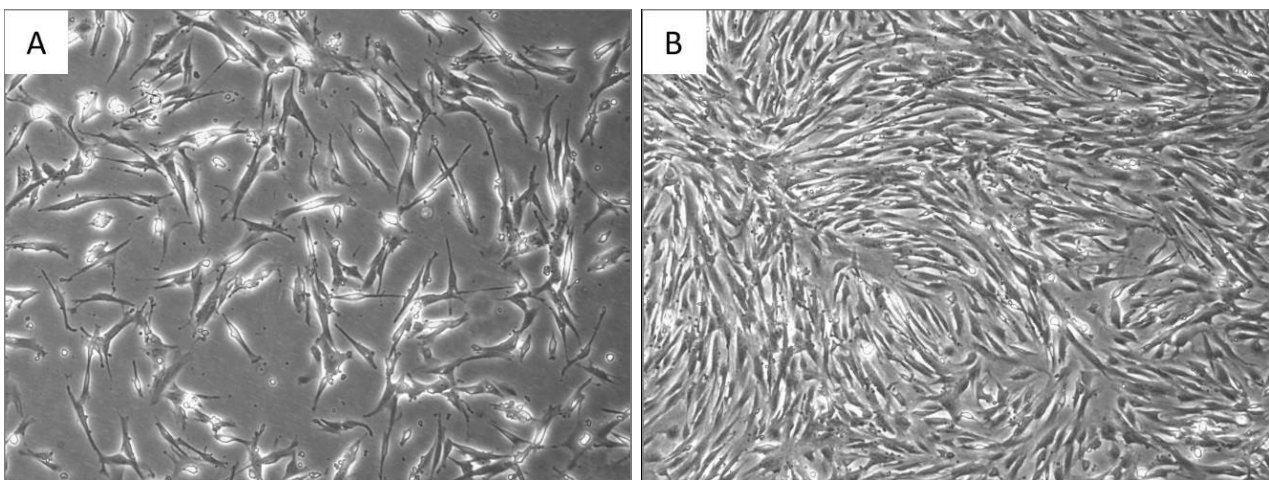


Figure 3.11: Phase-contrast morphology of MRC5 cells observed through a Leica DM IL Led inverted microscope. (A) Sparse MRC-5 cells, 5X magnification. (B) Confluent MRC-5 cells, 5X magnification. At confluency, they show a particular disposition which is not observed in NIH 3T3 cells, and a very elongated morphology.

## NIH 3T3

The NIH 3T3 cell line was established in 1963, from a spontaneous immortalization of the *M. musculus f. domestica* “Swiss mouse” embryo fibroblasts. 3T3 refers to the cell transfer and inoculation protocol for the line, and means “3-day transfer, inoculum  $3 \cdot 10^5$  cells”. Using this protocol, the immortal cell line begins to thrive and stabilize in cell culture after about 20-30 generations of *in vitro* growth. The cell line has since become a standard fibroblast cell line with morphologic characteristics best suited for transformation assays and one the most commonly used cell models for tissue engineering methods testing.

The cells are tetraploid, carrying 75 chromosomes [55]. It was demonstrated that mesenchymal cells could act in development also across species, therefore in addition to MRC-5 cells, we also tested NIH 3T3 behaviour on constructs used in this project.

NIH 3T3 cells (ATCC) were cultured in DMEM medium, supplemented with 10% fetal bovine serum, 1 mM sodium pyruvate, 2mM L-glutamine.

Confluent NIH 3T3 (Figure 3.12) tend to be spread and not organized in any particular disposition, in contrast to MRC-5 cells.

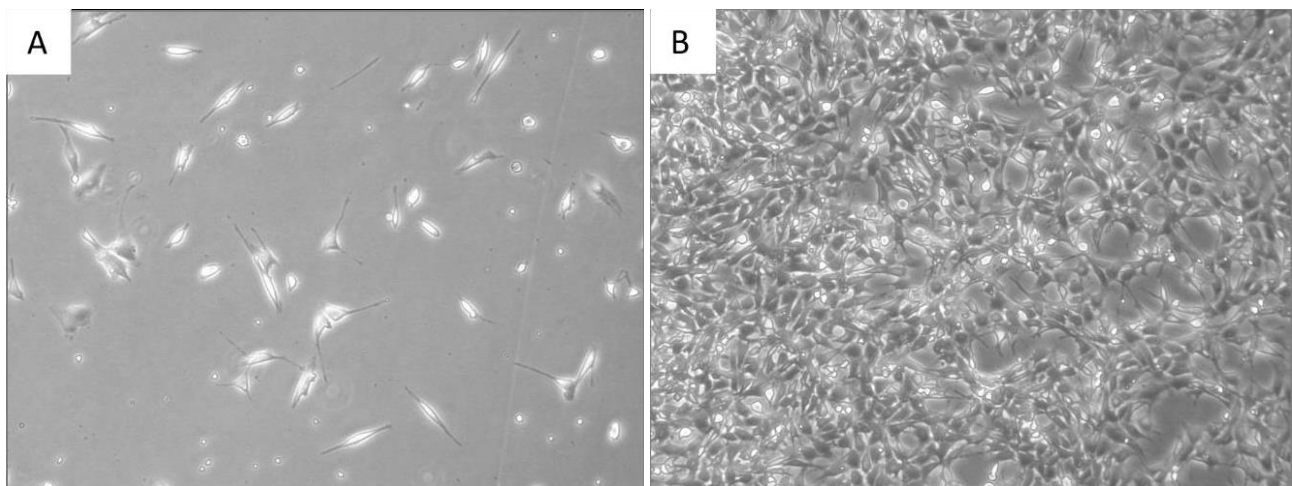


Figure 3.12: Phase-contrast morphology of NIH 3T3 cells observed through a Leica DM IL Led inverted microscope. (A) Sparse NIH 3T3 cells, 5X magnification. (B) Confluent NIH 3T3 cells, 5X magnification.

### 3.6.2 Design of cell culture

The samples used for cell cultures were:

- jellyfish collagen (PSC) and bovine type I collagen Tissue Culture Plate-well coating;
- Silk fibroin, jellyfish collagen/fibroin blend (weight ratio, 80:20), and jellyfish collagen coated fibroin films;
- Silk fibroin, jellyfish collagen/fibroin blend (weight ratio, 80:20), and jellyfish collagen coated fibroin 3D sponges.

Each disc was then inserted into the proper well (48 or 96 well plate) with a pair of tweezers, and pushed down to adhere the bottom of the plate.

Sterilization was carried out by covering samples with a 70% ethanol solution and waiting ethanol evaporation in sterility condition. Under a sterile laminar flow hood, samples were repeatedly washed in PBS to eliminate any possible residues of ethanol and a final wash was

performed with medium according to the specific fibroblast cell line. Scaffolds were then moved to new plates and, through confined drop technique (50  $\mu$ l), seeding was carried out. After 30 minutes of incubation at 37 °C, the medium was added. The MRC-5 and NIH 3T3 cell cultures were performed in an incubator at 37 °C and in a controlled atmosphere with 5% CO<sub>2</sub>. Changes of medium were made every 2-3 days.

For the *in vitro* testing, MRC-5 and NIH 3T3 cell lines were previously expanded in 2D flasks in order to achieve very high seeding concentrations.

### 3.6.3 Cytotoxicity: LDH-based assay

LDH *in vitro* assay (kit TOX7, Sigma Aldrich) was used to determine cytotoxicity of pepsin soluble collagen extracted from dried *Rhopilema hispidum* jellyfish. The enzyme, Lactate DeHydrogenase (LDH), a cytoplasmic enzyme, is a marker for cell membrane integrity. It can be correlated to cell viability since it is released when damage to the cytoplasmic membrane occurs (Figure 3.13). To perform LDH assay  $1 \cdot 10^4$  NIH 3T3 cells were seeded using a sterile culture medium with reduced serum, until they reached 70% confluency. Freeze-dried collagen was incubated for 24 hours in serum-reduces sterile medium and after incubation, it was used to culture the NIH 3T3 cells for 48 hours. LDH *in vitro* test was carried out following the manufacturer's instructions. Wells seeded with the same cells concentration, standard culture medium and 0.5% Triton-X in PBS were used as negative and positive controls, respectively. The absorbance of the assay mixture was measured at 492 nm and 690 nm (background) with a photometric microplate reader (Multiskan EX, ThermoLabsystems, Finland). Six reading were performed for each group: average value and standard deviation are reported.

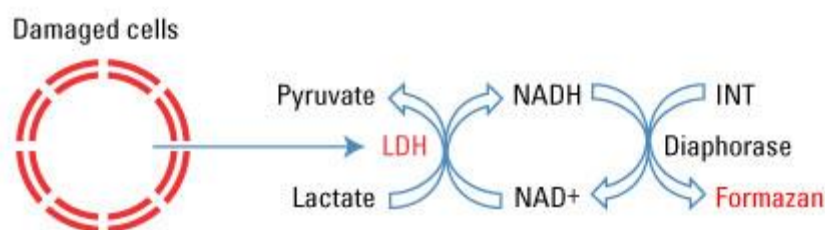


Figure 3.13: Lactate Dehydrogenase (LDH)-based *in vitro* cytotoxicity assay.



### 3.6.4 Image acquisition: confocal laser scanning microscopy

Confocal microscopy provides a useful tool to image virtual sections of the specimen, within a tissue or three-dimensional scaffold. The technique, patented in 1955 by Marvin Minsky, allows to visualise the samples with higher resolution and contrast compared to conventional widefield microscopy [56]. Briefly, the fluorescence light emitted by the laser source (excitation light) is converged from the objective lens at an extremely small point of the specimen at a specific depth by passing through a first pinhole aperture that stands on a focal plane conjugated with the specimen's one, a dichromatic mirror and an objective. The specimen is therefore emitting fluorescence upon excitation: the light is reflected by the same dichromatic mirror and hits a second pinhole aperture before reaching the detector (Figure 3.14). This allows to get rid of the fluorescence that comes from other planes of the specimen, because they are not confocal with the pinholes. Due to a very small area of the analyzed sample excited by laser, the resolution is very high and the characteristics of the resulting light (extreme coherence, high intensity and unique wavelength) allow to avoid phenomena of aberration and diffraction. By shifting the focus of the objective (vertical axis) after each optical section, another plane will be confocal with the pinhole planes: thus sections of the specimen can be imaged one by one allow to reconstructing an overall picture of the entire volume, where all planes are simultaneously in focus [57]. In conventional fluorescence microscopy instead, all the fluorescence emitted by the other planes of the specimen is detected as a background signal.

The fluorescent light, passed through the pinhole, can reach the photomultiplier, which converts the detected light intensity into an electrical signal proportional to the intensity itself. The electrical signal is then scanned and sent to a computer that records the light intensity at each point.

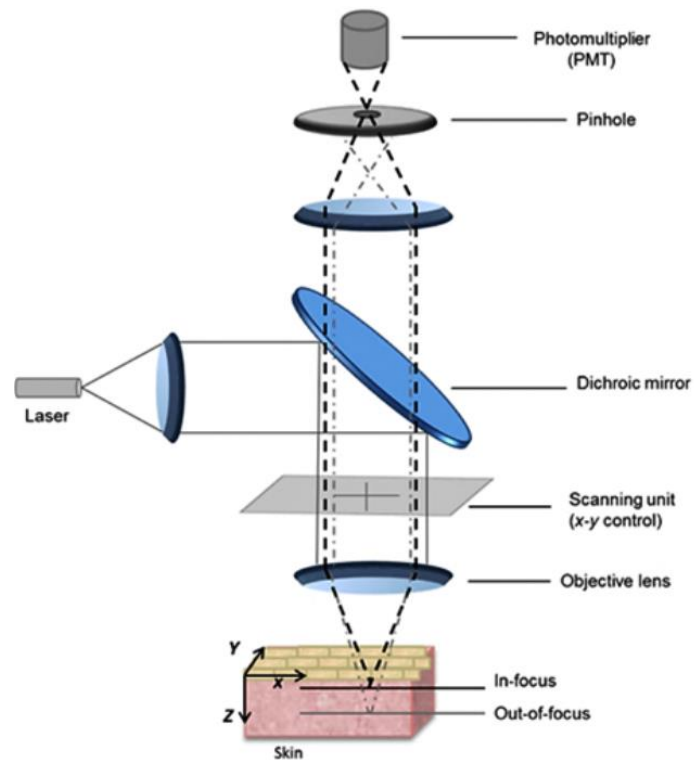


Figure 3.14: Confocal principle. The exciting laser pass through a first pinhole aperture which allows to concentrate the laser in a point of the specimen. The emitted fluorescence is then reflected by a beam splitter, pass through a second pinhole aperture which hampers the passage of the fluorescence coming from other planes. <http://www.medinfo.net/Technology/confocal-microscopy>.

Cells were imaged using a Nikon ECLIPSE Ti confocal laser scanning microscope linked with the NIS-Elements AR software (Figure 3.15), according to fluorescence staining with Calcein-AM and Propidium Iodide (Live/Dead assay) and immune staining against cell-specific antigens (Immunocytochemistry).



Figure 3.15: Nikon A1 ECLIPSE Ti confocal laser scanning microscope. <http://www.magersci.com>.

### 3.6.5 Cell viability: Live/Dead

MRC-5 and NIH 3T3 monocultures were seeded on top of silk fibroin and jellyfish collagen scaffolds and let them grow for 5 and 7 days, respectively. At day 1, 5 and 1, 5, 7 (MRC-5 and NIH 3T3, respectively) cell viability was estimated by fluorescence visualization (laser scanning confocal microscopy) of samples stained with calcein-AM/propidium iodide (Invitrogen, USA) (Figure 3.16). Calcein is a fluorescent lipophilic dye with excitation and emission wavelengths of 495/525 nm. Calcein-AM is derived non-fluorescent molecule that is transported through the cellular membrane into live cells. When in the cytoplasm, this molecule is cleaved by esterases becoming hydrophilic and fluorescent. Propidium iodide (PI) is a red fluorescent-intercalating agent able to bind nucleic acids (excitation and emission wavelengths: 535/617 nm). It can stain only necrotic or apoptotic cells due to the cell membrane permeability after activation of death cascade, leaving alive cells unstained due to their intact membrane. Samples were observed 1, 5 and 1, 5 and 7 days (for MRC-5 and NIH 3T3 cells, respectively) after cell seeding following standard protocols. In brief, samples were incubated for 30 min at 37°C in a solution of calcein (1  $\mu$ l of stock solution for 1 ml of DMEM). After that, the supernatant was removed, the samples were washed with a PBS w/ Ca<sup>2+</sup> solution. The procedure was repeated again at room temperature for 5 min with a solution of propidium iodide (100  $\mu$ l for 1 ml of PBS w/ Ca<sup>2+</sup>), followed by washings with PBS.

To validate results a negative control was used, represented by not-seeded constructs. All samples were carried out in twice (biological replicates).

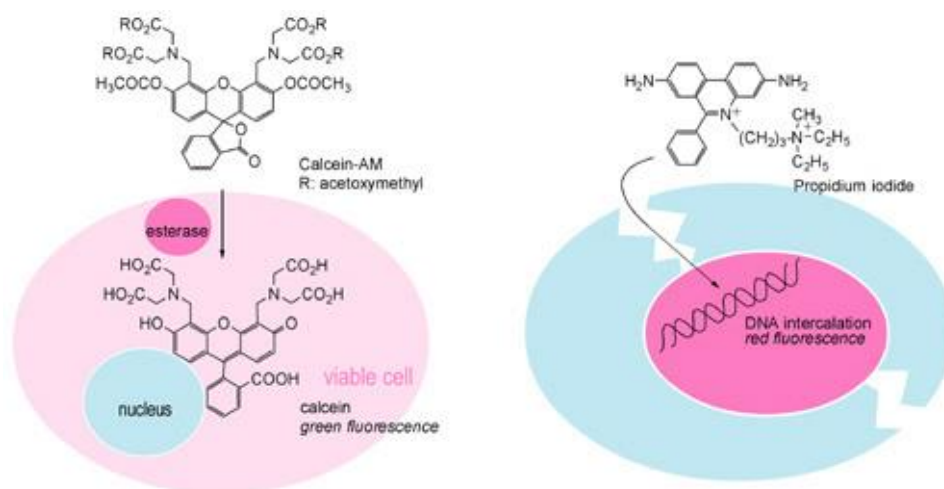


Figure 3.16: Mechanism of Calcein AM/PI staining. <http://bio530.wikispaces.com/Calcein+AM>.

### 3.6.6 Metabolic activity: Alamar blue® assay

MRC-5 and NIH 3T3 monocultures were seeded on top of silk fibroin and jellyfish collagen scaffolds and collagen well coating and let them grow for 5 and 7 days, respectively. The proliferation that is proportional to metabolic activity of cells was evaluated at the end of each time point (1, 5 and 1, 5, 7 days for MRC-5 and NIH 3T3 cells, respectively) after incubation of the constructs, by measuring the level of reduction of a blue, non-toxic compound named resazurin (AlamarBlue® Cell Viability Reagent, Life Technologies). A higher proliferation causes a larger absorbance value as well as a larger percentage of reduced AlamarBlue®. The cells metabolize the non-fluorescent resazurin, causing its reduction to resorufin, which gives a fluorescent signal if excited at 560 nm and shows a pinkish colour (Figure 3.17).

The assay was performed according to the manufacturer's instructions. Briefly, at each time point, the culturing medium was removed, the cell cultures were washed with PBS and incubated for 3 hours at 37 °C, 5% CO<sub>2</sub> with fresh culture medium (with reduced serum) supplemented with AlamarBlue® diluted according to manufacturer's data sheet (simply adding the AlamarBlue® reagent as 10% of the sample volume). A total of three biological replicates were used for each sample and each replicate was split into four wells (technical replicates) for the final reading. The references were taken from wells with unseeded scaffolds incubated with the AlamarBlue® working solution. Samples were washed with PBS

and fresh culturing media was added. Fluorescence was detected by using a Tecan Infinite M200 photometric microplate reader (excitation wavelength 565 nm, emission wavelength 595 nm) and the percentage of reduced alamarBlue® was calculated [58].

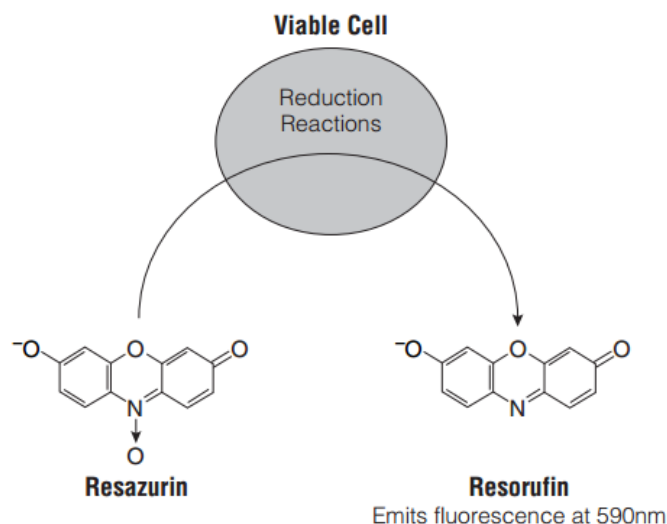


Figure 3.17: Reduction of Resazurin (AlamarBlue® Cell Viability Reagent, Life Technology) to the fluorescent molecule Resorufin. Adapted from [www.ita.promega.com](http://www.ita.promega.com).

### 3.6.7 Cell proliferation: PicoGreen assay

To evaluate the amount of NIH 3T3 cells growing on top of 2D-well coating and scaffolds, DNA quantification was performed at different time points: 1, 5 and 7 days. DNA extraction was performed by placing cells and scaffolds in a solution of 0.05% Triton X-100 in PBS w/o Ca<sup>2+</sup> (ThermoFisher, USA, 14040G091), while for 2D samples the solution was directly added to each well. After that, 10'' sonication (cycle; 1, amplitude 40%) was performed per each sample, washing with distilled water between samples. After the DNA was extracted, Quant-iT PicoGreen dsDNA Assay Kit (Invitrogen, catalog number: P11496) was used for the quantification. Fluorescence intensity of PicoGreen – DNA complex was measured in 96-well plates on a plate reader (485 nm excitation and 538 nm emission; Safire, Tecan, Austria). A calibration curve was built up using the DNA standard provided with the assay to correlate fluorescence intensity to the concentration of DNA.

### 3.6.8 Collagen synthesis: Immunocytochemistry

Immunofluorescence experiments were designed to evaluate Collagen I and III gene expression and assembly, since they represent fundamental markers synthesized by fibroblast cells in the early stages of wound healing process.

NIH 3T3 cells on collagen coated fibroin scaffolds were fixed with 4% paraformaldehyde (PFA) in PBS for 30 min at RT. Samples blocking and permeabilization were achieved by treating for 1 hour at RT with blocking buffer (1% BSA, 0,3% Triton X-100 in PBS). A secondary block was done by washing 3 x 10' with PBS/Glycine 100 mM. Glycine binds free aldehyde groups, preventing the antibodies to bind instead, leading to a lower background fluorescence [59]. Incubation with the primary anti-Collagen I (Abcam; 6308) and anti-Collagen III (Abcam; 7778) antibodies, diluted 1:200 in blocking buffer, was performed for 1 hour at RT or overnight at 4 °C. After 3 · 10 minutes PBS washing, the secondary goat-anti-rabbit Alexa-594 (Life Technologies; A11037) and goat-anti-mouse Alexa-488 (Life Technologies; A11029) antibodies were applied for 1 hour at room temperature (dilution 1:500). The samples were then counterstained with DAPI 1:1000 in PBS (Invitrogen; NL5995050) for 10 min. Finally, cells were washed three times with PBS w/ Ca<sup>2</sup> and results were analysed with the confocal microscope (Nikon).

### 3.6.9 Specific markers expression: Reverse transcription quantitative PCR in real time

In order to evaluate collagen I and collagen III synthesis by NIH 3T3 fibroblasts seeded on collagen coated fibroin scaffolds, reverse transcription real time quantitative polymerase chain reaction was performed at days 3, 7 and 14. Ribosomal Protein S18 (RPS18) was used as housekeeping gene.

Total mRNA extraction (three replicates for each group) was performed according to the QIAGEN mRNA extraction kit protocol. mRNA was re-suspended in a final volume of 30 µl with RNase-free water and its yield (in terms of concentration) was quantified by the NanoDrop spectrophotometer ND-1000, which allows to quantify nucleic acids by analysing 2 µl of sample.

Reverse transcription using 1 µg of total RNA was performed in a SensoQuest labocycler with SuperScript III Reverse Transcriptase (Invitrogen, UK) and oligo-dT primers, according to the manufacturer's protocol and following the reverse transcription thermocycler setup, in a 20 µl total reaction volume.

The mixture was put for 5' at 65° C to destroy any dimer-dimer bond or other RNA secondary structures and then placed back in ice. To each reaction mixture the following components were added, to reach 20 µl of total reaction volume.

After mixing and spin down, the synthesis was performed in a SensoQuest labocycler, the steps, following manufacture's protocol,

Transcribed cDNA was diluted 1 to 20 times till a final volume of 100 µl (100 ng/µl) in RNA-free water was obtained.

The qRT-PCR allows real-time quantification of the amount of a transcript present in a pool of mRNAs, through amplification. The total RNA has to be initially converted in cDNA; afterwards, using specific primers, the transcript of interest is amplified in the presence of a fluorescent dye (SYBR® green) which has the ability to intercalate the dsDNA quantitatively and in an aspecific way. It produces fluorescence only when bound to the dsDNA. Col I and III primers were selected from online primers bank PrimerBank [60]. RPS18 primers were designed (Table 3.1).

Oligo Name	Sequence (5' -> 3')
mCOL1a1_f	GCTCCTCTTAGGGGCCACT
mCOL1a1_r	CCACGTCTCACCATTGGGG
mCOL3a1_f	CTGTAACATGGAAACTGGGGAAA
mCOL3a1_r	CCATAGCTGAACTGAAAACCACC
mRPS18_f	AGTTCCAGCACATTTTGCAG
mRPS18_r	TCATCCTCCGTGAGTTCTCCA

Table 3.2: Primers sequence for RT-qPCR [60].

At any amplification cycle, the amount of detected fluorescence increases: this allows to record a sigmoid chart. The length of the linear ground phase is proportional to the initial amount of DNA molecules in the sample: there is a minimum level of fluorescence needed to be detectable by the machine. Standard curves are built by amplifying each gene of interest with a serial dilution of the template cDNA (1:1, 1:2, 1:5 and 1:10). The Ct (threshold cycle)

value of the collagens molecules amplification is normalized by subtracting the geometric average between the Ct values of the control housekeeping genes (RPS18). Then, the fold-change is calculated using the  $\Delta C_t$  method from Pfaffl [61].

Measurements were performed in quadruplicate for statistical analysis and amplification and detection were carried out using a CFX96 Touch™ Real-time PCR machine (BioRad, UK), using the default universal cycling conditions recommended by the manufacturer. Briefly, a mastermix (Table – manufactures' protocol) for each primer set was prepared using the reagents from the KAPA SYBR FAST Universal qPCR Kit (KAPA Biosystems, #KK4601) and then aliquoted in the 384-well plate. Then, 2  $\mu$ l/well of cDNA (therefore, a total of 25 ng each reaction) were added, to reach 10  $\mu$ l of total reaction volume.

The plate was then spun down, placed in the thermocycler and the reaction started. The reaction steps are the following (Table - manufactures' protocol):

The specificity of the SYBR® GREEN assay was further checked by SYBR® GREEN dissociation through gradual melting of the PCR products. By plotting the negative first derivative of the fluorescence signal versus the temperature, the melt profile presents a pick, which should be only one and corresponding to the  $T_m$  of the expected amplicon [62].

### 3.6.10 Statistical analysis

All statistical analysis was performed with GraphPad Prism® 6 software. Statistical analysis for more than two groups was carried out using two-way ANOVA with Bonferroni correction.  $P < 0.05$  was considered significantly different. Gene expression of cell culture day3 was set up as a control, and equal to 1. For gene expression analysis the  $ddC_T$  approach was applied. Targeted gene expression was calculated by the fold change related to the control group.



# 4. Results and discussion

## 4.1 Optimization of jellyfish collagen extraction

Specimens from *Rhopilema hispidum* jellyfish specie were collected from Thailand coast, and dried after being caught. In order to estimate the potential of these jellyfish species as a source of collagen, different collagen extraction procedures have been tested.

Few protocols for dried jellyfish collagen extraction were available in literature. For this reason, starting from a published basic procedure used to extract collagen from fresh jellyfish samples (Protocol 1), it has been necessary to change different parameters, in order to achieve a method suitable for this specific purpose.

As previously described (paragraph 3.1), different protocols have been carried out by BIOtech research group, before obtaining a better procedure in terms of yield (Protocol 6). Starting from the latter, my thesis project aimed to optimize the collagen isolation procedure, leading to increased yields with the final protocol (Protocol 9), working on *Rhopilema hispidum* dried jellyfish samples.

For the pre-treatment phase, about 10 g of tissue were used in each experiment. Following the basic procedure reported in literature (Protocol 1), the tissue was previously cleaned using bidistilled water in order to remove NaCl, which was necessary to preserve jellyfish samples. Size reduction was obtained by cutting the samples with scissor in order to facilitate acid action. After the sieve filtration, performed to separate the treated tissue from bidistilled water, the sample was ready for the subsequent extraction phase. Tissue was mixed with acetic acid solution, used for the solubilization of collagen. Then, the resulting mixture was centrifuged to obtain supernatant that include acid-soluble collagen (ASC) and a pellet that contain insoluble collagen. The choice of acetic acid as solubilizing agent was taken after that in previous studies were tested the influence of different acids on collagen extraction from marine organisms, including hydrochloric, citric, acetic and lactic acids, from which acetic and lactic acids revealed to be the ones rendering higher collagen extraction yields [67]. The first collagen extraction process normally returned an extremely low yield and to overcome this low efficiency, an enzymatic treatment (always coupled with acetic acid solution) by using a proteolytic enzyme, i.e. pepsin, non-specific for collagen, was applied. Pepsin help the solubilization process since it cleaves peptides specifically in telopeptide region of collagen, which are non-helical ends, and thus, by hydrolyzing some non-collagenous proteins,

increases the purity of collagen. By applying pepsin, the resulting extract is named Pepsin Soluble Collagen (PSC) or atelo-collagen. It results in a much more efficient collagen extraction, since it makes the sample ready to solubilize while reducing, at the same time, the antigenicity caused by telopeptides. For this reason, it is common to use this proteolytic procedure after the extraction of ASC, obtaining, thus, the above mentioned PSC.

For the recovery step, collagens (ASC and PSC) needs to be precipitated, generally achieved by adding NaCl, and the final precipitates were re-suspended in acetic acid and dialyzed against 0.1 M acetic acid solution in order to decrease the acetic acid content in the samples. In the end, the samples were freeze dried, resulting in the formation of dry acid soluble and pepsin soluble collagen sponges.

<b>Specie</b>	<b>Protocol</b>	<b>ASC (mg/g)</b>	<b>PSC (mg/g)</b>
<i>Rhopilema hispidum</i>	1	0.75	1.08
	2	0.71	1.36
	3	0.95	1.45
	4	1.06	2.35
	5	1.60	3.56
	6	2.15	4.57
	7	-	9.23
	8	-	20.87
	9	-	29.87 and 31.16

Table 4.1: Yield of collagen after acid and pepsin extraction, respectively. Values are indicated as mg of collagen per gram of tissue.

The extraction yields of both acid-soluble and pepsinized collagens from Protocol 1 shown very low yields, 6.33 mg and 9.12 mg respectively (Table 4.1), so some modifications were introduced by BIOtech research group in order to obtaining sufficient material for scaffold fabrication, as shown in the following table (Table 4.2).

Specie	Protocol	Modifications
<i>Rhopilema hispidum</i>	1	-
	2	Pre-treatment: add 0.1 M NaCl for 1 day + centrifugation; Extraction: 0.05% pepsin for 3 days
	3	Recovery: salted-out with 1.5 M NaCl, dialysis for 3 days
	4	Pre-treatment: add 0.1 M NaOH for 1 day + centrifugation (no NaCl); Extraction: 0.1% pepsin for 3 days
	5	Pre-treatment: add 0.1 M NaOH for 1 day + centrifugation (no NaCl); Extraction: 0.1% pepsin for 3 days
	6	Extraction: 0.2% pepsin for 3 days; Recovery: at 4 °C, salted-out with 2 M NaCl
	7	Pre-treatment: sample mincing with mixer; Extraction: ASC is discarded, centrifugation for 1 h
	8	Extraction: 0.5% pepsin for 3 days, ultra-centrifugation (20000 g for 1 h); Recovery: salted-out with 2.5 M NaCl, ultra-centrifugation (20000 g for 1 h);
	9	All steps at 4 °C; Pre-treatment: add 70% ethanol, besides NaOH, for 1 day; Extraction: 0.2% pepsin for 3 days, no ASC extraction; Recovery: salted-out with 2 M NaCl

Table 4.2: Modifications of protocols: each modification is refer to the previous procedure.

As shown in Table 4.2, each protocol was characterized from specific parameters and subsequently extraction yields of acid-soluble and pepsinized collagens were obtained, respectively (Table 4.1). Briefly, NaCl solution was used and then increased in concentration in order to remove non-collagenous proteins from the tissue and to achieve greater precipitate. The length of the pepsin extraction was then extended to 3 days and the time of dialysis was prolonged to better separate the collagen from residual substances. Successively,

the NaCl solution used for sample pre-treatment was replaced by a solution of NaOH that result in a higher effectiveness. Antigenicity of collagen is not only derived from its telopeptides, being also related to the presence of non-collagenous proteins, cells and cell remnants, being the above-mentioned method of NaOH treatment of raw materials important for the removal of this source of antigenicity.

This thesis project aimed to optimize the collagen isolation procedure, starting from Protocol 6, where a higher concentration of pepsin was used, in order to verify if this parameter was critical to obtain good results, and the salting-out was carried out with 2 M NaCl solution. It was found a way to perform the recovery phase at a temperature of 4 °C, decreasing the risk of denaturing the collagen. In Protocol 7, the starting tissue was mincing with a mixer in order to facilitate the acid action and the ASC was discarded because of the very low yields obtained with the above-mentioned procedures. In Protocol 8, a key step was introduced: ultra-centrifugation, thanks to which samples were better separated and they were then coupled with high concentrations of pepsin and NaCl. In this way, the results starting to be satisfactory. At the end (Protocol 9), an additional step was introduced: a 70 % ethanol solution was used in order to remove pigment and fat residues. Moreover, proper concentrations of pepsin (risk of over-pepsinization) and NaCl were carried out and all phases were performed at 4 °C to avoid collagen denaturation. The modifications performed in the extraction procedures were then compared to the respective yields (Table 4.3).

<b>Specie</b>	<b>Protocol</b>	<b>ASC (mg/g)</b>	<b>PSC (mg/g)</b>	<b>Modifications</b>
<i>Rhopilema hispidum</i>	1	0.75	1.08	-
	2	0.71	1.36	Pre-treatment: add 0.1 M NaCl for 1 day + centrifugation; Extraction: 0.05% pepsin for 3 days
	3	0.95	1.45	Recovery: salted-out with 1.5 M NaCl, dialysis for 3 days
	4	1.06	2.35	Pre-treatment: add 0.1 M NaOH for 1 day + centrifugation (no NaCl); Extraction: 0.1% pepsin for 3 days
	5	1.60	3.56	Pre-treatment: add 0.1 M NaOH for 1 day + centrifugation (no NaCl); Extraction: 0.1% pepsin for 3 days

6	2.15	4.57	Extraction: 0.2% pepsin for 3 days; Recovery: at 4 °C, salted-out with 2 M NaCl
7	-	9.23	Pre-treatment: sample mincing with mixer; Extraction: ASC is discarded, centrifugation for 1 h
8	-	20.87	Extraction: 0.5% pepsin for 3 days, ultra-centrifugation (20000 g for 1 h); Recovery: salted-out with 2.5 M NaCl, ultra-centrifugation (20000 g for 1 h);
9	-	29.87 and 31.16	All steps at 4 °C; Pre-treatment: add 70% ethanol, besides NaOH, for 1 day; Extraction: 0.2% pepsin for 3 days, no ASC extraction; Recovery: salted-out with 2 M NaCl

Table 4.3: Yield of collagens compared with the performed modifications. Red circles indicate the samples used for the following studies.

In the first four protocols, it is possible to observe as the yields of both ASC and PSC are very low, especially for ASCs. The only significant increase occurred in Protocol 4 where, due to the introduction of NaOH and the doubling of pepsin concentration, slightly better results were obtained. Starting from Protocol 6, performed on *Rhopilema hispidum* samples, better results are shown, especially in Protocol 8 and in the final protocol. The key factors that seem to have affected the results have been definitely the introduction of ultra-centrifugation, the size reduction through sample mincing, the balancing of pepsin concentration (too high pepsin concentration leads to over-pepsinization) and the addition of ethanol in the cleaning step. These improvements have led to good yields of freeze dried PSC, as reported in Table 4.3, Protocol 8 with 203.45 mg, and subsequently, in Protocol 9 with 302.58 mg and 627.87 mg. It is difficult to find the perfect balance in order to obtain the best suited protocol for each sample type, furthermore the entire procedure required at least 15 days for its implementation and these long period make the protocol optimization a real challenge. Red circles in Table 5 highlights the samples used for the characterization of the materials, ASC

and PSC, Protocol 6, were used for SDS-PAGE analysis, while PSC, Protocol 9, were utilized in order to observe collagen type, structure and physical-chemical properties.

## 4.2 Jellyfish isolated collagen characterization

The characteristics of collagens *in vivo* are unique and when the goal is to mimic the collagen role in extracellular matrix, as is the case of tissue engineering approaches producing collagen-based scaffolds for cell culture, it is of extremely importance the evaluation of collagen properties. Since there are so many sources from where collagens can be extracted, and so many types, it is crucial to study its characteristics with particular care and accuracy.

There are several techniques that can be used to characterize collagen samples (in solution or in solid state), addressing structural, chemical and morphological features. With a good characterization and, consequently, a better knowledge of the sample, it is easier to have a desired biological response or to establish a relationship between results and features of the produced structure. The goal is to continuously improve the results, by trying to control the sample features, resulting in a more predictable and accurate biological response.

One of the methods used to characterize collagen purity and breakdown was the sodium dodecyl sulfate polyacrylamide gel electrophoresis (SDS-PAGE), from which, it is possible to compare the collagen sample with collagen obtained from other sources, taken as reference and propose an identification of the collagen type when the collagen bands are similar.

In the case of collagens from the same type but from different species, where the amino acid sequence is changed although the same chain types are present (for instance,  $\alpha 1$ ,  $\alpha 2$  and  $\beta$  chains in type I collagen), slightly shifts in the position of the bands may be observed. This is most probably caused by small differences in the molecular weight as a consequence of different amino acid sequences. In Figure 4.1, it is shown a SDS-PAGE pattern of ASC and PSC extracted from dried *Rhopilema hispidum* jellyfish compared with a commercial Bovine type I collagen as reference.

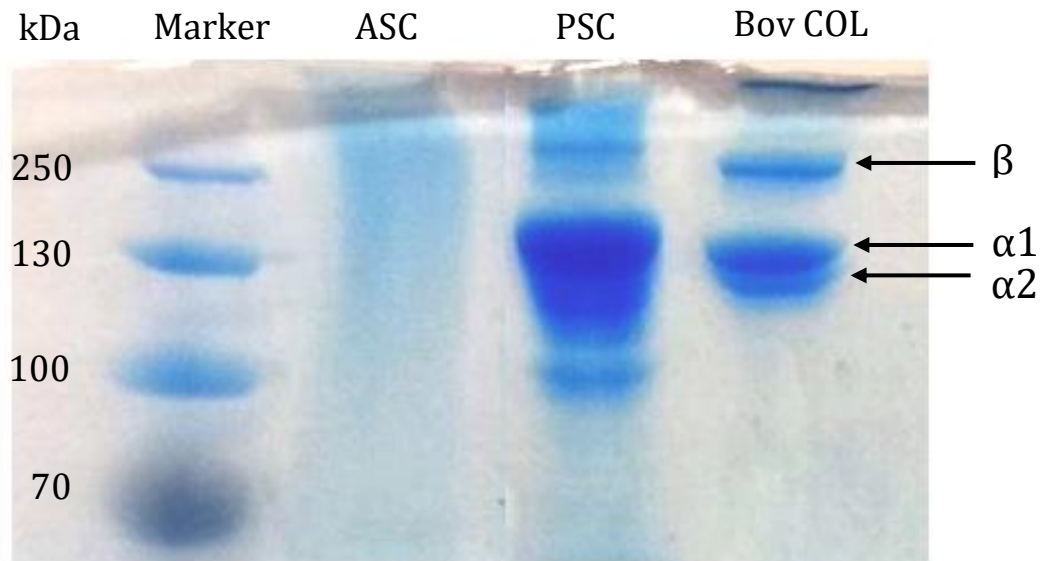


Figure 4.1: SDS-PAGE pattern of collagens extracted from dried *Rhopilema hispidum* jellyfish specie by acetic treatment (ASC) and in the presence of pepsin (PSC). Commercial Bovine type I collagen was used as control. The position of molecular mass markers (kDa) is indicated on the left of the gel.

As it is possible to observe from the image, ASC of jellyfish sample shows no bands and this probably indicate that the first collagen isolation (Protocol 6) with acetic acid was not sufficient to extract pure collagen; moreover the ASC yields reported for each extraction were too low to be used for subsequent analysis. In contrast to ASC, PSC of *R. hispidum* shows at least two different  $\alpha$  chains, probably  $\alpha_1$  of about 130 kDa and  $\alpha_2$  of about 105 kDa, and their cross-linked chains can also be observed. These results are similar to Bovine type I collagen although the position of the bands is slightly shifted, probably due to different amino acid sequences between species. Additionally, jellyfish PSC finds crosslinked component,  $\beta$ -sheet band at 260 kDa ( $\alpha_1 + \alpha_1$ ), indicating that some of  $\alpha$  chains do not completely dissociate under denaturing condition. The intensity of this band seems to be lower than Bovine sample ones, but this can be explained by conversions of some  $\beta$ -sheets in  $\alpha$ -chains due to the action of pepsin. Pepsin removes the crosslink containing telopeptide, and concomitantly one  $\beta$ -chain is converted to two  $\alpha$ -chains. The  $\alpha_3$  chain could not be observed under the electrophoretic conditions employed, because  $\alpha_3$  migrates electrophoretically to the same position as  $\alpha_1$ . In general, the pattern of  $\alpha$  chains in the pepsinized extract is more complex than in bovine sample. These differences are evident in the presence of additional and faster migrating chains. These bands being collagenase-sensitive, they could represent an over-pepsinization of the collagen chains and these degradation products might correspond to the presence of thermally unstable regions in these collagen molecules, which are more sensitive

to protease digestion. However, based on electrophoretic mobility and subunit composition, it is suggested that PSC from jellyfish sample could refer to type I collagens.

Despite efforts focusing in other techniques, the most used to assess the helical content of a collagen sample is circular dichroism (CD), which addresses the structure of proteins. When the chromophores of the amides of the polypeptide backbone of proteins are aligned in arrays, their optical transitions are shifted or split into multiple transitions due to “exciton” interactions. The result is that different structural elements have characteristic CD spectra, as shown in Figure 4.2 [68].

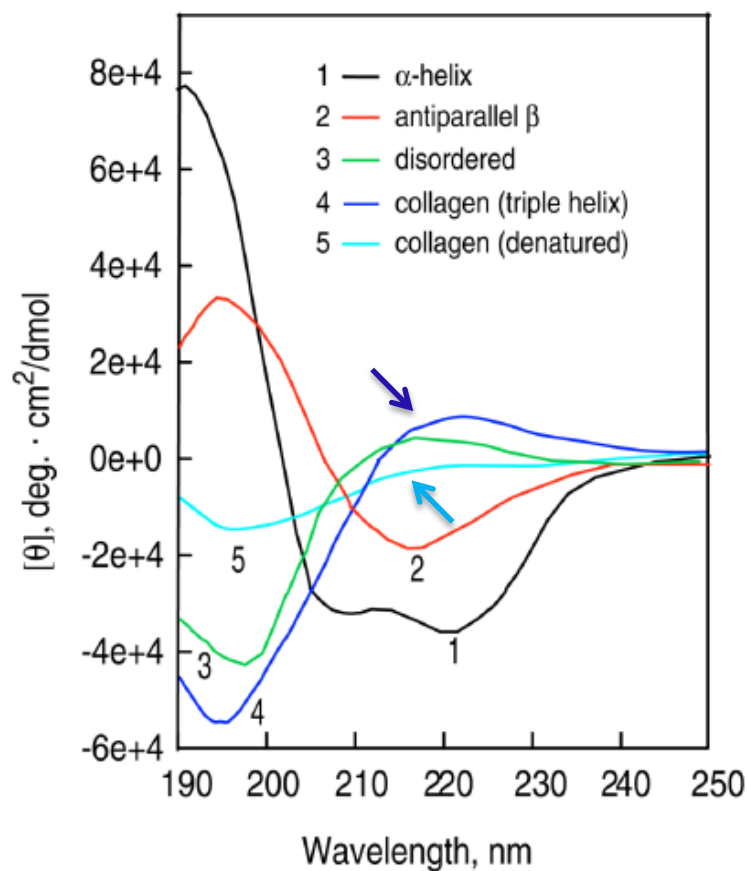


Figure 4.2: Circular dichroism (CD) spectra of polypeptides and proteins with representative secondary structures [68]. Arrows indicate the value of the peaks discussed in the text.

The figure shows the trend of the various protein structures:  $\alpha$ -helical proteins have negative bands at 222 nm and 208 nm and a positive band at 193 nm. Proteins with well-defined antiparallel  $\beta$ -pleated sheets have negative bands at 218 nm and positive bands at 195 nm, while disordered proteins have very low ellipticity above 210 nm and negative bands near 195 nm. The collagens are a unique class of proteins, which have three chains that wrap



together in a triple helix. Collagen is a sort of optically active protein and adopts the polyproline II-like helical conformation with a negative minimum absorption band around 195 nm and a weak positive maximum absorption band at 210-230 nm (blue arrow) [68]. On the other hand, when collagen is denatured, the positive maximum peak disappear (cyan arrow). CD spectra of *Rhopilema hispidum* samples used in this work are shown in Figure 4.3.

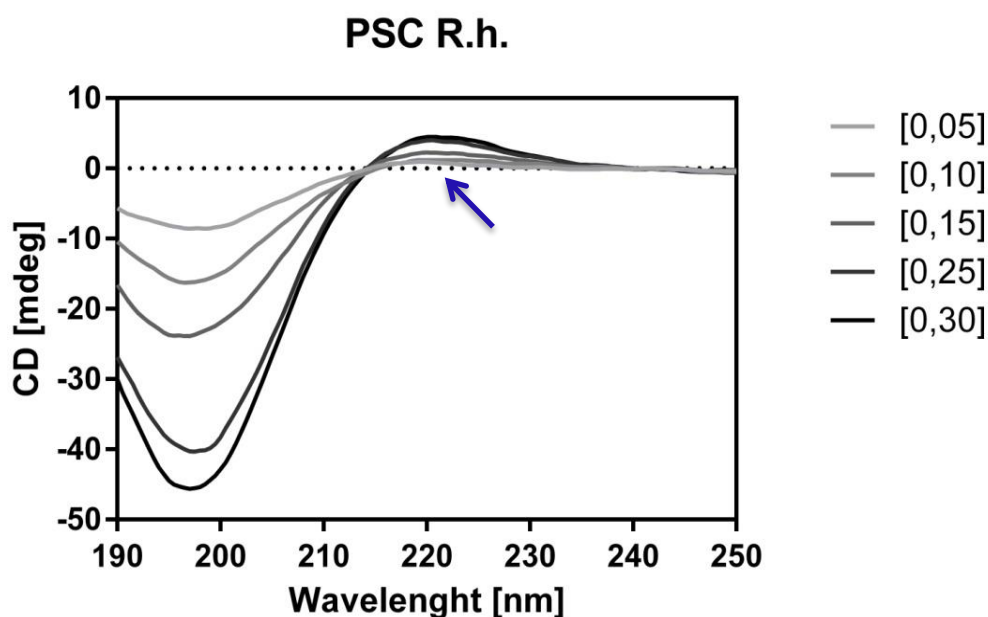


Figure 4.3: CD spectra of *Rhopilema hispidum* pepsin soluble collagen (PSC) samples. Arrow indicate the value of the peak discussed in the text.

Collagen fraction isolated from *Rhopilema hispidum* have a positive maximum peak at 220.5 nm (blue arrow) and a negative minimum peak at 197 nm, suggesting the typical triple helical conformation (as reported in Figure 4.2). However, the triple helix can partly reform for not-classified specie collagen when the temperature of the sample falls below the gelation temperature.

The sample, tested at five different concentrations, shows an increase of peaks in proportion to the degree of concentration. This is a further confirmation that the presence of the positive peaks represent the effective secondary structure of collagen. Unfortunately, this is only a qualitative analysis and therefore the peaks cannot be quantified.

Fourier Transform Infrared Spectroscopy (FTIR) is a powerful tool to investigate and identify the chemical composition of a sample, like the presence of collagens and eventually their different types. In the case in which collagen is extracted from a new marine source, it can also

be used to check the presence of triple helix, as shown by the spectra in Figure 4.4, exhibiting the characteristic amide peaks of collagens.

The amide A band of both PSC sponges are found at 3306 and 3280  $\text{cm}^{-1}$ , respectively. This band is generally associated with the NH stretching vibration and shows the existence of hydrogen bonds, probably with a carbonyl group of the peptide chain. A free NH stretching vibration occurs in the range of 3400 - 3440  $\text{cm}^{-1}$ , whereas when the NH group of a peptide is involved in a hydrogen bond, the position is shifted to lower frequency, usually 3300  $\text{cm}^{-1}$ . Amide B band of PSC sample, representing the asymmetrical stretch of  $\text{CH}_2$ , is observed at 2925  $\text{cm}^{-1}$ , while the sharp amide I band is observed at 1649  $\text{cm}^{-1}$ . The latter, with characteristic frequencies in the range from 1600 to 1700  $\text{cm}^{-1}$ , is mainly associated with stretching vibrations of the carbonyl groups ( $\text{C}=\text{O}$  bond) along the polypeptide backbone, which is a sensitive marker of the peptide secondary structure.

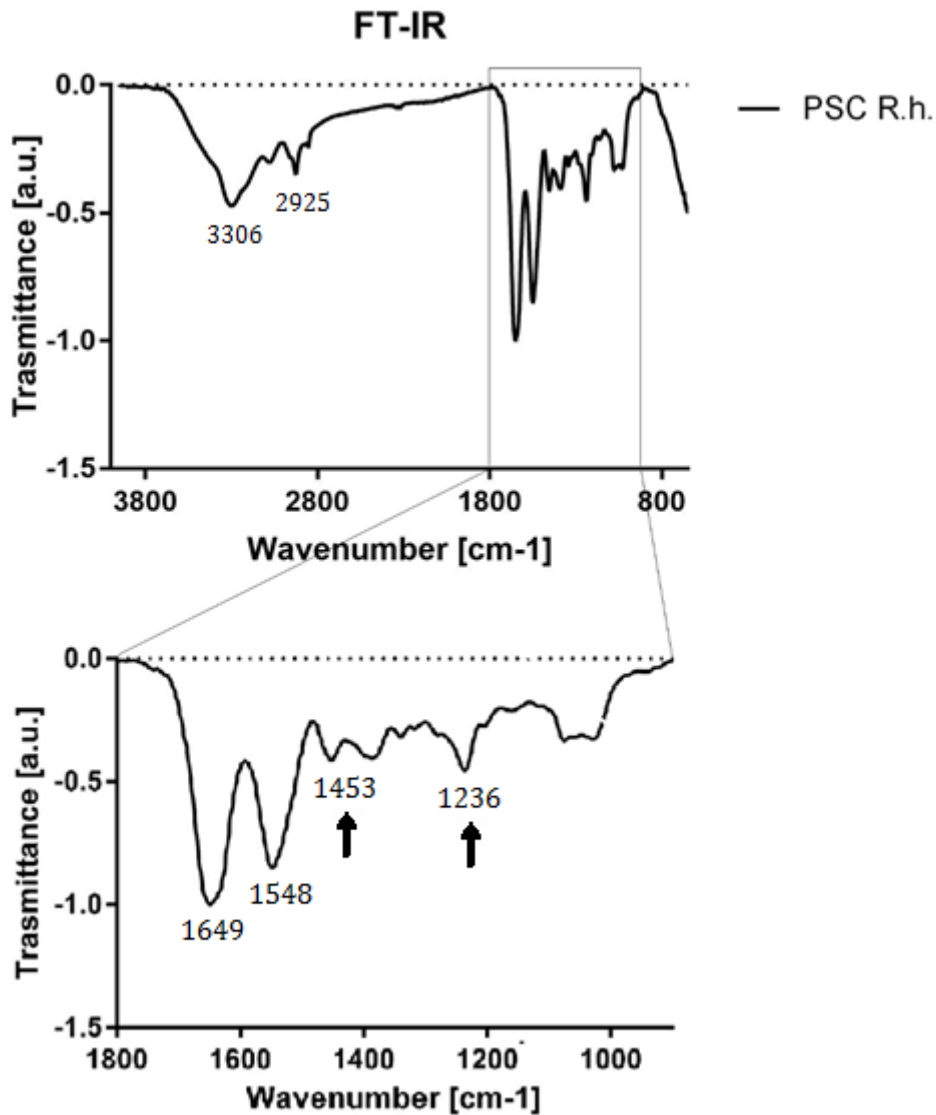


Figure 4.4: FTIR spectra of PSC from *Rhopilema hispidum* jellyfish specie. Arrows indicate the peaks that determine the triple-helical conformation.

The amide I peak underwent a decrease in absorbance, followed by a broadening accompanied by the appearance of additional shoulders when collagen is heated at higher temperature. The amide II pepsin soluble collagen appears at  $1548\text{ cm}^{-1}$  and results from NH bending vibration coupled with CN stretching vibration. Due to the amplitude, it could be supposed that *R. hispidum* collagen were most likely not denatured during the extraction. Moreover, this powerful tool can also be used to check the presence of triple-helical structure of collagen: if absorptions ratio of amide III ( $1236\text{ cm}^{-1}$ ) and the peak at  $1453\text{ cm}^{-1}$  (represented by the arrows in the Figure 4.4) is close to 1, it is indicative that triple helix structure is preserved [69]. In this study, the collagen extracted from *Rhopilema hispidum* shows the typical structure of collagen, reaching a ratio of 1.06, confirming the results

obtained with CD spectroscopy. Also, according to Belbachir K. et al. (2009), the investigation of collagen types and structure only by analysis of absorptions and infrared wavelength is not possible, however it presents a discrimination potential between studied collagen types and could represent a preliminary study for the material characterization.

The thermal stability of collagen can be addressed by thermal analysis, namely differential scanning calorimetry (DSC), by measuring the flux of calorimetric energy associated to material transitions, namely collagen denaturation, as a consequence of the heating process. As the heating process starts, protein absorbs heat, causing protein to unfold, at a temperature range specific to that protein, in this case, collagen. The maximal transition temperatures and denaturation temperatures vary from different marine sources and, even if extracted from the same species, those temperatures are different [70].

When collagen is heated, the crystalline triple helix is transformed into amorphous randomly coiled peptide chains that results in shrinkage of the collagen fibers formed. The determination of denaturation temperature of PSC from *Rhopilema hispidum* jellyfish by DSC is illustrated in the thermograph in Figure 4.5.

In this study, thermal denaturation temperature of the freeze dried PSC of *R. hispidum* is found at 73,83°C and it is a very important characteristic to account with, as it will influence the temperature that can be used in collagen processing into structures and its biomedical application.

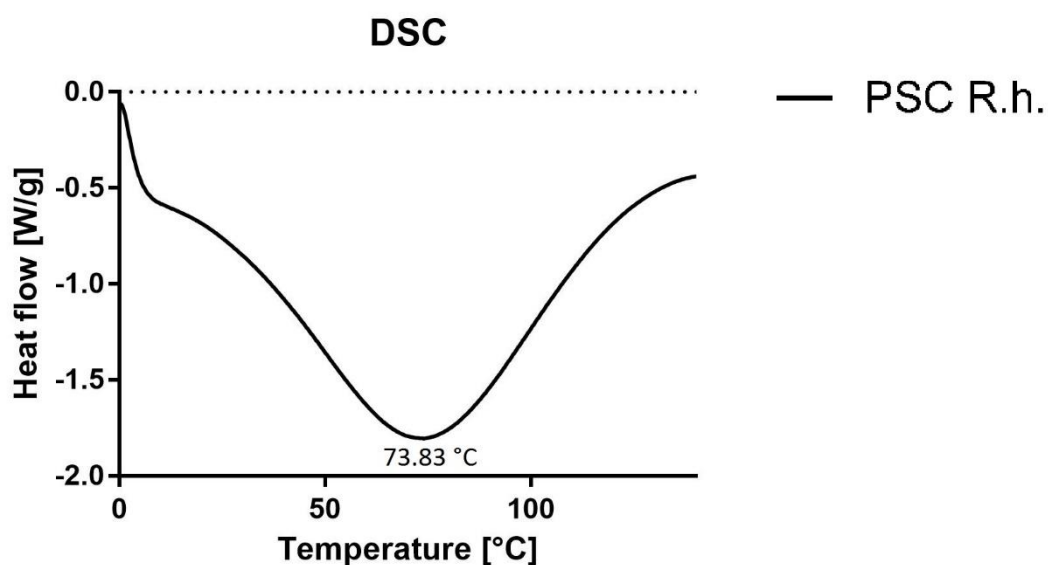


Figure 4.5: DSC thermograph of PSCs extracted from the studied species of jellyfish.

The thermal denaturation of collagen is related to the thermal stability of collagen by amino acid content and hydroxyproline content; in particular, denaturation temperature is known to increase with increasing amounts of amino acids residues [71].

Table 4.4 shows the amino acid composition, expressed as residues per 1000 total residues, of pepsin soluble collagen extracted from *Rhopilema hispidum* jellyfish, as well as of bovine collagen (Sigma, St. Louis, MO, USA, type I collagen of calf skin origin). As collagen is triple helical in nature with characteristic amino acid repeat, (Gly-Pro-Hyp)<sub>n</sub>, glycine is the most abundant with the amount of 185 and 330 of the total amino acid present in the jellyfish and bovine collagen, respectively. For these reason, Jellyfish collagen shows also high values of proline and hydroxyproline content, which represent an important factor expressing thermal stability in collagen. Generally, mammalian collagen contains more imino acids (Pro and Hyp) than fish collagen [72]. In the present study, jellyfish collagen shows slightly higher imino acid content than mammalian collagen. Despite their similarities, differences between jellyfish and bovine collagen are detected in their amino acid composition. In particular, jellyfish collagen has a relatively high content of threonine and alanine than calf-skin collagen. Pepsin soluble jellyfish collagen also contains a small amount of tyrosine, suggesting that the collagen is atello-collagen of high purity [72].

Amino acids	Jellyfish pepsin soluble collagen	Bovine collagen
Aspartic acid	55	45
Threonine	20	18
Serine	25	31
Glutamic acid	58	75
Glycine	185	330
Alanine	70	119
Cysteine	1	-
Valine	19	21
Methionine	-	6

Isoleucine	10	11
Leucine	22	23
Tyrosine	4	3
Phenylalanine	15	3
Lysine	25	26
Histidine	6	5
Arginine	43	50
Hydroxyproline	138	94
Proline	82	121
Imino acids <sup>1</sup>	220	215

Table 4.4: Amino acid composition of pepsin soluble collagen extracted from jellyfish *Rhopilema hispidum* and bovine collagen (results are expressed as residues/1000 residues). <sup>1</sup>Imino acids mean proline and hydroxyproline.

### 4.3 Scaffold characterization

The necessity of natural polymeric scaffolds, artificial skin substitutes for wound healing or model membranes for penetration studies has promoted the development of a biocompatible natural-derived polymeric substrate within which fibroblasts can grow [74].

Among them, collagen, one of the major components of the extracellular matrix, is known to play an important role in adhesion and growth of mammalian cells and contain the amino acid sequence, arginine-glycine-aspartic acid (RGD) that stimulates cell attachment and protein expression in cells [75]. In particular, fibroblast and endothelial cells require the presence of additional coating to adhere and proliferate. The principal sources of collagen are calf skins and bones. However, due to religious constraints related with avoidance of porcine and bovine products, association with a higher risk of bovine spongiform encephalopathy (BSE) and transmissible spongiform encephalopathy (TSE), and strong immunogenic reactions reported in clinical trials, other collagen source are being debated, such as marine organisms (squid, marine sponge, fish and jellyfish). Thanks to wide availability of the raw material and strong similarity between species, this study focused on jellyfish samples, being also infesting animals present in all over the world and possessing good amount of collagen. Firstly, we used

collagen fraction isolated from dried *Rhopilema hispidum* in order to create Tissue Culture Plate-well coating on the bottom of plates, with the aim to test its ability in promoting cell adhesion and proliferation. This innovative material was then compared with bovine type I collagen, already available commercially.

Another natural polymer, silk fibroin produced by silkworm, *Bombyx mori*, was considered in this study for its advantaging properties of tunable biodegradability, biocompatibility and low inflammatory response [76]. Additionally, it had found that silk fibroin film has several useful properties, for example, adjustable mechanical strength, high oxygen permeability and drug permeability [42]. In this study, we tried to improve the properties of silk fibroin film by blending with collagen and then created a collagen coated fibroin constructs. Apart the superior mechanical and physical properties of blended constructs to SF films, collagen contains RGD sequences that could facilitate cell attachment and proliferation [42].

Finally, in this study, three-dimensional scaffolds were prepared using freeze drying technique as constructs for wound dressing, tissue templates, etc. To achieve this goal, biomimetic scaffolds with appropriate pore size, high mechanical properties, porosity and interconnecting pores are characteristics needed for polymeric scaffold design that provides temporary framework for supporting cell attachment, proliferation and extracellular matrix formation. In this context, collagen has been reported to inhibit the unwanted aggregation in fibroin scaffold during the preparative processes producing scaffolds with high porosity [42].

Silk fibroin films from 4% silk aqueous solution and jellyfish collagen/fibroin blend (weight ratio, 80:20) were fabricated by solvent casting method. Jellyfish collagen coated fibroin films were also prepared by immersion of fibroin films in a 1 mg/mL jellyfish pepsin soluble collagen solution. It was not possible to produce jellyfish collagen films due to the high amount of material necessary for their manufacture. Furthermore, by solvent casting technique the resulting collagen films were not water-stable, extremely thin and subject to easy breakage.

Scanning electron microscopy of water-insoluble silk-based films prepared by solvent casting technique followed by water-vapour stabilization are shown in Figure 4.6. The three constructs are macroscopically smooth and uniform at a lower magnification (Figure 4.6 A, B, C). At higher magnification, occasional islands are found on the surface and they are probably indicate some aggregates in solution prior to solvent casting. However, the overall surface is relatively smooth with micro-roughness and regular streaks (Figure 4.6 D, E), which seem to

be absent in fibroin/collagen films (Figure 4.6 F). The thickness of the solvent-cast films was about 50  $\mu\text{m}$ .

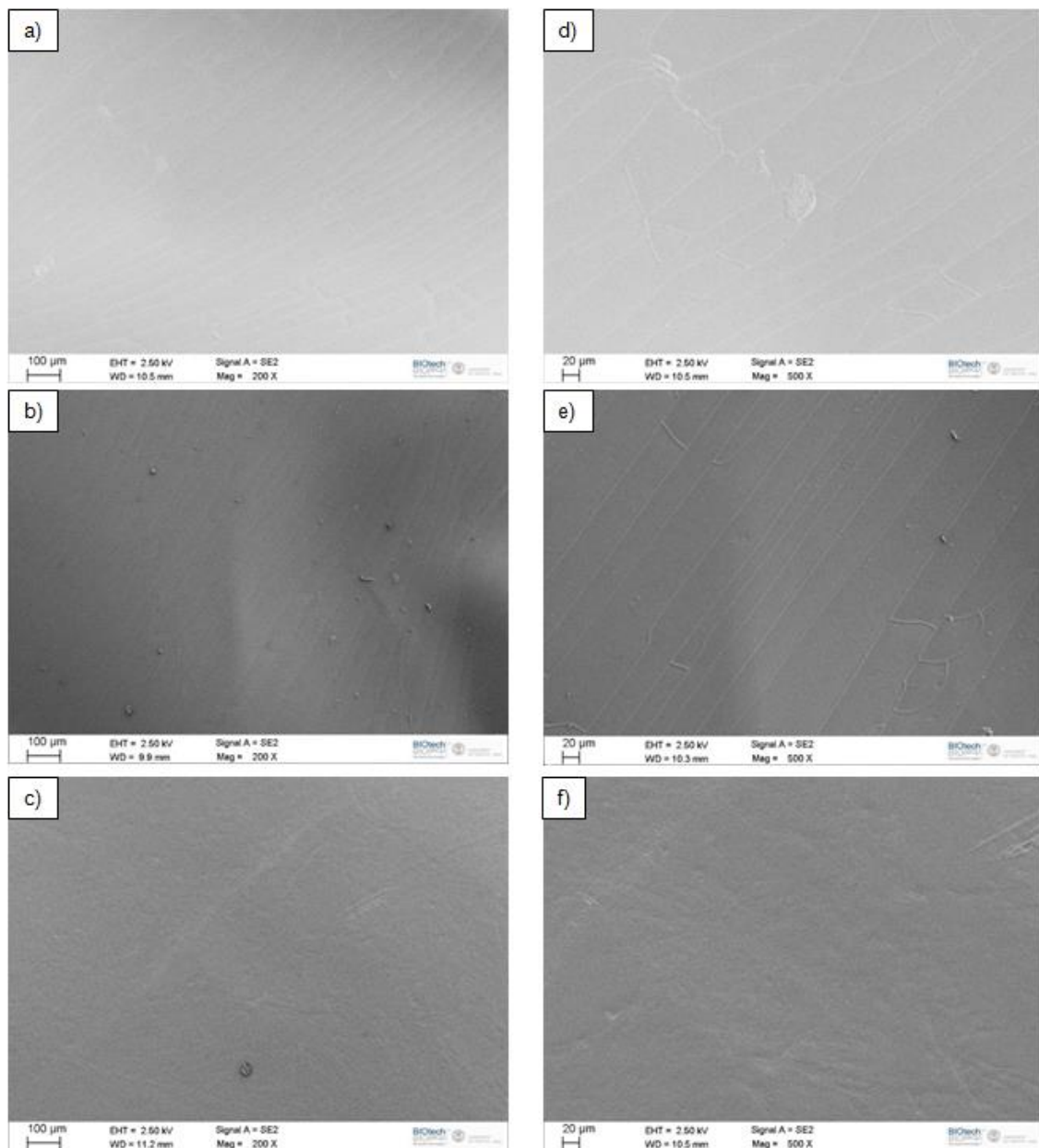


Figure 4.6: Representative scanning electron microscopy images of films prepared by solvent casting method: 4% silk fibroin film; collagen-coated 4% silk fibroin film; fibroin/collagen film containing 20% collagen and 80% silk fibroin (total fraction 4%). A, C, E images are at lower magnification, whereas B, D, F images are at higher magnification.

Pore size, porosity and surface area are widely recognized as important parameters for scaffolds used in tissue engineering. In addition, other architectural features such as pore shape, pore wall morphology and interconnectivity between pores of the scaffold material have also been suggested as important parameters for cell seeding, migration and



proliferation, mass transport, gene expression and new three dimension tissue formation [77].

In this context, Figure 4.7 shows SEM images of freeze-dried scaffolds prepared from silk fibroin solution, fibroin solution followed by collagen coating and jellyfish collagen/fibroin blend (weight ratio, 80:20) solution. Porous 4% jellyfish collagen scaffolds were also prepared by lyophilisation of a dilute acid solution of pepsin soluble collagen. Collagen scaffolds reveal an interconnected network pore configuration and high porosity throughout the cross-section (Figure 4.7 A). As discussed above, this type of construct is not stable in aqueous environment, such as cell culture medium, and for this reason it was decided to combine it with another natural polymer: silk fibroin. Fibroin usually self-assembles separate sheets in freeze-drying process, which make it difficult to prepare porous structure and this make them frangible (Figure 29 B). As also reported in previous researches [41], it was found that collagen could form hydrogen bonds with fibroin to prevent the formation of separate sheets in freeze-drying process. Interestingly, following the adding of collagen, the fibroin/collagen scaffolds prepared from blend solutions show interconnected porous and reticulate structures, in which less sheet was formed (Figure 29 C). The result indicates that when containing 20% collagen, porous fibroin/collagen scaffolds could be easily prepared with freeze-drying method because collagen probably prevents fibroin from forming irregular sheets. On the other hand, bioabsorbable collagen coating on 4% silk fibroin scaffolds does not have the same positive effect like blending. In fact, it creates a sort of covering on fibroin scaffolds, which exhibited the same matrices generally composed of sheets (Figure 29 D). However, it could play an important role in promoting fibroblast adhesion in the early stage of cell culture.

Additionally, freeze dried PSC appears like irregular porous structure with a size of pores on the surface ranging from 50 to 70  $\mu\text{m}$ . When 20% collagen was added into 4% fibroin solution, the pores in blend scaffolds change to lower values. Considering that the decrease of pore size will increase the surface area and mechanical properties, the scaffold made up of fibroin and collagen would become more propitious for tissue engineering than fibroin scaffolds. On the other hand, since the adding of collagen increases the viscosity of solution and then restrains the unwanted fibroin aggregation in freezing process, the three-dimensional scaffolds with different pore sizes can be easily prepared by adjusting the solution concentration to meet the different application requirements.

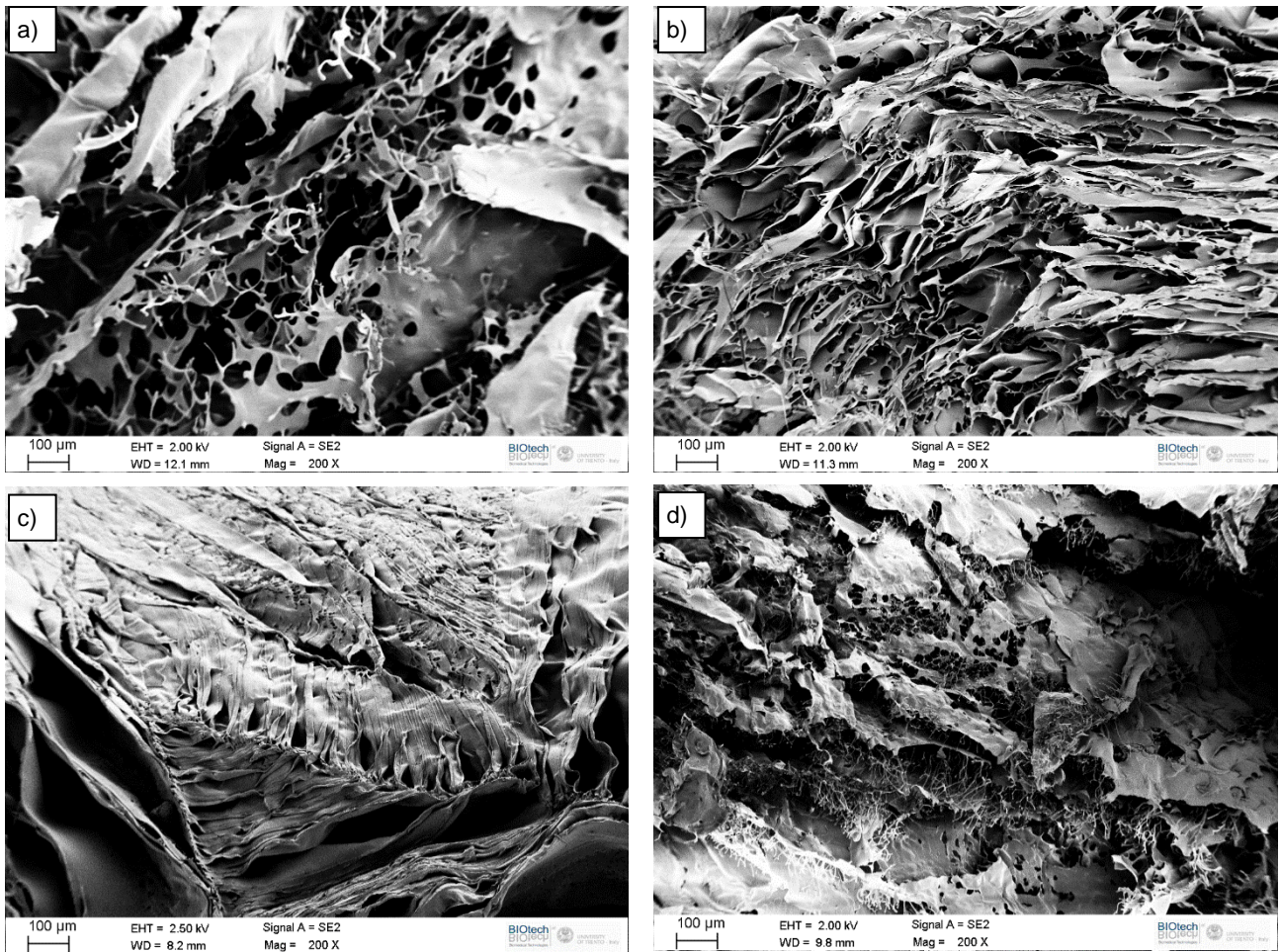


Figure 4.7: Representative scanning electron microscopy images of the freeze-dried scaffolds: porous jellyfish pepsin soluble collagen scaffold (A); 4% silk fibroin scaffold (B); collagen-coated 4% silk fibroin scaffold (C) and fibroin/collagen scaffold containing 20% collagen and 80% silk fibroin (total fraction 4%) (D).

Regenerated silk-based materials are normally stabilized by the induction of  $\beta$ -sheet formation through the use of solvent or by physical stretching [78], which represent not green-friendly methods. The  $\beta$ -sheets serve as physical cross-links in silk-based scaffolds, providing mechanical stability, water insolubility and relating directly to the rate of degradation via proteolytic action. In this work, water-insoluble silk films have been prepared with a low  $\beta$ -sheet content by all aqueous solvent casting method followed by water vapour drying. Thus, this approach satisfies some of the requirements for more green-friendly degradable biomaterials when compared with traditional methanol-treated films. Structural changes in the silk fibroin films after the different processes were analysed by FT-IR (Figure 4.8). The infrared (IR) spectral region within  $1700\text{-}1500\text{ cm}^{-1}$  is assigned to absorption by the peptide backbones of amide I ( $1700\text{-}1600\text{ cm}^{-1}$ ) and amide II ( $1600\text{-}1500\text{ cm}^{-1}$ ), which have been commonly used for the analysis of different secondary structures of silk fibroin. The

peaks at 1610-1630  $\text{cm}^{-1}$  (amide I) and 1510-1520  $\text{cm}^{-1}$  (amide II) are characteristic of silk II secondary structure. In particular, some researchers have suggested that the absorption at 1648-1554  $\text{cm}^{-1}$  (amide I) and 1535-1542  $\text{cm}^{-1}$  are indicative of random coil structure [79]. In the present study, we compare silk fibroin film with stabilized silk fibroin film. The amide I band for not stabilized silk fibroin film shows one strong peak at 1645  $\text{cm}^{-1}$ , while in the water-annealed sample the same peak at 1644  $\text{cm}^{-1}$  appears with a shoulder at 1623  $\text{cm}^{-1}$ , which represents an increase in  $\beta$ -sheet content at the expense of random coil conformation. The same trend in structural change is also found in the amide II region. From water-annealed SF the peak at 1533  $\text{cm}^{-1}$  (random coil structure) decreased, while the peak at 1517  $\text{cm}^{-1}$  ( $\beta$ -sheet conformation) increased.

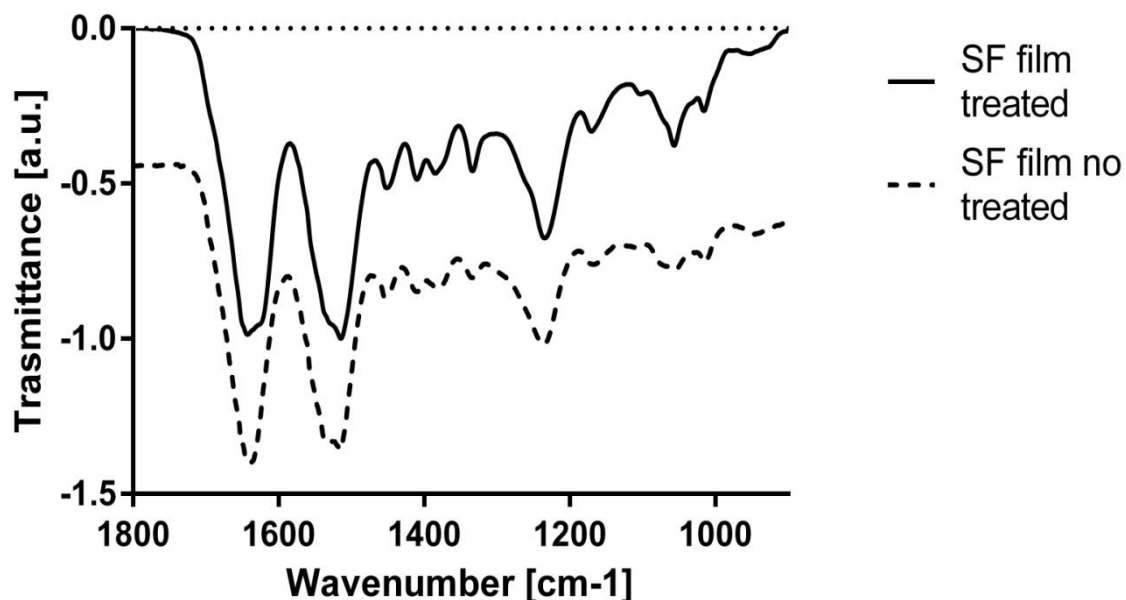


Figure 4.8: FTIR spectra of silk fibroin films prepared by two different processes: SF film, water-annealed silk film; SF no treat, water-soluble silk film.

In order to determine the conformational structure of the fibroin, collagen-coated silk fibroin and collagen/fibroin films from their IR spectra, we closely observe the amide I region between 1600 and 1700  $\text{cm}^{-1}$ , which is the most useful for IR structural analysis of proteins. The amide I band represents primarily the C=O stretching vibration depends on the strength of hydrogen bonding between the C=O and N-H groups, which in turn is determined by the particular conformational structure of the protein backbone. In general, the amide I mode associated with the  $\alpha$ -helical conformation occurs at 1650-1660  $\text{cm}^{-1}$ , the random coil

conformations give bands in the range of 1640-1650  $\text{cm}^{-1}$ , and the  $\beta$ -sheet conformation results in IR bands between 1620 and 1640  $\text{cm}^{-1}$  [79].

The FT-IR spectra of silk fibroin film, collagen-coated silk fibroin film and fibroin/collagen film are shown in Figure 4.9. All the spectra possess the same trend with absorption bands at 1700-1660  $\text{cm}^{-1}$  (amide I) and 1600-1500  $\text{cm}^{-1}$  (amide II) corresponding to the SF silk II structural conformation ( $\beta$ -sheet). Another absorption band is observed in all curves at 1235  $\text{cm}^{-1}$  (amide III), which are characteristic of the silk I conformation (random coil and  $\alpha$ -helix). This indicates that silk I and silk II structures are presented simultaneously in all films; however, the poor solubility of these films indicates the predominance of the silk II structure. FT-IR spectra of collagen coated SF films and SF/PSC films show an amide I band with a strong peak centred at 1621  $\text{cm}^{-1}$ . Such a peak cannot be observed in the spectrum of the SF film, in fact it is more shifted toward random coil conformation. As known, the peak at 1621  $\text{cm}^{-1}$  is characteristic of antiparallel  $\beta$ -structure frequencies. Therefore, we believe that the  $\beta$ -sheet structure could be formed in both the silk films combined with jellyfish collagen probably due to the acidification linked to the presence of acetic acid in which collagen is dissolved.

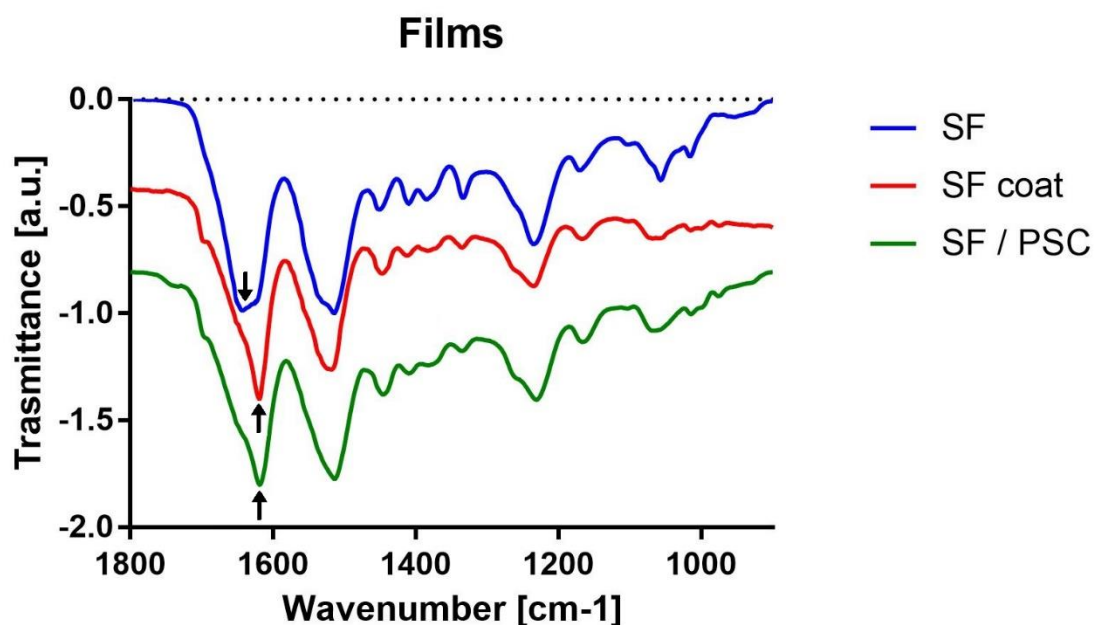


Figure 4.9: FT-IR spectra of films prepared by solvent casting method: silk fibroin film, collagen-coated 4% silk fibroin film and fibroin/collagen film containing 20% collagen and 80% silk fibroin (total fraction 4%). Arrows represent peaks discussed in the text.

Structural changes in the silk fibroin sponges before and after water vapour drying treatment were also analysed by FT-IR (Figure 4.10). As in the previous reported films, the same infrared spectral regions corresponding to amide I ( $1700\text{-}1600\text{ cm}^{-1}$ ) and amide II ( $1600\text{-}1500\text{ cm}^{-1}$ ) are observed. As expected as a result of stabilization in water vapour dryer, silk fibroin sponge shows a strong increase in  $\beta$ -sheet content with a peak at  $1626\text{ cm}^{-1}$  when compared with not stabilized SF sponge, which displays one strong peak at  $1640\text{ cm}^{-1}$  (random coil structure).

On a comparison to water-annealed silk fibroin film, the stabilized SF sponge reveals a larger  $\beta$ -sheet component with respect to the random coil conformation. A possible explanation of this result lies in the structure of the film, which is more dense and for this reason the chains are more difficult to rearrange in a more stable  $\beta$ -sheet conformation.

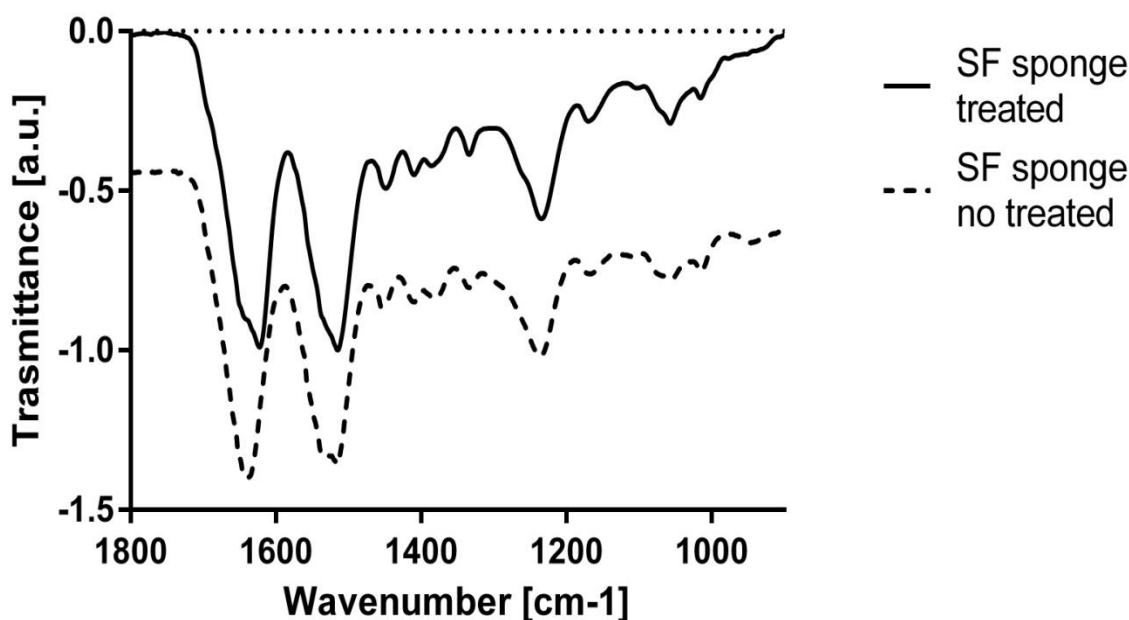


Figure 4.10: FTIR spectra of silk fibroin sponges before and after stabilization by water vapour dryer: SF sponge, water-annealed silk sponge; SF sponge no treated, water-soluble silk sponge.

FT-IR was then used to determine the structural changes in the silk fibroin sponge, jellyfish collagen coated fibroin sponge and jellyfish collagen/fibroin blend (weight ratio, 80:20).

Figure 4.11 displays FT-IR spectra of the three freeze-dried scaffold, which are shown comparatively. All the spectra show characteristic amide I, amide II and amide III peaks. The intensities of the absorption bands at around  $1623\text{ cm}^{-1}$  (amide I),  $1521\text{ cm}^{-1}$  (amide II) and  $1237\text{ cm}^{-1}$  (amide III) are roughly comparable in all the samples. FT-IR spectra of collagen-coated SF sponge and PSC/SF blend show an amide I band with a strong peak centred at about

1623  $\text{cm}^{-1}$ , particularly marked in the collagen-coated sponge, while in the silk fibroin sponge it is slightly shifted toward the random coil conformation (black arrows). The result indicates that acetic acid used in the collagen processing facilitated the transformation from random conformation into  $\beta$ -sheet crystal, which might partly result in the increase of mechanical strength. This behaviour is not observed in the case of the amide II peak (indicated by arrow). This result is confirmed, especially in the SF coat sample, by the presence of a shoulder in the absorption peak at 1261  $\text{cm}^{-1}$  (black arrow), which indicates the transition to the stable state Silk II. However,  $\beta$ -sheet structure transition is just partial, as evidenced by the presence of a weak peak at 1698  $\text{cm}^{-1}$ , characteristic of turns and bends structure.

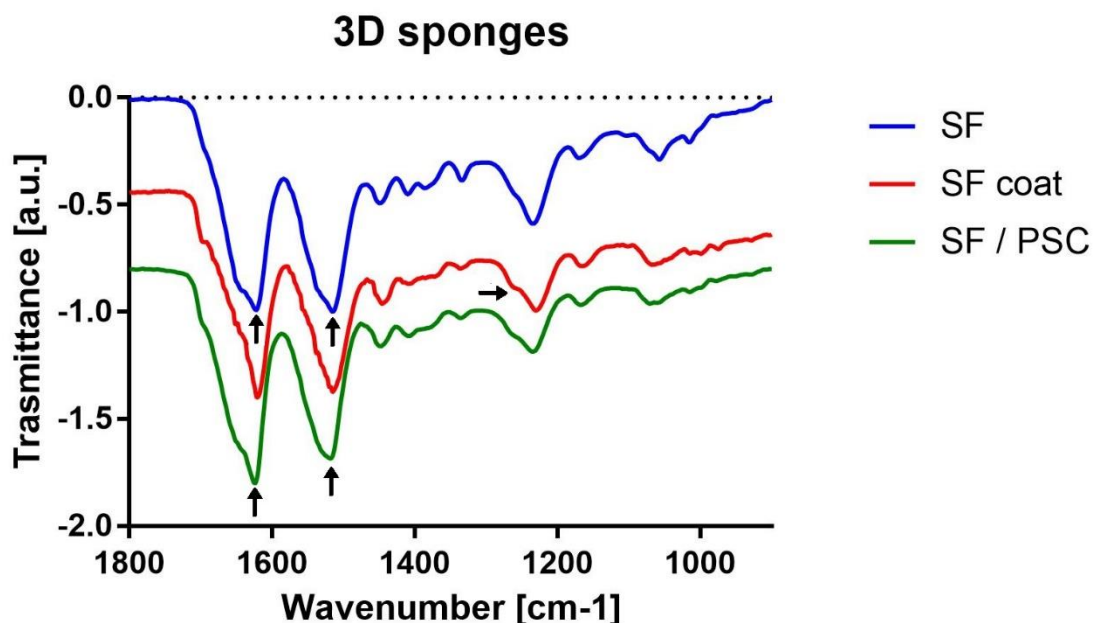


Figure 4.11: FT-IR spectra of freeze-dried scaffolds: 4% silk fibroin sponge, collagen-coated 4% silk fibroin sponge, and fibroin/collagen sponge containing 20% collagen and 80% silk fibroin (total fraction 4%). Arrows represent peaks discussed in the text.

Differential scanning calorimetry (DSC) has been used extensively as a sensitive technique to quantify the addition of covalent bonds and reductions in triple-helical content, as well as determine thermal properties of different biomaterials.

Figure 4.12 illustrates standard DSC curves for silk fibroin film, jellyfish collagen-coated silk fibroin film and silk fibroin/collagen blend. All the samples show an endothermic peak at around 100  $^{\circ}\text{C}$ , a glass transition temperature ( $T_g$ ) at around 210  $^{\circ}\text{C}$  and a degradation peak at around 280  $^{\circ}\text{C}$  (as indicated by arrows). The endothermic peak at around 100  $^{\circ}\text{C}$  is due to the

evaporation of bound and not-bound water and indicates that silk fibroin interacts with water. At the crystallization peak, unstable non-crystal structures are transformed to  $\beta$ -sheet. After the appearance of the glass transition temperature, samples start to degrade, with an endothermic peak at around 280 °C. In literature, in the thermal analysis of random coil conformation silk fibroin it was also observed an exothermic peak at around 230 °C [80]. Its absence confirms the findings in the FT-IR analysis: the transition of silk fibroin toward stable state Silk II with  $\beta$ -sheet structures formation. In the SF sample, the endothermic peak related to the evaporation of the adsorbed water is less marked than SF coat and SF/PSC films, probably because of its less dense structure. However, this endothermic peak is maintained because the silk I crystal is a hydrated structure [81]. The degradation peak in the SF film is at around 282 °C but decreases to 277 °C in SF/PSC blend film, indicating a lower thermal stability of SF/PSC film than SF film.

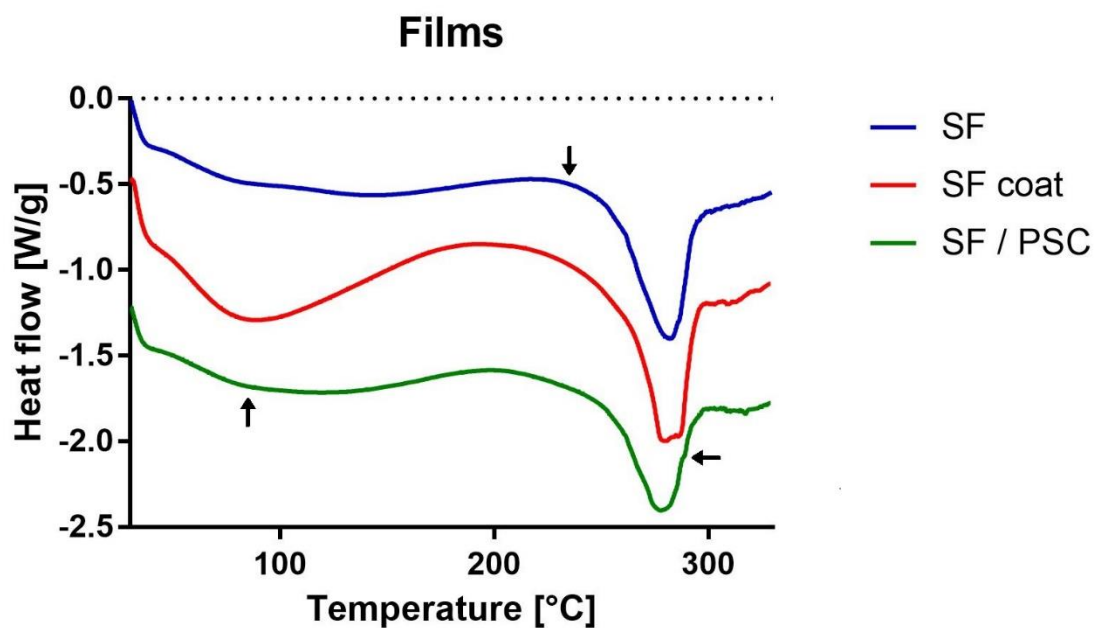


Figure 4.12: Differential scanning calorimetry spectra for 4% silk fibroin film, collagen-coated 4% silk fibroin film, and fibroin/collagen film containing 20% collagen and 80% silk fibroin (total fraction 4%). Arrows represent peaks discussed in the text.

The thermal properties of fibroin and collagen are very sensitive to moisture, which acts as plasticizing agent to depress thermal transition temperatures. Figure 4.13 shows the DSC thermographs for silk fibroin, jellyfish collagen coated fibroin sponges and jellyfish collagen/fibroin blend. All the samples show an endothermic peak below 100 °C, a glass

transition temperature at around 210 °C and a degradation peak at around 280 °C (as indicated by arrows). Denaturation temperature ( $T_d$ ) values of fibroin and fibroin/collagen scaffolds are similar. The result implies that the interaction between fibroin and collagen has little effect on  $T_d$  of fibroin/collagen scaffold without crosslinking. Moreover, though the endothermic peak become slightly broader than that of fibroin scaffolds because of the effect of collagen, the fibroin/collagen sponge has the prominent endothermic peak at 287 °C, attributed to the thermal decomposition of silk fibroin with un-oriented  $\beta$ -sheet structure [82]. The result confirm that fibroin/collagen sponge has enough  $\beta$ -sheet content, which makes this scaffold water-stable.

When compared to films, sponges exhibit the endothermic peak related to the evaporation of the adsorbed water more marked, probably due to their less dense structure, which tends to absorb a larger amount of water. This peak is particularly pronounced in the coated SF sponge, probably related to the specific fabrication process.

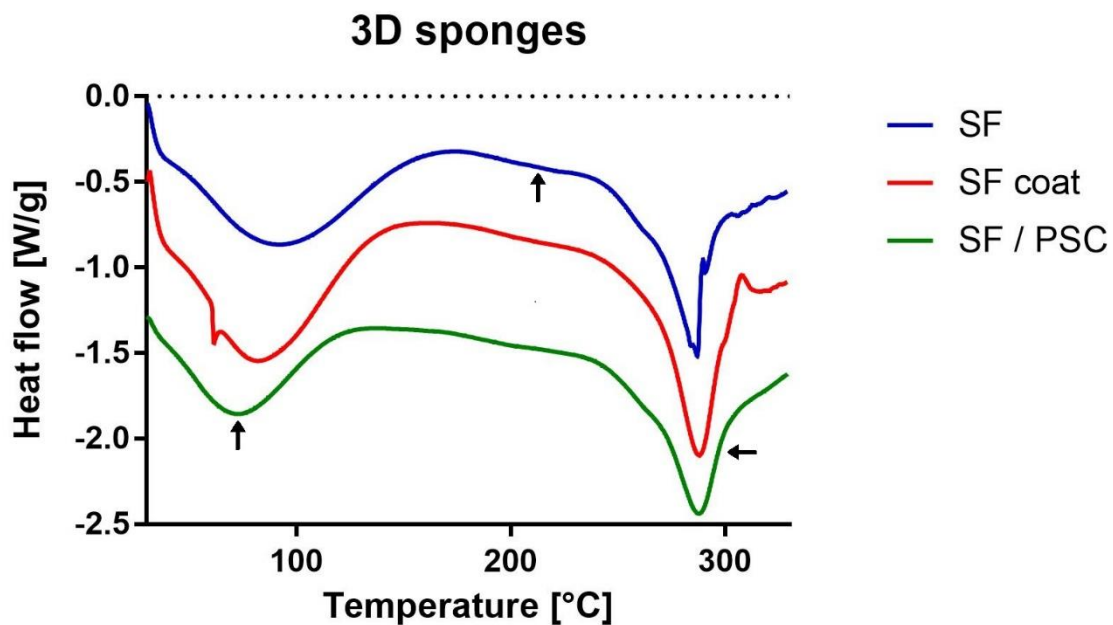


Figure 4.13: DSC spectra for 4% silk fibroin sponge, collagen-coated 4% silk fibroin sponge, and fibroin/collagen sponge containing 20% collagen and 80% silk fibroin (total fraction 4%). Arrows represent peaks discussed in the text.



## 4.4 Material evaluation on MRC-5 cell culture

The main goal of the following experiment is to evaluate the effect of jellyfish collagen on fibroblast cell behavior, in particular the ability of collagen to stimulate cell adhesion and proliferation, firstly in 2D cell culture and then in 3D constructs, with the aim to use it in scaffold fabrication. The human lung fibroblast cell line (MRC-5) was selected to represent the first cell type involved in the early stages of wound healing process and it represents a good model for biocompatibility analysis accepted by scientific community.

A MRC-5 culture was seeded on different substrates (Tissue Culture Plate-well coating, film and 3D sponge) and cell viability and proliferation were analyzed with Live/Dead analysis and AlamarBlue® assay, respectively. Different time points were considered to elucidate the contribution of jellyfish collagen in the microenvironment, depending on its presence in the substrate. TCP and Bovine type I collagen were used as 2D control samples, whereas silk fibroin film and sponge were considered as 3D control constructs.

For Live/Dead qualitative staining, we developed 3D porous scaffolds starting from jellyfish collagen, silk fibroin and silk fibroin/collagen using freeze drying technique with water vapor treatment. However, as expected, the scaffolds built from the isolated collagen were not stable in aqueous medium. For this reason, collagen blended with silk fibroin were used, in order to avoid any chemical cross-linking. Moreover, for the AlamarBlue® assay we introduced film morphology as 3D scaffold, with the intent to discriminate chemical and morphological factors affecting cell adhesion and growth. Collagen-coated silk fibroin sponges were also fabricated to verify the effective bioactive role of jellyfish collagen in promoting cell adhesion on silk fibroin scaffolds.

Live/Dead analysis by Calcein AM and Propidium Iodide staining was performed to check cell viability in a qualitative way. Figure 4.14 shows MRC-5 monoculture seeded on 2D standard culture well plates and Tissue Culture Plate-well coated with the extracted jellyfish collagen or standard bovine type I collagen. The results are roughly comparable on all samples analysed. After 24 hour from seeding, the cells are slightly more spread on jellyfish and bovine collagen than TCP and these samples most seem to promote cell adhesion and growth. At day 5 of cell culture, fibroblasts develop adhesion and cell-cell connective structures when plated on jellyfish collagen and they seem to align according to the specific network of the underlying coating. A similar morphology of contacts and cell spreading was observed with fibroblasts

adhering to TCP. MRC-5 cells also adhere and proliferate on bovine type I collagen, but alignment seem to be slightly diminished by comparison with cell morphology and organization on jellyfish collagen, probably due to increased cell spreading. However, no significant differences were found among these experimental groups. Live/dead assay revealed few detectable dead cells while the majority of cells was alive as stained green after 5 days of culture.

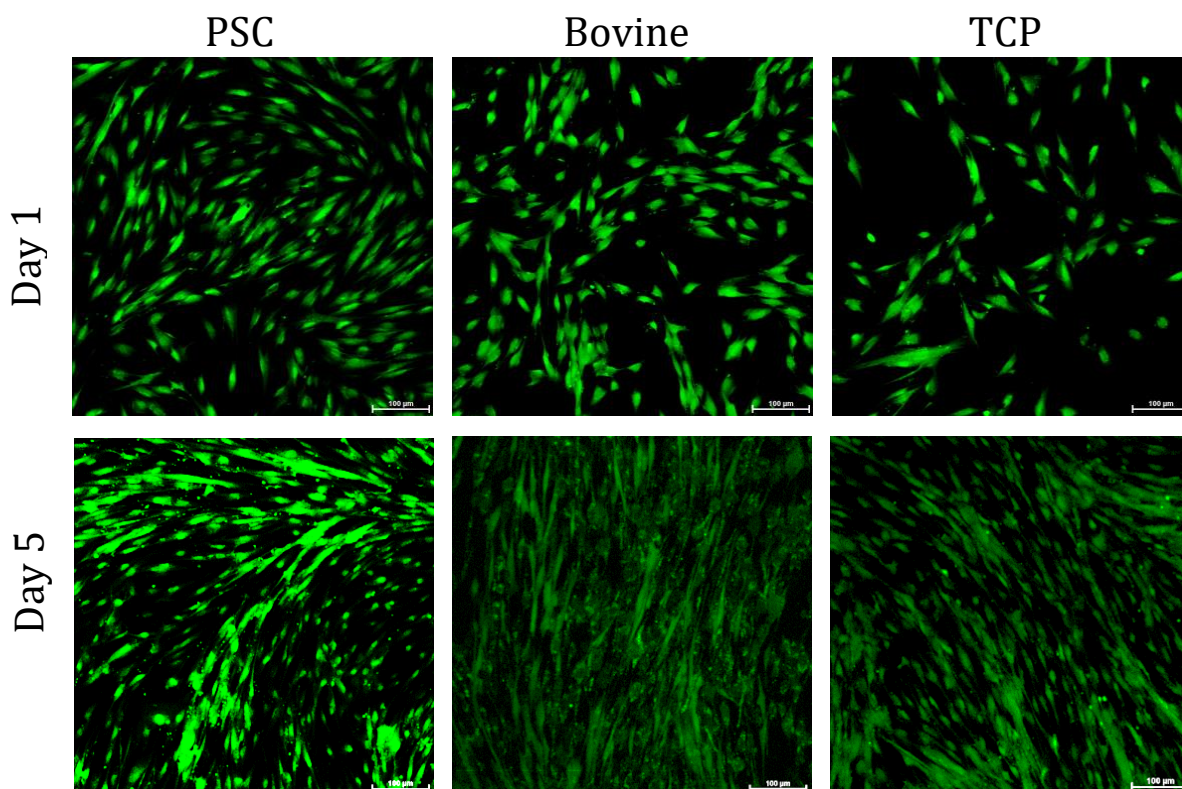


Figure 4.14: Viability test of MRC-5 cell monoculture seeded in 3 different conditions and observed with confocal laser microscopy. Viability for day 1 and 5 was tested using the Calcein/propidium iodine test for 2D jellyfish collagen coating (A, D), Bovine type I collagen coating (B, E) and TCP as control (C, F). Green color indicates viable cells, red color represents dead cells. Scale bar = 100 μm.

The same qualitative cell viability test was performed on MRC-5 cells seeded on freeze dried porous 3D scaffolds, composed by jellyfish collagen, silk fibroin and silk fibroin/jellyfish collagen blend. The results of the Calcein AM/Propidium Iodide staining are shown in Figure 4.15. As previously mentioned 3D collagen scaffold are not stable in aqueous environment, so after about 12 hours from culture medium addition, collagen scaffold collapsed forming a kind of filaments and fibers in the medium. Its presence as additional component of culture medium seems to promote cell proliferation and adhesion after just 24 hour from seeding. Silk fibroin and silk fibroin/collagen scaffolds show comparable results. MRC-5 cells seem to

reveal some difficulties in adhering on 3D scaffolds, even after 5 days of culture. In order to discriminate if cell growth is disadvantaged by the material used for scaffold fabrication or by the morphology, in the subsequent experiments we introduce film-like structures. They represent flat two-dimensional surfaces on which cells can adhere and proliferate more easily.

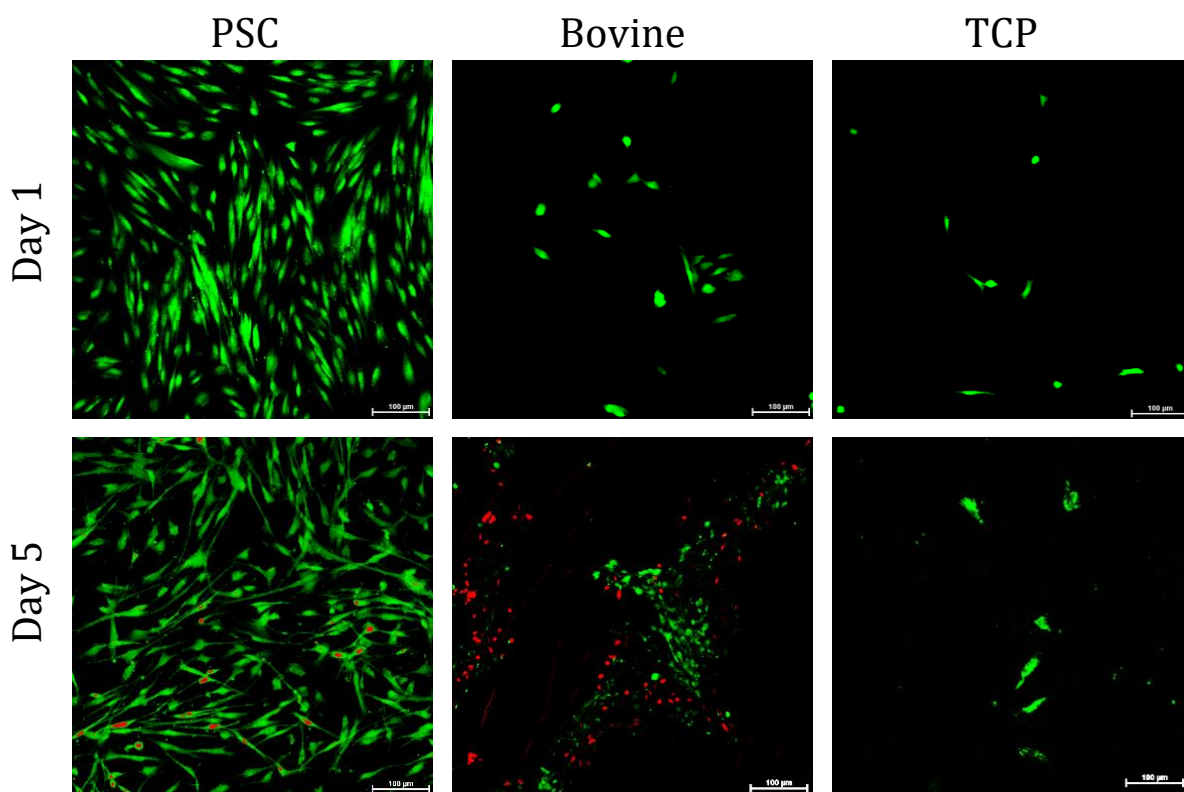
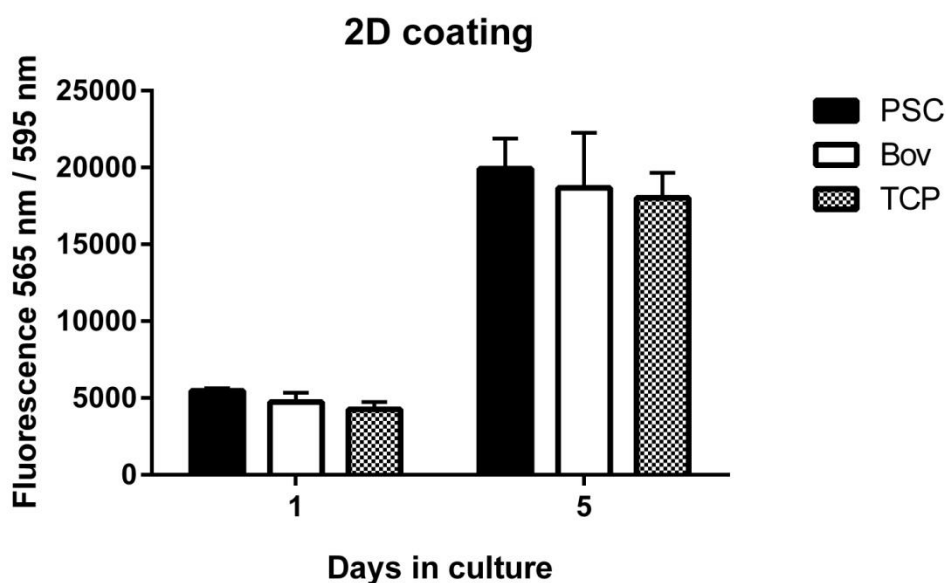


Figure 4.15: Viability test of MRC-5 cell monoculture seeded in 3 different conditions and observed with confocal laser microscopy. Viability for day 1 and 5 was tested using the Calcein/propidium iodine test for jellyfish collagen 3D sponge (A, D), silk fibroin sponge (B, E) and silk fibroin/jellyfish collagen sponge (C, F). Green color indicates viable cells, red color represents dead cells and fibroin sponge background. Scale bar = 100 µm.

The AlamarBlue® assay is a quantitative colorimetric assay employed to assess cell proliferation during 5 days of culture. Since the resulting fluorescence of reduced Alamar Blue by metabolically active cells, is proportional to the number of viable cells in the sample, MRC-5 cell proliferation on different samples could be assessed. The results reveal that MRC-5 cells seeded on 2D coating well plates (Figure 4.16) own a growth rate of about 103 times higher than that found on 3D scaffolds (Figures 4.17 and 4.18). On 2D coating (Figure 4.16), there are no significant differences among groups on day 1 as well as day 5 and the number of MRC-5 cells in all 2D groups significantly increase during culture, which suggests that the presence of

marine collagen not have a negative effect on cell proliferation and adhesion. Silk fibroin, collagen coated silk fibroin sponges and silk fibroin/collagen blend, as well as films, exhibit an opposite growth trend, with a slight decrease in cell number on day 5, regardless the presence of jellyfish collagen. As already supposed following the viability analysis, we might expect that the MRC-5 cell line could have some difficulties in adhering and proliferating on 3D scaffolds compared to 2D samples, regardless the material. Moreover, because of these problems, it might be possible that non-adherent cells could be washed away particularly from films after the first time point. However, the reduction in cell number detected on films and sponges is not statistically significant, in fact it can be regarded as approximately constant.

On the basis of these results, adhesion and proliferation of MRC-5 cells appear to be affected by three-dimensionality of the constructs, regardless the material used. For this reason, further analyses have been carried out using a different cell type in order to assess the potential role of jellyfish collagen in promoting or supporting cell adhesion and proliferation.



2

Figure 4.16: Metabolic activity of MRC-5 cells growth on 2D jellyfish collagen coating, Bovine type I collagen coating and standard tissue plate. AlamarBlue® assay was used to monitor cell proliferation during static culture at day 1 and day 5. Two-way ANOVA with Bonferroni correction.

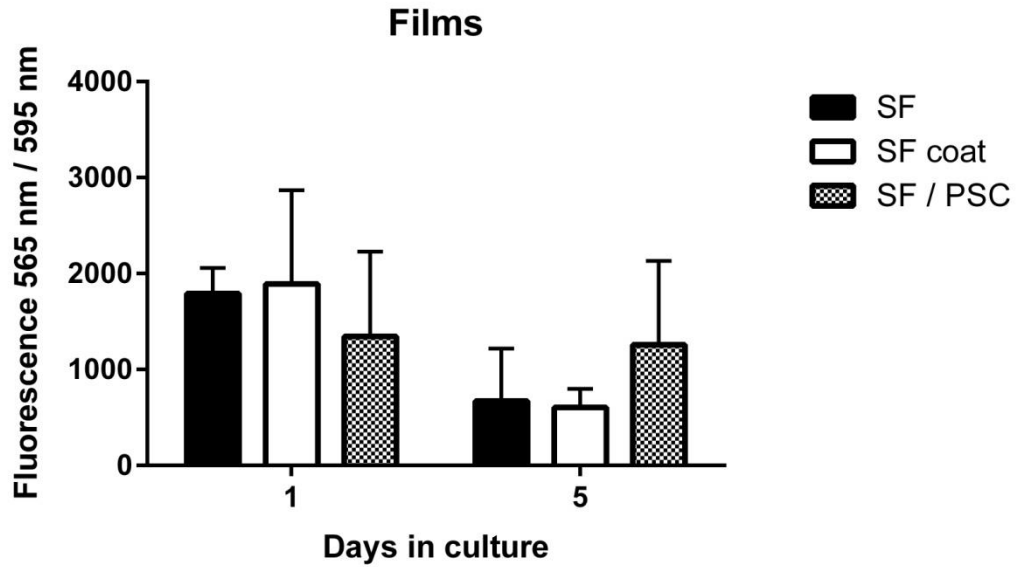


Figure 4.17: Metabolic activity of MRC-5 cells growth on silk fibroin film, collagen-coated silk fibroin film and silk fibroin/collagen film. AlamarBlue® assay was used to monitor cell proliferation during static culture at day 1 and day 5. Two-way ANOVA with Bonferroni correction.

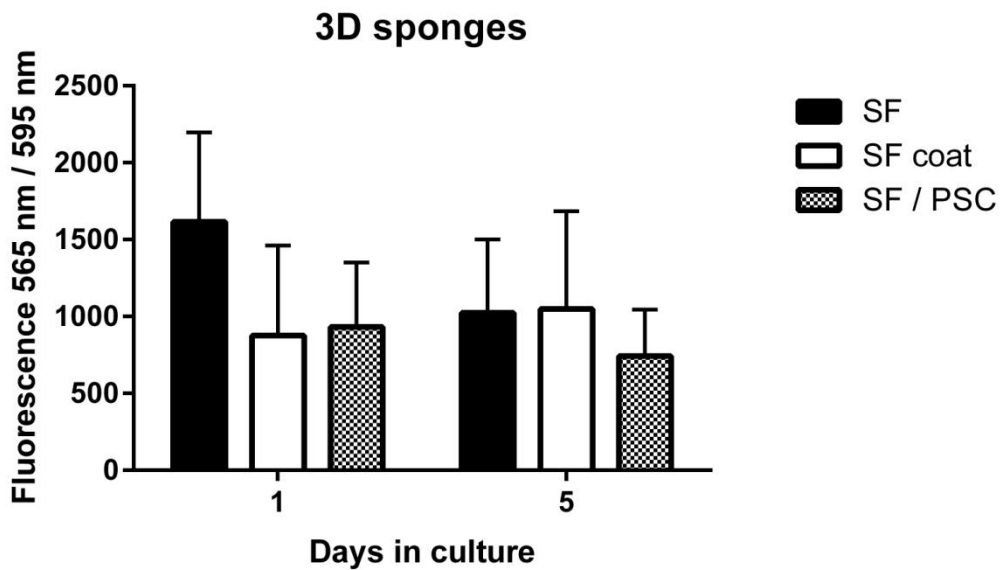


Figure 4.18: Metabolic activity of MRC-5 cells growth on silk fibroin 3D sponge, collagen-coated silk fibroin 3D sponge and silk fibroin/collagen sponge. AlamarBlue® assay was used to monitor cell proliferation during static culture at day 1 and day 5. Two-way ANOVA with Bonferroni correction.

## 4.5 Material evaluation on NIH 3T3 cell culture

The mouse embryonic fibroblast cell line (NIH 3T3) was utilized in the successive biological analysis as a good and representative model of fibroblast for cytotoxicity and cytocompatibility studies in the tissue engineering field.

The *in vitro* cytotoxicity of the marine collagen (pepsin soluble collagen, PSC) was investigated using fibroblast-like NIH 3T3 cells by LDH-based assay, which relies on fluorescence values emitted by Lactate Dehydrogenase, an enzyme released into the media as a marker of dead cells. The cytotoxicity results of the isolated collagen are shown in Figure 4.19. This cytotoxicity was compared with that of PBS, which represents the negative control, and Triton X-100, used as positive control. From the results is evident that cell mortality cultivated in presence of a concentration of 200  $\mu\text{g}/\text{mL}$  of collagen shows values comparable to physiological values reported in the negative control sample, whereas the positive control register high fluorescence values which indicate high cell death rate. These results confirm that the isolated jellyfish collagen is biocompatible and nontoxic in nature.

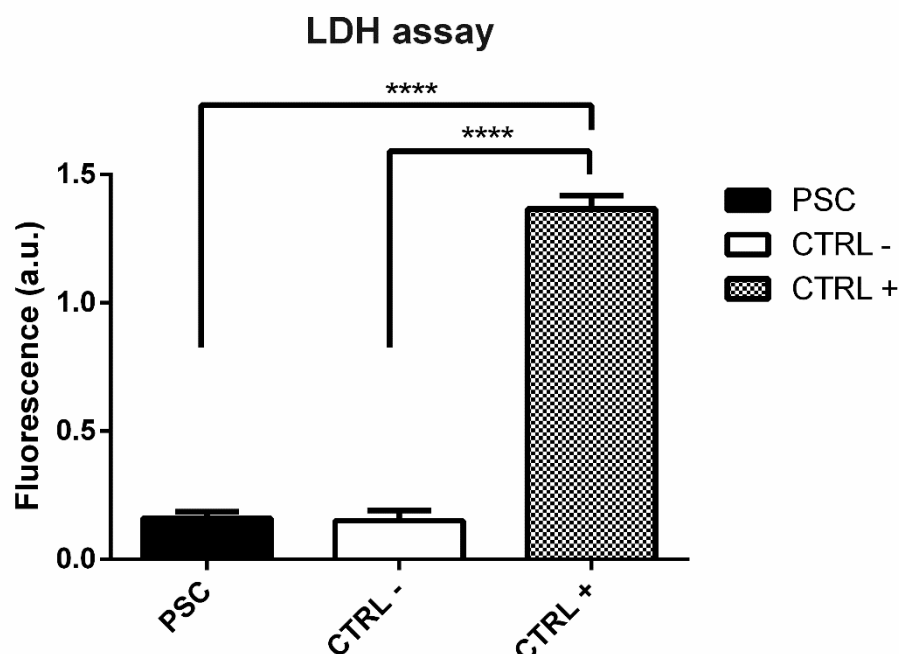


Figure 4.19: Cytotoxicity of pepsin soluble collagen isolated from *Rhopilema hispidum* jellyfish, tested by Lactate Dehydrogenase (LDH) Assay. One-way ANOVA with Bonferroni correction (confidence interval 95%).

NIH 3T3 cell monoculture was then used to evaluate the *in vitro* influence of the extracted jellyfish pepsin soluble collagen on metabolic activity, viability and cell proliferation by AlamarBlue® assay, viability analysis and DNA quantification (PicoGreen). In these studies, different experimental groups were analyzed. In particular, 2D cultures with jellyfish collagen well coating were used and compared with commercially available bovine type I collagen coating and standard tissue culture plates, as control. Additionally, films and 3D porous scaffolds composed by silk fibroin, jellyfish collagen coated silk fibroin and silk fibroin/collagen blend were fabricated, in order to discriminate which factors affect cell spreading and to verify the bioactive role of jellyfish collagen in promoting cell adhesion on silk fibroin scaffolds.

Cell proliferation was assessed using AlamarBlue® assay, which is based on a tetrazolium-based dye as oxidation–reduction indicator that yield colorimetric changes and a fluorescent signal in response to metabolic activity, which can be accurately measured.

Culturing cells on innovative material like jellyfish collagen, led to the necessity to check also cell viability. For this analysis, it was chosen to use the confocal laser microscope after staining with Calcein acetoxymethyl ester (AM) and Propidium Iodide. This because the analysis of samples stained with Calcein AM (viable cells) and Propidium Iodide (dead cells) not only allows to evaluate cell viability, but also to observe shape and three-dimensional cell distribution on the surface and inside the 3D like sponge scaffold. Successively cell distribution was observed by using the confocal laser microscope.

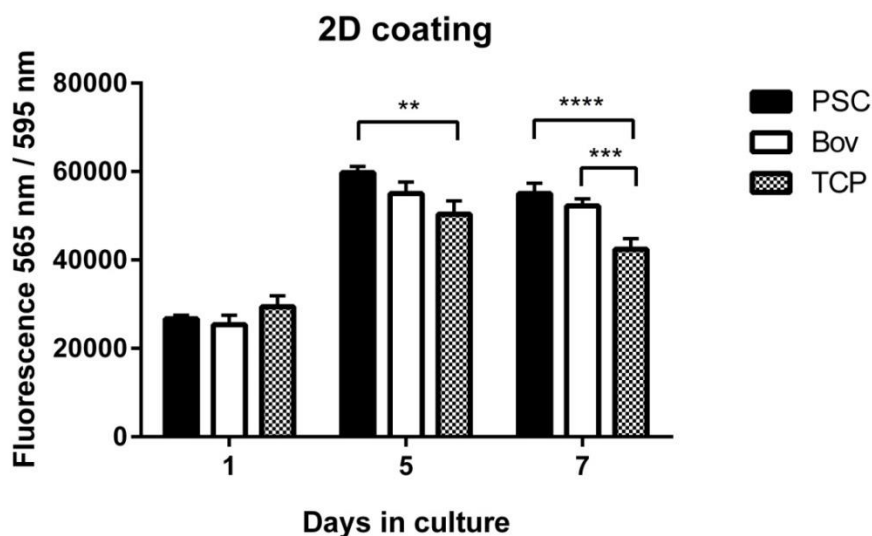


Figure 4.20: Metabolic activity of NIH 3T3 cells growth on 2D jellyfish collagen coating, Bovine type I collagen coating and standard tissue plate. AlamarBlue® assay was used to monitor cell proliferation

during static culture at 1, 5 and 7 days after cell seeding. Two-way ANOVA with Bonferroni correction (\*\* pvalue < 0.01, \*\*\* pvalue < 0.001, \*\*\*\* pvalue < 0.0001).

Based on the results of AlamarBlue® assay concerning 2D coating cell culture (Figure 4.20), the initial proliferation was substantially very high and comparable in all groups considered. After just 24 hours from cell seeding, fluorescence values were substantially high in both marine and bovine collagen coating well plates, as well as in the control, tissue culture well plate (TCP). These results reveal a rapidly growing of the cell type on two-dimensional substrates, including jellyfish collagen. The relative fluorescence difference of Alamar Blue between control sample and both collagen coating increased exponentially with time. The increase in Alamar Blue fluorescence with time was significantly higher for marine collagen coating than TCP on day 5, while metabolic activity on Bovine coating assumed an intermediate values between the two. At the last time point, 7 days, a plateau in the cell proliferation could be observed for all the samples produced. A plateau in dye reduction was produced with high cell densities and/or extended incubation times for the percentage of reduction, followed by a slight decline in fluorescence. However, the values of the AlamarBlue® assay of seeded marine and bovine collagen coating were higher than the control sample. This fact might be due to the presence of micro- and nano-roughness in the two-dimensional structure of the coating that provide to the cells a greater surface area on which to adhere and proliferate.

These observations were further confirmed by CLM imaging analyses after staining the seeded samples with Calcein AM and Propidium Iodide. Cell attachment, proliferation and viability are shown in Figure 4.21. In all the samples proliferation and cell migration increased with incubation time. At early time points scaffolds showed single, unorganized cluster of cells. At later time points, cells started to communicate each other and to interact. Therefore, they created a connected network and a morphological pattern, up to cover the entire surface of the well plate creating a sort of holes but always remaining in contact with each other. The qualitative results are almost comparable on all the constructs, at all the experimental time points.



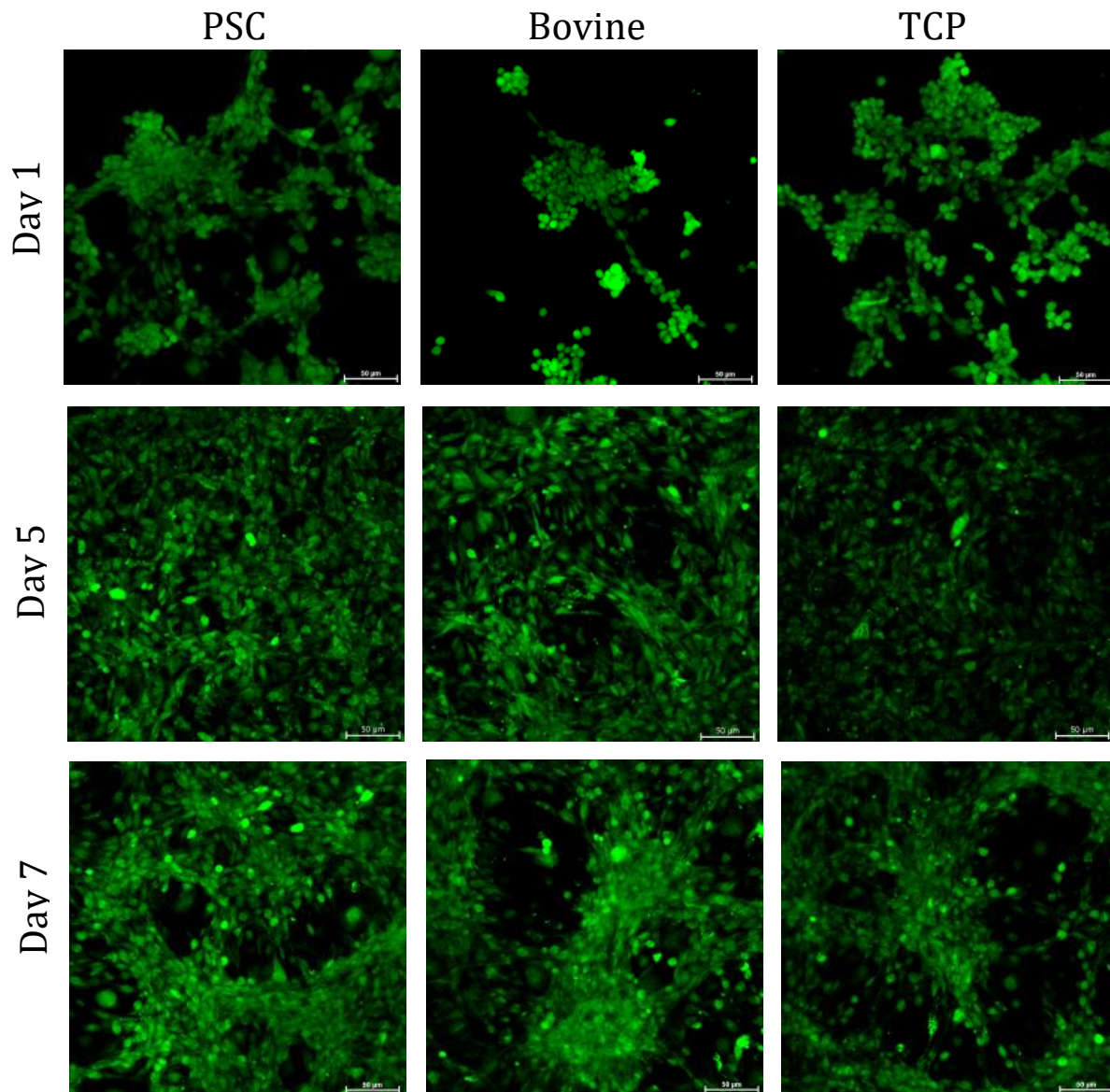


Figure 4.21: Viability test of NIH 3T3 cell monoculture seeded in 3 different conditions and observed with confocal laser microscopy. Viability for day 1, 5 and 7 was tested using the Calcein/propidium iodine test for 2D jellyfish collagen coating, Bovine type I collagen coating and TCP as control. Green color indicates viable cells, red color represents dead cells. Scale bar = 50 µm.

Proliferation rate of NIH 3T3 monoculture on different sample was also evaluated through the DNA quantification (PicoGreen) (Figure 4.22). At the first time point - day 1 - the number of cells was fluctuating around the same values. At day 5 great increase in cell number indicates higher amount of cell for all the sample analyzed, especially for jellyfish collagen coating

(PSC), followed by Bovine type I collagen (Bov) coating. At the last time point, the results reveal a plateau phase, because cell probably reached confluency in 2D samples, but significant higher value is reported for jellyfish collagen respect to Bovine and TCP constructs. Of particular interest the comparison between the isolated jellyfish and the commercially available bovine collagens. Data were analyzed using GraphPad Prism® software and the statistical test applied is the two-way ANOVA with Bonferroni correction for the multiple comparisons, in order to consider the variability linked to the specific material as well as the time point considered.

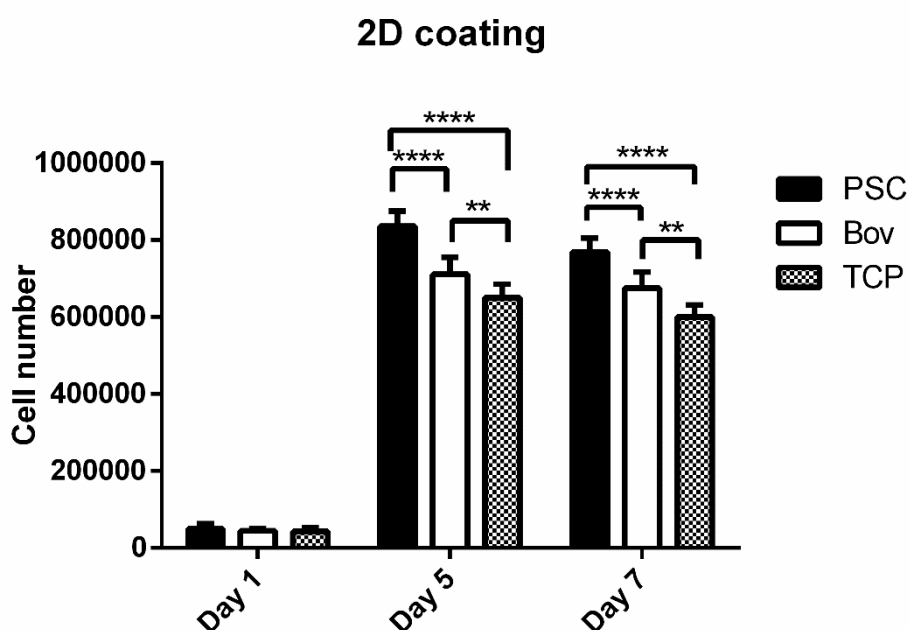


Figure 4.22: DNA quantification analysis through DNA content – PicoGreen, performed at 1, 5 and 7 days of NIH 3T3 monoculture growth on Jellyfish collagen well coating (PSC), Bovine type I collagen coating (Bov) and Tissue Culture Plate well (TCP). Two-way ANOVA with Bonferroni correction (\*  $p < 0.05$ ; \*\*  $p < 0.01$ ; \*\*\*  $p < 0.001$ ; \*\*\*\*  $p < 0.0001$ ).

While the bulk structure and properties of cast fibroin and fibroin/collagen films are of significant importance, the surface characteristics appear to be equally important, especially in connection with growing interest in biomedical applications of the films. The surface properties of a material are key factors controlling the interactions that occur when it is exposed to biological environments. The proliferation of NIH 3T3 cells seeded on silk fibroin film, jellyfish collagen coated silk fibroin film and jellyfish collagen/silk fibroin film was evaluated on day 1, day 5 and day 7 using AlamarBlue® assay (Figure 4.23), where cell proliferation is proportional to the collected fluorescence signal. As first consideration, we can

observe how the fluorescence values related to film-like scaffolds appear significantly lower when compared to that of the 2D coating well plates. This result could be due to the fact that film was treated as a 3D scaffold during manufacturing process and cell seeding. Additionally, it presents a substantially flat and smooth surface, on which adhesion might take more time. For these reasons, it might be possible that detachment of a greater number of cells was favoured and/or not well adherent cells were washed away. However, fibroblasts in contact with collagen coated SF construct proliferate significantly after just 24 hours of culture, when compared with the other two samples (Figure 4.23). This evidence might be attributable to the presence, on the surface of the construct, of the jellyfish collagen as bioactive component able to promote cell adhesion. At day 5, the relative fluorescence difference of Alamar Blue between the samples is retained and also in this case cells seem to prefer adhering and growing on the collagen coated fibroin film, as their number increased a lots. At day 7 of cell culture, the growth profile is comparable to the previous time points, with fluorescence value significantly greater for the collagen coated fibroin film than the other two samples (Figure 4.23).

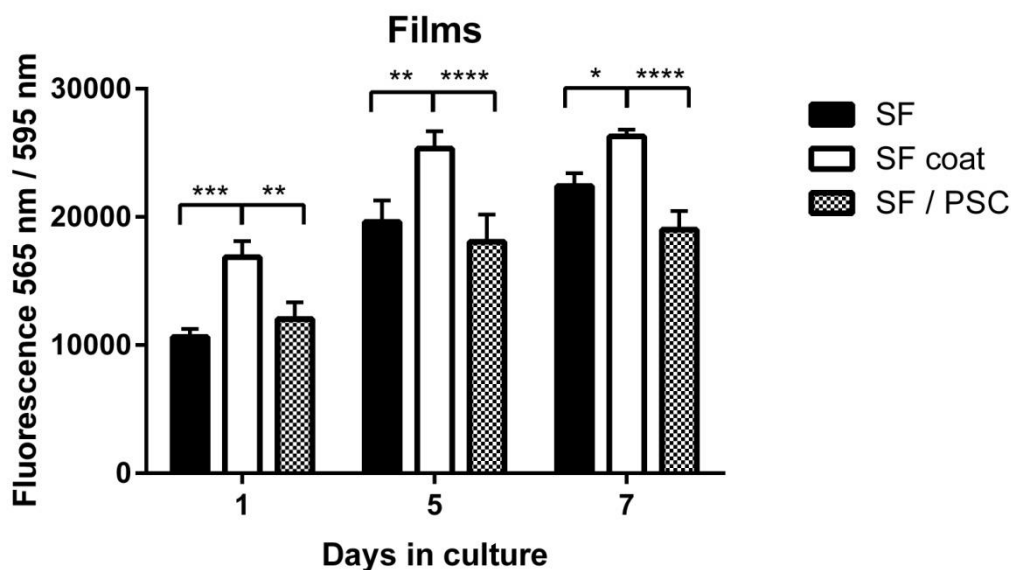


Figure 4.23: Metabolic activity, which is proportional to cell proliferation, of NIH 3T3 cells growth on silk fibroin film, collagen-coated silk fibroin film and collagen/silk fibroin film. AlamarBlue® assay was used to monitor cell proliferation during static culture at 1, 5 and 7 days after cell seeding. Two-way ANOVA with Bonferroni correction \* pvalue < 0.1, \*\* pvalue < 0.01, \*\*\* pvalue < 0.001, \*\*\*\* pvalue < 0.0001.

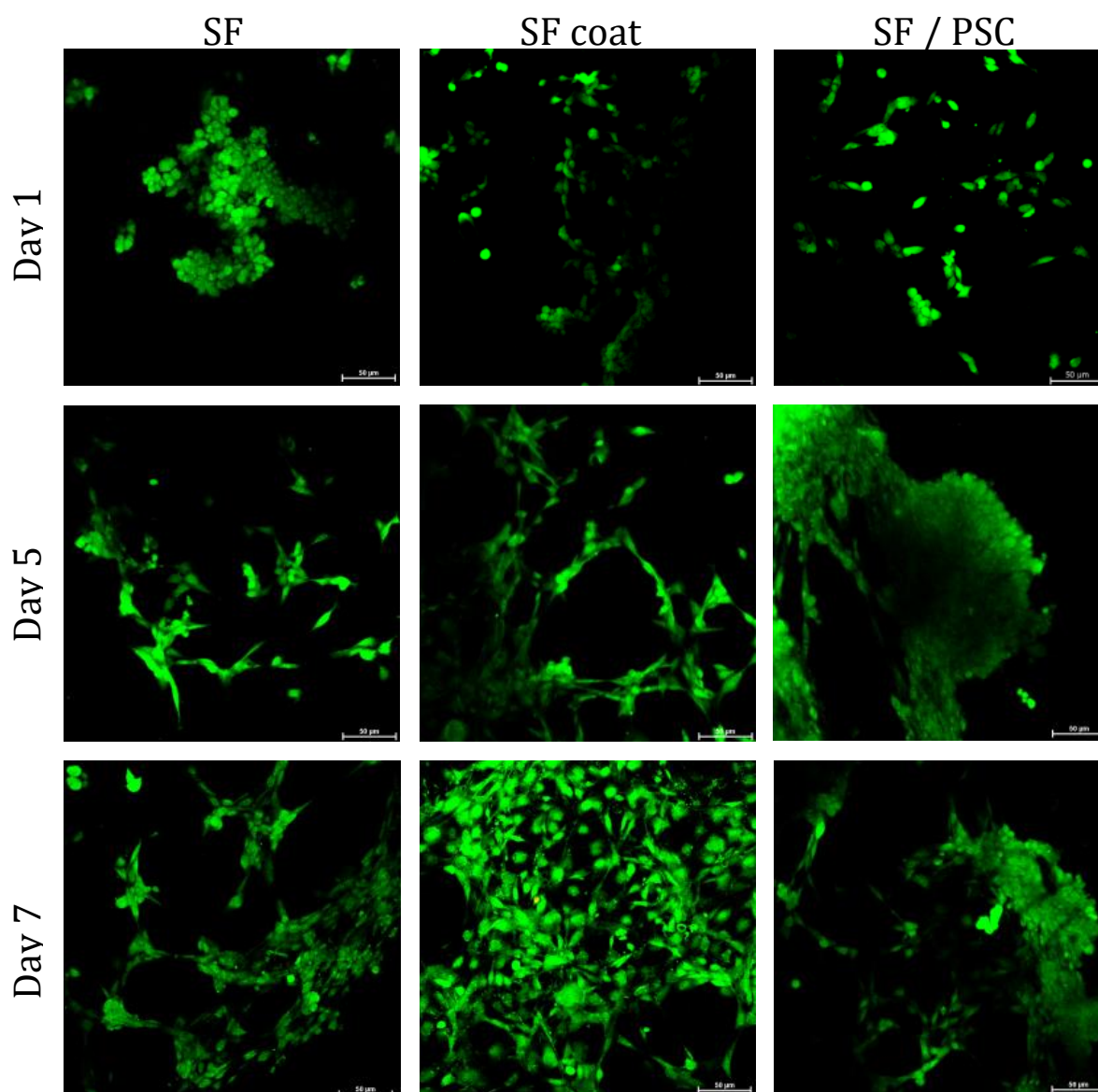


Fig. 4.24: Viability test of NIH 3T3 cell monoculture seeded in 3 different conditions and observed with confocal laser microscopy. Viability for day 1, 5 and 7 was tested using the Calcein/propidium iodine test for silk fibroin film, collagen-coated silk fibroin film and silk fibroin/collagen film. Green color indicates viable cells, red color represents dead cells. Scale bar = 50 µm.

These metabolic activity results are further confirmed by qualitative imaging analysis after staining with Calcein AM and Propidium Iodide (Figure 4.24).

After 24 hours from cell seeding, NIH 3T3 cells seeded on silk fibroin film tend to aggregate with each other and form clusters, whereas on films composed also by marine collagen they are more spread and start to migrate over the whole surface available. At later time points, cells start to interact and proliferate on all the constructs. However, on silk fibroin film cells appear less spread out and always in lower numbers. On fibroin plus collagen films, cells show a more developed and spread out cytoskeleton compared with fibroin sample where they are

more isolated and have primarily spherical shapes. These morphology and greater proliferation are particularly evident on collagen coated silk fibroin film (Figure 4.24).

However, in general the distribution of NIH 3T3 cells was less homogeneous with respect to what was found previously with these cells seeded on 2D samples.

Proliferation rate of NIH 3T3 monoculture on the different film matrices was evaluated through the DNA quantification (Figure 4.25). At the first time point – days 1 – the number of cells was fluctuating around the same low values. At day 5 and 7 great increase in cell number indicates high amount of cell for all the film considered, with no statistical differences between samples. In the jellyfish collagen coated fibroin substrate the superficial bioactive component could leave the flat surface of film, probably due to the instability of collagen its. Moreover, in the silk fibroin/collagen blend, the weight ratio of 20% represented by jellyfish collagen are not sufficient or not bio-available for cell in order to promote their adhesion and proliferation.

Data were analyzed using GraphPad Prism® software and the statistical test applied is the two-way ANOVA with Bonferroni correction for the multiple comparisons, in order to consider the variability linked to the specific material as well as the time point considered.

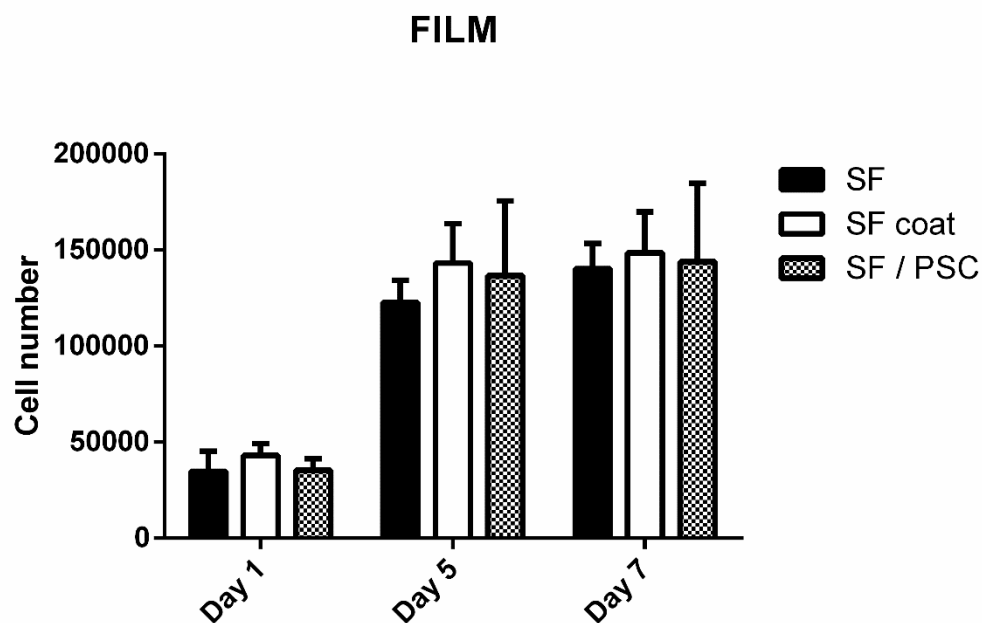


Figure 4.25: DNA quantification analysis through DNA content – PicoGreen, performed at 1, 5 and 7 days of NIH 3T3 monoculture growth on silk fibroin film, jellyfish collagen coated fibroin film, and silk fibroin/collagen film. Two-way ANOVA with Bonferroni correction (\*  $p < 0.05$ ; \*\*  $p < 0.01$ ; \*\*\*  $p < 0.001$ ; \*\*\*\*  $p < 0.0001$ ).

Since the resulting fluorescence of the AlamarBlue® assay is proportional to the number of viable cells in the sample, proliferation of NIH 3T3 cells on the different types of freeze dried 3D sponges could be also assessed and they are shown in Figure 4.26.

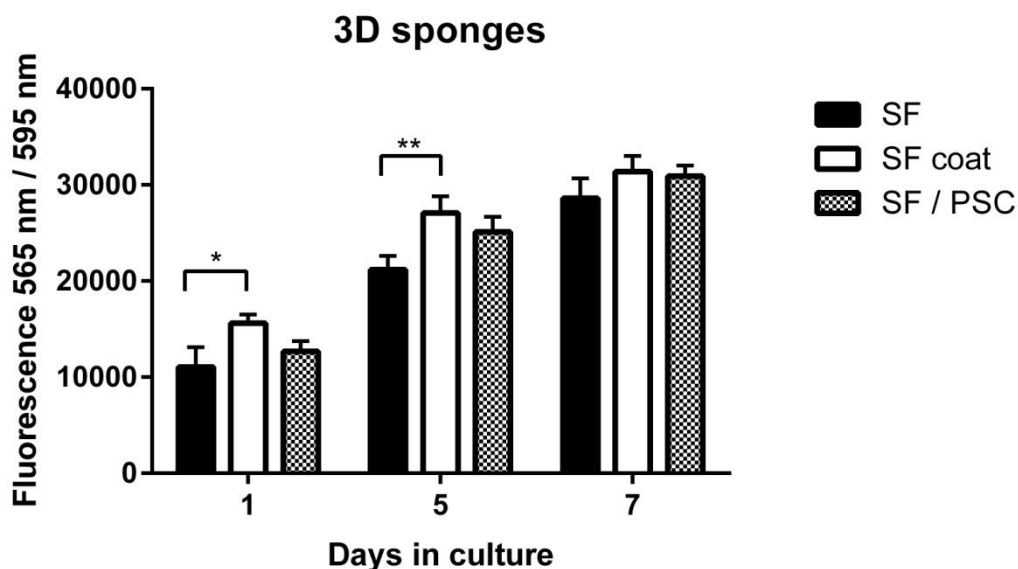


Fig. 4.26: Metabolic activity, which is proportional to cell proliferation, of NIH 3T3 cells growth on silk fibroin sponge, collagen-coated silk fibroin sponge and silk fibroin/collagen sponge. AlamarBlue® assay was used to monitor cell proliferation during static culture at 1, 5 and 7 days after cell seeding. Two-way ANOVA with Bonferroni correction (\* pvalue < 0.1, \*\* pvalue < 0.01).

The cell density used for these constructs was much greater than that used for seeding of 2D well coating and films. The reason for this choice lies in the fact that 3D like sponge structures offer less favorable environmental to cell adhesion. However, at day 1 of cell culture the results reveal fluorescence values comparable to those related to films. Even in the case of 3D scaffolds, the collagen coated fibroin sponge presents values of metabolic activity significantly higher than fibroin and fibroin/collagen sponges, which indicate stronger and more favourable adhesion of cells on this type of construct (Figure 4.26). At day 5, the relative fluorescence difference of Alamar Blue between samples is retained and significantly greater proliferation could be observed on collagen coated fibroin scaffold. At the last time point, 7 days, unlike the previous studied 2D samples, fluorescence values on all 3D groups significantly increase (Figure 4.26).

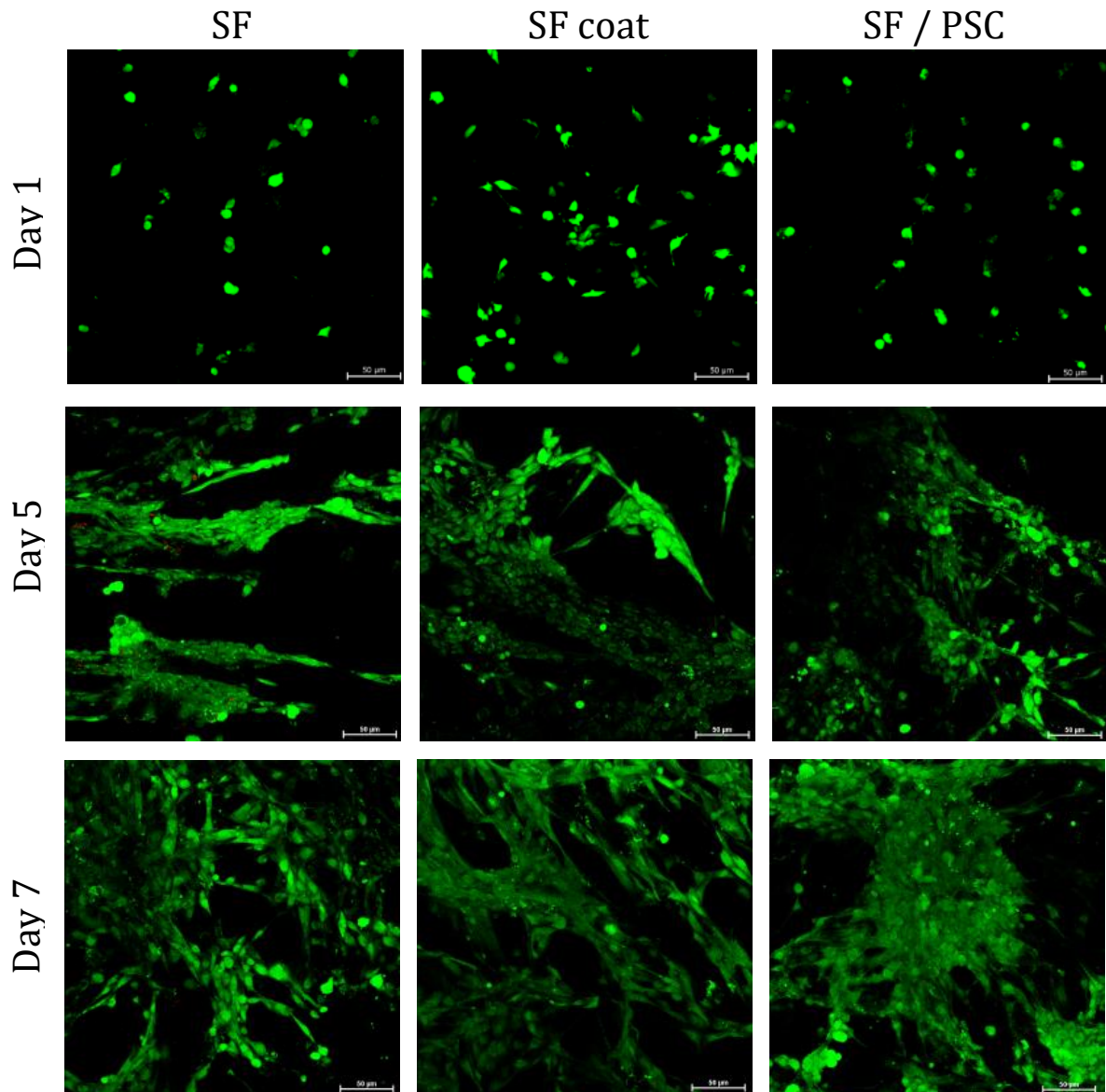


Fig. 4.27: Viability test of NIH 3T3 cell monoculture seeded in 3 different conditions and observed with confocal laser microscopy. Viability for day 1, 5 and 7 was tested using the Calcein/propidium iodine test for silk fibroin sponge, collagen-coated silk fibroin sponge and silk fibroin/collagen sponge. Green color indicates viable cells, red color represents dead cells. Scale bar = 50  $\mu\text{m}$ .

The lack of a marked plateau phase could be explained by the three dimensional morphology of sponges, which allow cell migration in the three dimensions of the construct and prevent contact inhibition. These make such a construct the best model in order to better adhesion, proliferation and cell migration.

The viability of fibroblasts on fibroin, collagen coated fibroin and fibroin/collagen sponges after 1, 5 and 7 days of culture was then assessed using a Live/Dead analysis and confocal laser microscopy. The collected images for SF, SF coat and SF/PSC samples are reported in Figure 4.27. At the same time, a very high seeding density is achieved with all the 3D scaffolds

even after 5 days of culture. Freeze dried sponges, at the first analyzed time point, show cell distribution mainly on the outer surface, where cells were previously seeded. Afterward, cells start invading scaffold pores and adhering to the matrix. Furthermore, at longer culture time, a deeper migration of cells inside and between the pores is visible until they populate all scaffolds throughout their volume, since live cells are detected also almost in the center of each sample. We could therefore suggest that pore sizes are large enough to permit ingress of cells, with concurrent bridging of cells between pore walls. Confocal microscopy results also give a view of cell-cell and cell-material interactions. At the last time point, cells appear well attached on all the constructs, but with slightly different adhesion morphology and distribution. Interestingly, cells seem to prefer to bridge between pore walls so that a new architecture is formed (Figure 4.27).

Proliferation rate of NIH 3T3 cells on the sponge-like constructs was evaluated through the DNA quantification (PicoGreen assay) (Figure 4.28). At the first time points – day 1 – the number of cells was fluctuating around the same values on the all sample analyzed. At day 5 initial great increase in cell number indicates higher amount of cell for the collagen coated fibroin scaffold, followed by the pure fibroin scaffold and fibroin/collagen blend. At day 7 in all the samples the number of cells little increase showing with collagen coated SF sponge showing significant difference with the other two samples in promoting fibroblast adhesion and proliferation. Data were analyzed using GraphPad Prism® software and the statistical test applied is the two-way ANOVA with Bonferroni correction for the multiple comparisons, in order to consider the variability linked to the specific material as well as the time point considered.



## SPONGE

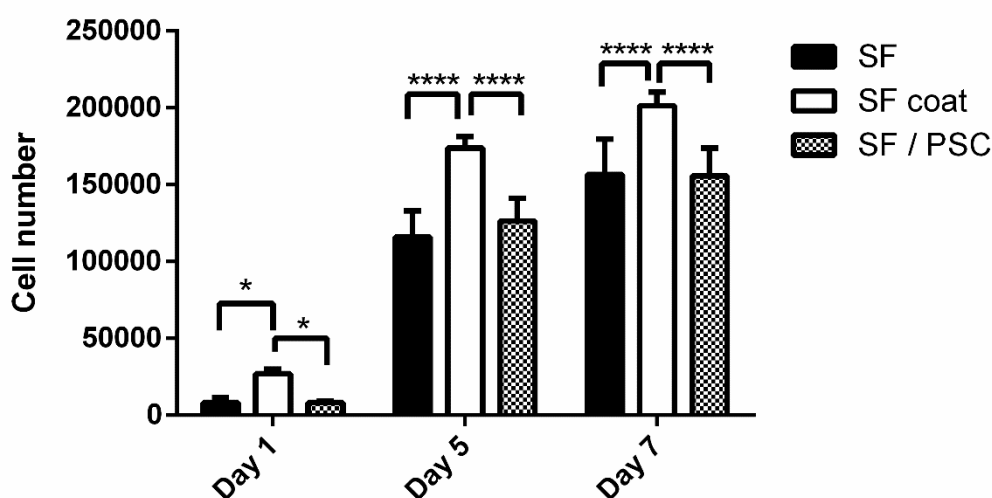


Figure 4.28: DNA quantification analysis through DNA content – PicoGreen, performed at 1, 5 and 7 days of NIH 3T3 monoculture growth on silk fibroin sponge, jellyfish collagen coated fibroin sponge, and silk fibroin/collagen sponge. Two-way ANOVA with Bonferroni correction (\*  $p < 0.05$ ; \*\*  $p < 0.01$ ; \*\*\*  $p < 0.001$ ; \*\*\*\*  $p < 0.0001$ ).

In the end, a morphological analysis by using scanning electron microscopy (SEM), following the protocol for the biological sample chemical fixation, through a treatment with glutaraldehyde and cacodylic buffer, was performed as a qualitative analysis to confirm the presence of cells on fabricated scaffolds. The samples selected for this study are the scaffolds that showed the best performing in the previous biological evaluations: film and sponge of silk fibroin with marine collagen coating. This analysis was carried out after the seventh day of AlamarBlue® assay with NIH 3T3 cell line. An advantage that offer this assessment is the ability to observe clearly the interactions between cells and the material, unlike from Live/Dead analysis, which highlights cell behavior only. The Figure 4.29 underline the different conformation of two scaffolds, showing a ordered cell arrangement for the film, typical of cells seeded on 2D surfaces, whereas a more chaotic distribution in the sponges, so creating morphological artifacts into the matrix and in cell morphology as well. However, this is an expected result, since cell adhesion is more difficult on porous and not-regular surfaces. SEM images show in all samples differences in morphology with very heterogeneous structures within them and complicated structures can be determined. Unfortunately, through these images it is impossible to understand if the structures are related to a characteristic of the sample or the structures are just artifacts induced by the fixation protocol. For those

reasons data analysis will be not included into the discussion part, but just reported in the results section.

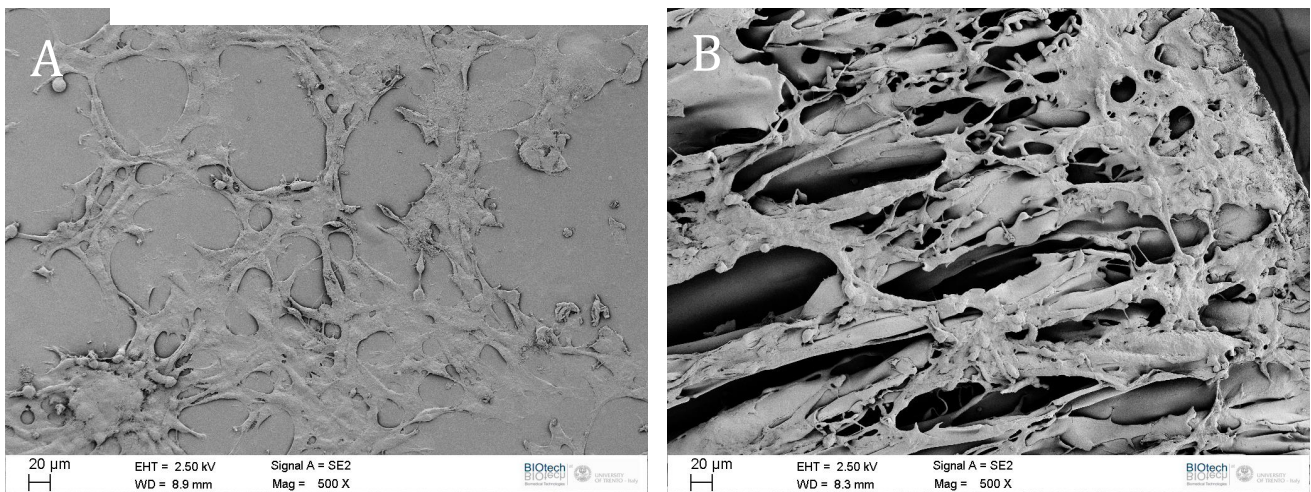
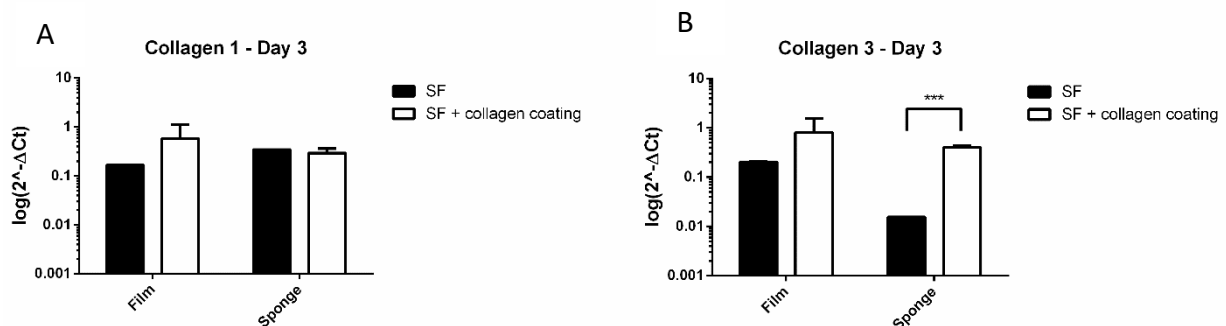


Figure 4.29: Scanning electron microscopy of NIH 3T3 culture on collagen-coated silk fibroin film (A) and collagen-coated silk fibroin sponge (B). Images were acquired 7 days after cells seeding, at the same magnification.

## 4.6 Collagen expression and assembly

The ability of pepsin soluble collagen (PSC), as superficial coating in 3D fibroin sponges, to induce the production of collagen type I and collagen type III in NIH 3T3 cells, was assessed by gene expression analysis through quantitative Real Time Polymerase Chain Reaction (qRT-PCR) at three time points: 3, 7 and 14 days after seeding. Both fibroin films and sponges were coated with PSC collagen and compared with the non-coated fibroin samples. At each time point, the RNA was extracted and retro-transcribed, and eventually analysed by real-time PCR in a 384-well plate format. The results are shown in Figure 4.30.



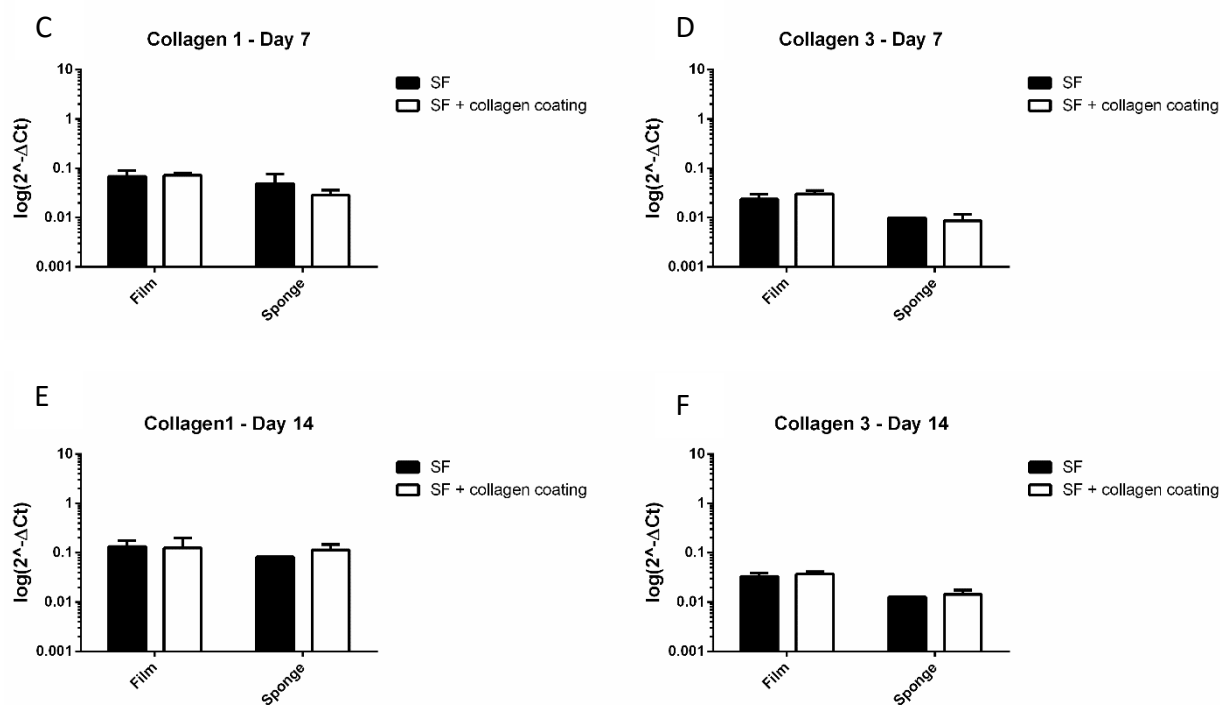


Figure 4.30: Quantification through quantitative Real Time Polymerase Chain Reaction (qRT-PCR – Gene expression) of the Collagen 1 and Collagen 3 transcripts produced at day 3, 7 and 14 by the NIH 3T3 cells, seeded on silk fibroin scaffolds and collagen coated silk fibroin scaffold. The values are relative to the expression of the RPS18 housekeeping gene. Unpaired T-test, confidence level 95% (\* $p < 0.05$ ; \*\* $p < 0.01$ ; \*\*\* $p < 0.001$ ; \*\*\*\* $p < 0.0001$ ).

As it can be observed from the plots, at day 3 there is an increase in collagen III expression in the PSC-coated sponge. A difference in expression is observed also in the coated films during the first three days, even if it is not statistically significant, due to the high variability within the biological replicates. This inconstancy between replicates could mainly be due to two reasons: the unevenness and the instability of the coating. During crosslinking, the fibroin fibers arrange in a way that leads to the formation of crystalline and amorphous parts, which will interact differently with the jellyfish collagen. Therefore, there is a substantial difference between the samples surfaces, which is reflected by a difference in cell behaviour. Moreover, the collagen coating seems not to be stable: in fact, at days 7 and 14 there are no more differences between the coated and the non-coated samples. It is likely that the PSC coating gradually dissolved in the cell culture medium, and was drew during media changes.

As it can be seen from DNA content data (Figure 4.22 and 4.28), the PSC coating improves cell adhesion and proliferation both on 2D TCP and sponges. We therefore hypothesize that the PSC coating could also enhances the production of Collagen I and III by NIH 3T3 cells, as it is

also suggested by our preliminary data. However, this hypothesis needs to be tested by stabilizing the coating in order to impair its dissolution in the cell culture medium.

Type I and type III collagens are synthesized by fibroblasts and are considered as major biomarkers in the wound healing process. In particular, type I collagen is the most abundant type of collagen in normal dermis (approximately 80% to 90%). During the early stages of wound healing, fibroblasts actively produce type III collagen, which may account for 30% of the collagen in a healing wound. By week 2, type I collagen again becomes the principal collagen produced by fibroblasts. The presence of these markers and their specific assembly in the collagen coated fibroin 3D sponges were tested with the relevant primary and secondary antibodies and then compared with the non-coated fibroin samples. The immunocytochemistry of 3D constructs seeded with NIH 3T3 fibroblasts at days 3, 7 and 14 is shown in Figure 4.31. A fluorescent DAPI was used to stain NIH 3T3 nuclei.

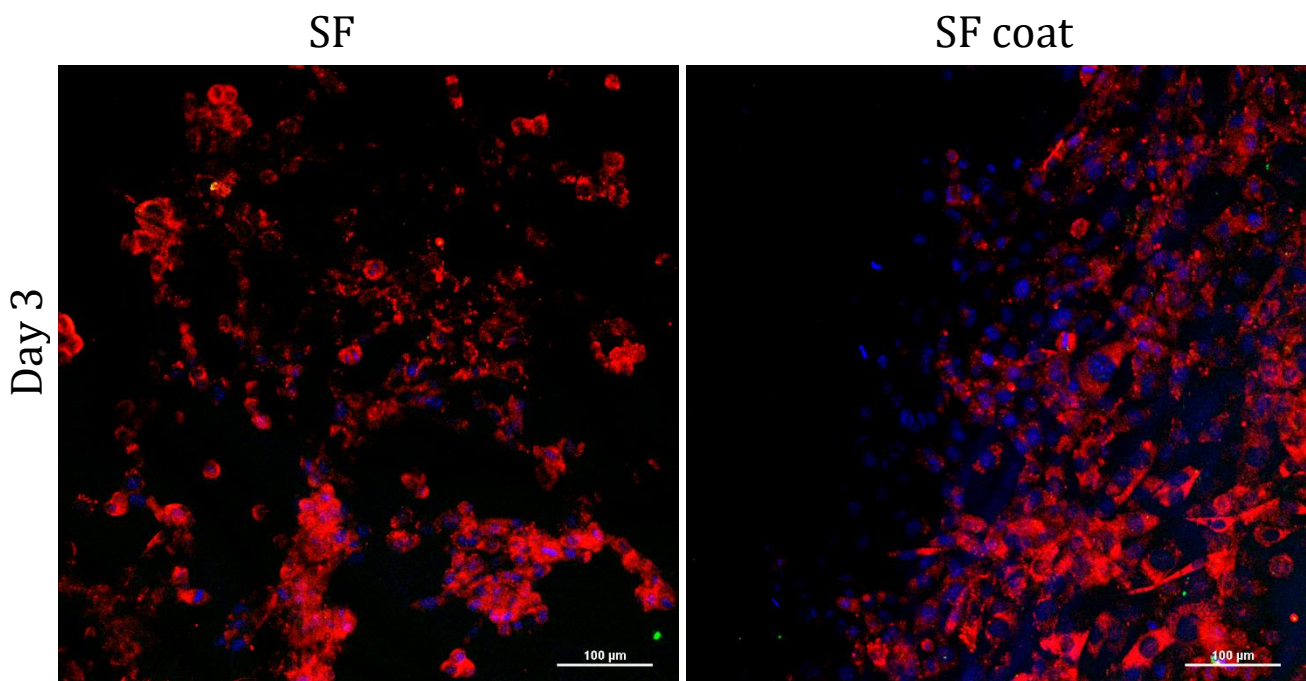
For what concerns film-like scaffolds at day 1 (Figure 4.31), the constructs considered not show substantial differences linked to type III collagen (red color), which represents the most present in both constructs with respect to type I collagen (green color) that is instead almost absent. It is possible to observe a different morphology assumed by NIH 3T3 cells, which change organization creating nearly homogeneous single layer on collagen coated SF film but denser region and less homogeneous background layer on SF film. This observation might be due to the presence of collagen on the surface, which could promote cell adhesion. At day 7, the results show substantial changes in the ECM molecules synthesis, especially on collagen coated SF construct, on which fibroblasts, together with type III collagen, start producing type I collagen, which represents the most abundant type of collagen in normal dermis. On the contrary, on silk fibroin film the type III collagen remains the most plentiful ECM marker. At the last time point, synthesis and secretion of type I collagen further increase on collagen coating matrix and seems to induce cells to assume particular conformations. Collagen I results, instead, almost absent on fibroin film and the same is reported for type III collagen.

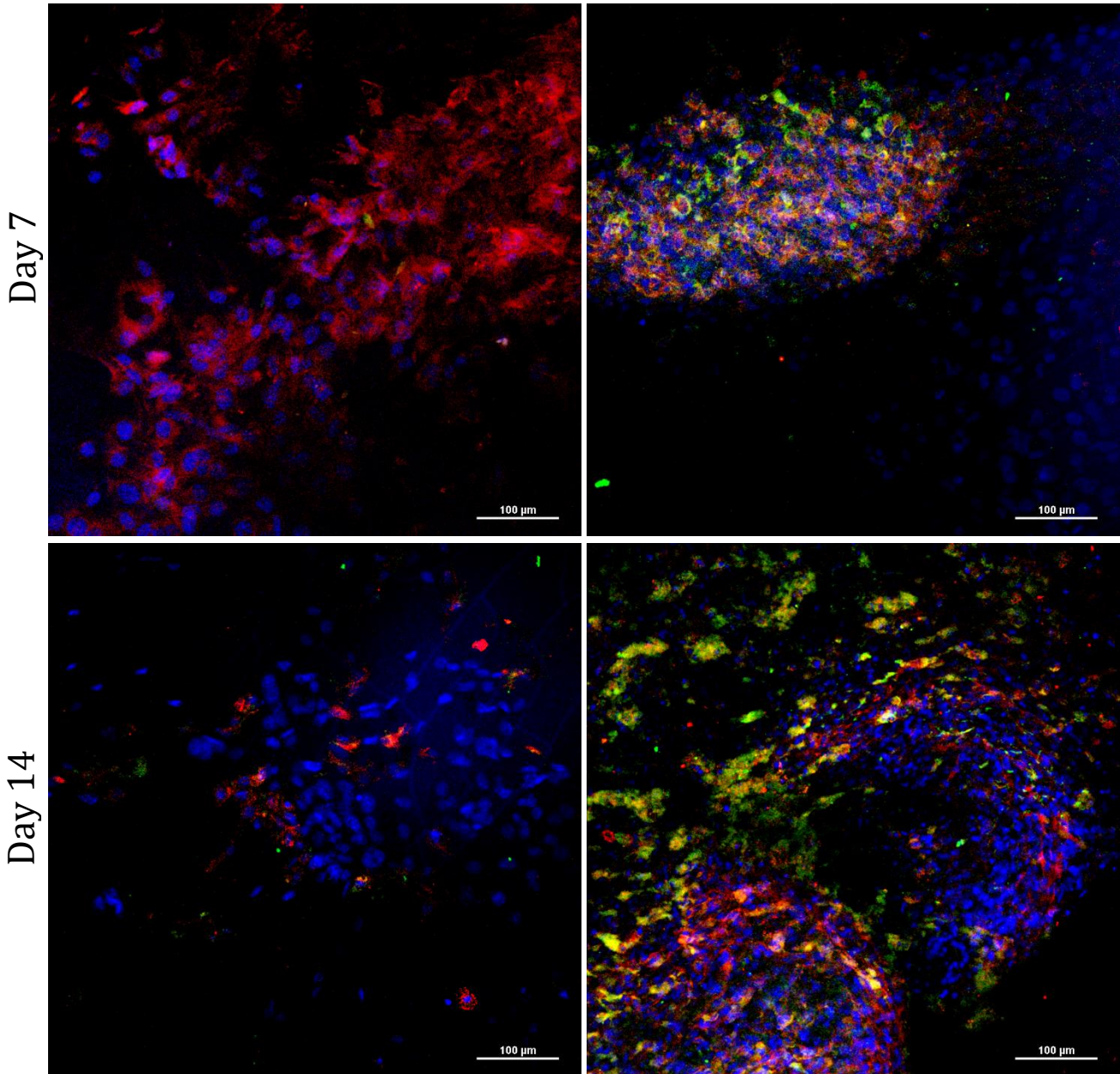
Observing the immunocytochemistry results for 3D-like sponge (Figure 4.32) at day 1, the images are similar to those revealed for films, where fibroblasts tend to form clusters on silk fibroin sponge and this lower adhesion is reflected in a lower collagens synthesis, for both

type I and type III collagen. Scattered type III collagen staining is detected most in collagen coated fibroin sponge.

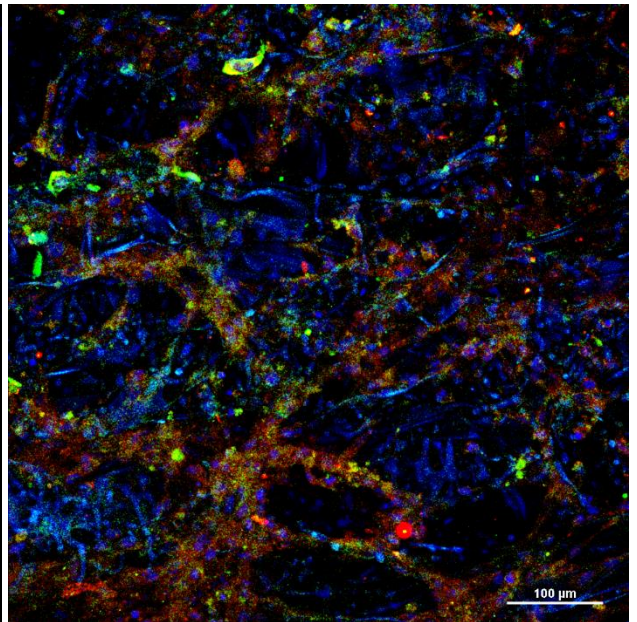
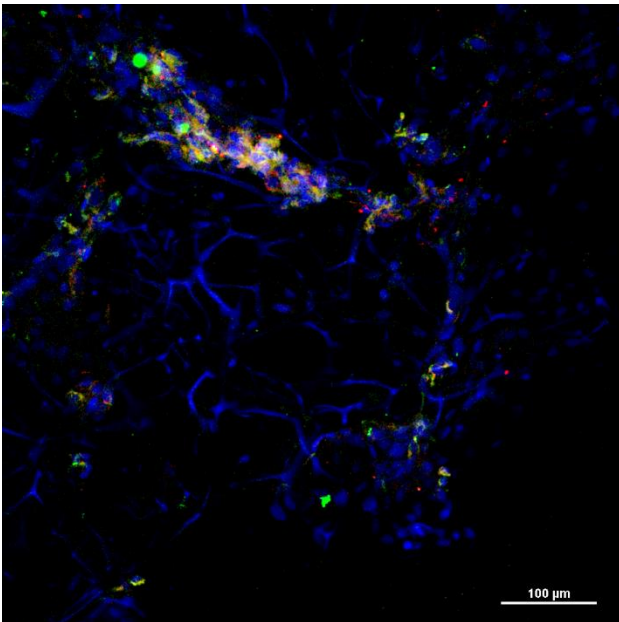
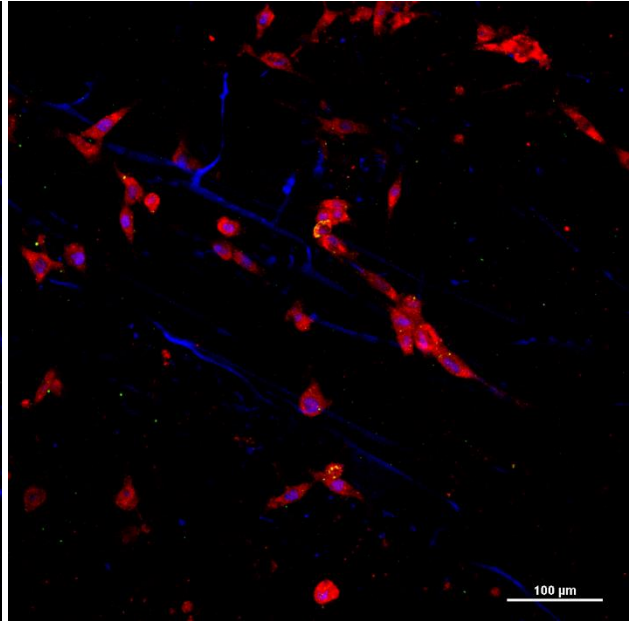
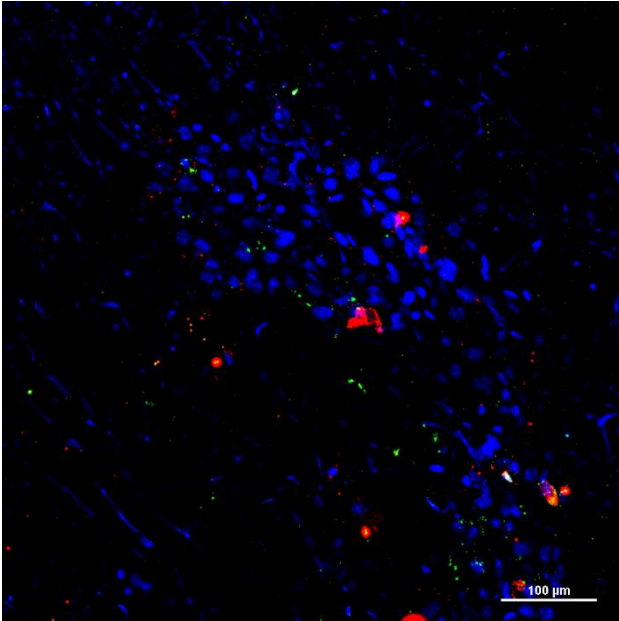
At day 7, as revealed in film-like samples, NIH 3T3 cells, grown on collagen coated SF sponge, start producing type I collagen as ECM specific fibroblast marker, which co-localize with type III collagen, whereas on SF sponge persists mainly type III collagen. At day 14, type I collagen synthesis further increases by fibroblasts seeded on collagen coated fibroin sponge and particular evident results the formation of ordered structures, which follow the scaffolds shape.

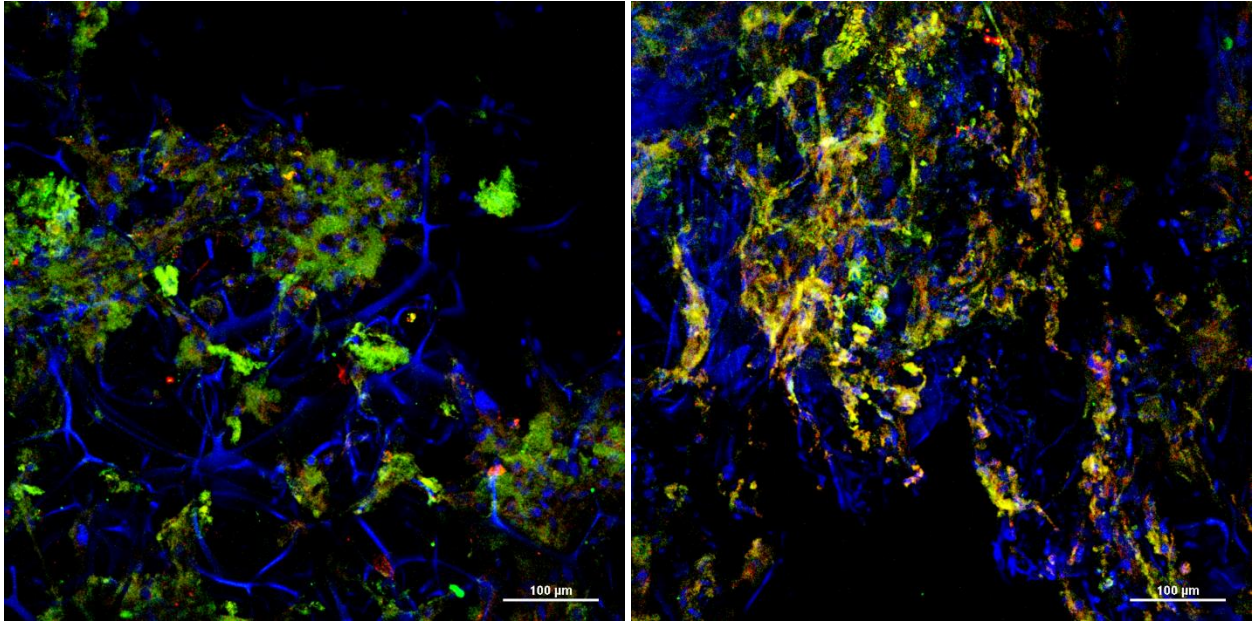
In conclusion, addition of collagen like coating to the silk fibroin scaffolds not only improves cell viability and proliferation of SF scaffold as previously reported but also greatly affects on the biological properties of fibroblast cultivation, especially the correct type III and type I collagen deposition, which represents the sequential ECM biomarkers during the early and less early stages of wound healing process.





Confocal microscopy images for NIH 3T3 monoculture, growth on silk fibroin films and jellyfish collagen coated fibroin films, were investigated at day 3, 7 and 14 for Collagen type I and Collagen type III synthesis. Green-labeled secondary antibody (Alexa 488) was used against the Collagen type I and red-labeled secondary antibody (Alexa 594) was used for Collagen type III. Blue DAPI was used to label NIH 3T3 nuclei. Scale bar: 100  $\mu\text{m}$ .





Confocal microscopy images for NIH 3T3 monoculture, growth on silk fibroin sponge and jellyfish collagen coated fibroin sponge, were investigated at day 3, 7 and 14 for Collagen type I and Collagen type III synthesis. Green-labeled secondary antibody (Alexa 488) was used against the Collagen type I and red-labeled secondary antibody (Alexa 594) was used for Collagen type III. Blue DAPI was used to label NIH 3T3 nuclei. Scale bar: 100  $\mu\text{m}$ .

## 5. Conclusion and future perspectives

In this study, we managed to optimize collagen extraction protocol from dried *Rhopilema hispidum* jellyfish, obtaining sufficient material for scaffolds fabrication. After several attempts, the yields assumed significant values, reaching 2.9 and 3.1%, for the pursuit of the study. It was then necessary to characterize the isolated collagen, studying its molecular weight, its conformational structure, its thermal properties and its amino acid composition. The results revealed molecular weight comparable to bovine type I collagen, the existence of triple helical arrangements, its fair closeness in  $T_d$  (denaturation temperature) and amino acid composition with mammalian collagen.

Silk fibroin, a natural fibrous biopolymer, was also used in this specific work with the final objective of skin replacement fabrication.

Instead of introducing a chemical or physical crosslink, jellyfish collagen coated silk fibroin construct and marine collagen/silk fibroin blend were used in order to produce water-stable scaffolds. Chemically and morphologically different types of scaffolds, such as Tissue Culture



Plate-well coating, film and 3D sponge, were produced in order to discriminate which factors affected cell adhesion and growth. The conformational structures and the thermal properties of films and 3D sponges were quite comparable. The sponge morphology represents the main constructs investigated for a possible application in wound healing process as wound dressing or tissue templates. In particular, we successfully developed collagen coated silk fibroin 3D sponge using a freeze drying technique without methanol treatment. This scaffold exhibited a high porosity, an interconnected pore structure and high water adsorption, which could provide better environment for cell proliferation. Additionally, its specific morphology resulted suitable to mimic the functional and physiological structure of the skin. The final step of this project focused on the preliminary *in vitro* biological evaluations, in order to understand if these scaffolds, especially sponges, were suitable for cell adhesion and growth. *In vitro* cell viability and proliferating studies, using jellyfish collagen well coating, revealed that jellyfish collagen did not induce any significant cytotoxic effect and had higher cell viability than other biomaterials, including bovine type I collagen. MRC-5 and NIH 3T3 fibroblast monocultures, grown on film- and sponge-like structures, highlighted promising properties for collagen coated silk fibroin films and sponges, such as biocompatibility and the ability of marine collagen in promoting cell adhesion and proliferation, when compared with silk fibroin and silk fibroin/collagen scaffolds.

In conclusion, Jellyfish collagen should be a true alternative source for replacing bovine or human collagens in selected biomedical applications, thanks to its good *in vitro* biological properties and its bioavailability. Additionally, this marine species presents a distinct advantage as a lower known risk of transmission to human of infection-causing agents and is thought to be far less associated with cultural and religious concern regarding the human use of marine derived products.

For these reasons, it would be necessary to focus on better characterization of the extracted collagen, performing several tests such as mass spectrometry to identify amount and type of chemicals present in a sample and solid phase NMR, a specific technique to investigate the triple helix conformation. It would be also important to understand if 3D fabricated scaffolds are the best solutions as possible applications in wound healing process and if collagen coating could be stabilized through some chemical-physical technique. Additionally, the results of this study provide the foundation for a novel multicomponent approach wherein other biopolymers can be added in fibroin and collagen blend solutions to generate different scaffolds with synergistic properties. After that, more stringent biological evaluations are

necessary in order to observe the real ability of the scaffolds in mimicking specific skin functions. Additional research on scaffold is needed because, as engineering of skin tissue continues to grow, so will the need for tissue-specific scaffolds. In the nearly future, scaffolds will become more sophisticated, supplying cells in all their needs. Future developments will gain more insight into the complexity of interactions of cytokines and cells on the cellular level involved in the wound healing process. At the end, the hypothesis to advance current skin grafting technologies using autologous derivable stem or progenitor cells that possess the potential to generate skin and its appendages might be a promising approach in order to regenerate injured skin.

## Acknowledgement

I would never have been able to finish my dissertation without the guidance of BIOtech laboratory members, help from my friends, and support from my family and, especially, my boyfriend and Sabrina.

# Bibliography

- [1] Paul A.J. Kolarsick, BS, Maria Ann Kolarsick, MSN, ARNP-C, Carolyn Goodwin, APRN-BC, FNP (2011) Anatomy and Physiology of the Skin. Journal of the Dermatology Nurses' Association: Volume 3 - Issue 4 - pp 203-213
- [2] A. B. Wysocki (1999) Skin anatomy, physiology and pathophysiology. The Nursing clinics of North America.
- [3] McLafferty E, Hendry C, Alistair F. (2012) The integumentary system: anatomy, physiology and function of skin. Nurs. Stand. Sep 19-25;27(3):35-42.
- [4] Anthony D. Metcalfe and Mark W. J. Ferguson (2007) Tissue engineering of replacement skin: the crossroads of biomaterials, wound healing, embryonic development, stem cells and regeneration. J. R. Soc. Interface 4, 413–437.
- [5] Stuart Enoch David John Leaper (2007) Basic science of wound healing. Surgery (Oxford) Volume 26, Issue 2, February, Pages 31–37.
- [6] Rostislav V. Shevchenko, Stuart L. James, and S. Elizabeth James (2010) A review of tissue-engineered skin bioconstructs available for skin reconstruction. J R Soc Interface. Feb 6; 7(43): 229–258.
- [7] Alastair Young, Clare Mcnaught (2011) The physiology of wound healing. Surgery (Oxford) 29(10):475–479.
- [8] Li J, Chen J, Kirsner R. (2007) Pathophysiology of acute wound healing. Clin Dermatol. Jan-Feb;25(1):9-18.
- [9] Martin P. (1997) Wound healing – Aiming for perfect skin regeneration. Science. Apr 4;276(5309):75-81.
- [10] Laplante AF, Germain L, Auger FA, Moulin V (2001) Mechanisms of wound reepithelialization: hints from a tissue-engineered reconstructed skin to longstanding questions. FASEB J. 15(13):2377-89.
- [11] Bayat A., McGruther D. A. & Ferguson M. W. (2003) Skin scarring. Br. Med. J. 326, 88–92.
- [12] Ferguson M. W. J. & O’Kane S. (2004) Scar-free healing: from embryonic mechanisms to adult therapeutic intervention. Phil. Trans. R. Soc. 359, 839–850.
- [13] Armstrong J. R. & Ferguson M. W. (1995) Ontogeny of the skin and the transition from scar-free to scarring phenotype during wound healing in the pouch young of a marsupial, *Monodelphis domestica*. Dev. Biol. 169, 242–260.
- [14] Groeber F, Holeiter M, Hampel M, Hinderer S, Schenke-Layland K. (2011) Skin tissue engineering – In vivo and in vitro applications. Adv Drug Deliv Rev. Apr 30;63(4-5):352-66.
- [15] R. Lanza, R. Langer, J. Vacanti. (2007) Principles of Tissue Engineering 3rd edition. Elsevier Academic Press.
- [16] Chen, G., Ushida, T. & Tateishi, T. (2001) Development of biodegradable porous scaffolds for tissue engineering. Materials Science and Engineering: C 17, 63-69.
- [17] J. B. Park, J. D. Bronzino. (2003) Biomaterials, principles and applications. CRC Press.
- [18] W. Swieszkowsky Et al, Repair and regeneration of osteochondral defect in the articular joint. Biomolecular Engineering 24 (2007), 489-495.
- [19] Peter X Ma (2008) Biomimetic Materials for Tissue Engineering. Adv Drug Deliv Rev 4; 60(2): 184–198.

- [20] Lutolf, M. P, Gilbert, P. M, & Blau, H. M. (2009) Designing materials to direct stem-cell fate. *Nature* 462, 433–41.
- [21] Dutta, R. C & Dutta, A. K. (2010) Comprehension of ECM-cell dynamics: a prerequisite for tissue regeneration. *Biotechnology advances* 28, 764–9.
- [22] Williams, D. F. (2008) On the mechanisms of biocompatibility. *Biomaterials* 29, 2941–53.
- [23] D.T. Woodley, H.D. Peterson, S.R. Herzog, G.P. Stricklin, R.E. Burgeson, R.A. Briggaman, D.J. Cronce, E.J. O'Keefe, Burnwounds resurfaced by cultured epidermal autografts show abnormal reconstitution of anchoring fibrils, *JAMA* 259 (1988) 2566–2571.
- [24] D.N. Herndon, R.E. Barrow, R.L. Rutan, T.C. Rutan, M.H. Desai, S. Abston, (1989) A comparison of conservative versus early excision. *Therapies in severely burned patients*, *Ann. Surg.* 209 547–5528 discussion 552–543.
- [25] M. Nomi, A. Atala, P.D. Coppi, S. Soker, (2002) Principals of neovascularization for tissue engineering, *Mol. Aspects Med.* 23 463–483.
- [26] Evans, Nicholas D., and Eileen Gentleman. (2014): The role of material structure and mechanical properties in cell–matrix interactions. *Journal of Materials Chemistry B* 2.17: 2345-2356.
- [27] Liang C.C., A.Y. Park, and J.L. Guan. (2007). In vitro scratch assay: a convenient and inexpensive method for analysis of cell migration in vitro. *Nat Protoc.* 2:329-333. <http://dx.doi.org/10.1038/nprot.2007.30>
- [28] Sheila MacNeil (2008) Biomaterials for tissue engineering of skin. *Materials Today* 11(5).
- [29] Tiago H. Silva, Joana Moreira-Silva, Ana L. P. Marques, Alberta Domingues, Yves Bayon, Rui L. Reis (2014) Marine Origin Collagens and Its Potential Applications. *Mar Drugs.* 12(12): 5881–5901.
- [30] Brinckmann, J. (2005) Collagen, eds. Brinckmann, J, Notbohm, H, & Müller, P. K. (Springer), pp. 1–6.
- [31] Veit, G, Kobbe, B, Keene, D. R, Paulsson, M, Koch, M, & Wagener, R. (2006) Collagen XXVIII, a novel von Willebrand factor A domain-containing protein with many imperfections in the collagenous domain. *The Journal of biological chemistry* 281, 3494–504.
- [32] Shoulders, M. D & Raines, R. T. (2009) Collagen structure and stability. *Annual review of biochemistry* 78, 929–58.
- [33] Gelse, K. (2003) Collagens-structure, function, and biosynthesis. *Advanced Drug Delivery Reviews* 55, 1531–1546.
- [34] Lodish, H, Berk, A, Zipursky, S. L, Matsudaira, P, Baltimore, D, & Darnell, J. (2000) *Molecular cell biology*. Freeman, New York.
- [35] Berisio, R, Vitagliano, L, Mazzarella, L, & Zagari, A. (2002) Crystal structure of the collagen triple helix model [(Pro-Pro-Gly)<sub>10</sub>]<sub>3</sub>. *Protein science: a publication of the Protein Society* 11, 262–70.
- [36] Brazel, D, Oberbäumer, I, Dieringer, H, Babel, W, Glanville, R. W, Deutzmann, R, & Kühn, K. (1987) Completion of the amino acid sequence of the alpha 1 chain of human basement membrane collagen (type IV) reveals 21 nontriplet interruptions located within the collagenous domain. *European journal of biochemistry / FEBS* 168, 529–36.
- [37] Sourour Addad, Jean-Yves Exposito, Clément Faye, Sylvie Ricard-Blum, and Claire Lethias, (2011) Isolation, characterization and biological evaluation of Jellyfish collagen for use in biomedical applications. *Mar Drugs.* 9(6): 967–983.
- [38] Jean-Yves Exposito, Ulrich Valcourt, Caroline Cluzel, Claire Lethias (2010) The fibrillary collagen family. *Int J Mol Sci.* 2010; 11(2): 407–426.
- [39] Kundu, Banani, et al. (2013) Silk fibroin biomaterials for tissue regenerations. *Advanced drug delivery reviews* 65.4: 457-470.

- [40] A. Motta; M. Floren; C. Migliaresi, (2014) Silk fibroin in medicine. P. Aramwit, Silk: properties, Production and Uses, New York, USA: Nova Science Publishers, Inc., Hauppauge, p. 189-222. - (science and Technologies-Materials Science). - ISBN: 9781621006923
- [41] Qiang L, Quingling F, Kun H, Fuzhai C. (2005) Three-dimensional fibroin/collagen scaffolds derived from aqueous solution and the use for HepG2 culture. *Polymer* 46, 12662-12669.
- [42] Chomchalao et al. (2013) Fibroin and fibroin blended three-dimensional scaffolds for rat chondrocyte culture. *BioMedical Engineering*, 12:28.
- [43] Santin M, Motta A, Freddi G, Cannas M. (1999) In vitro evaluation of the inflammatory potential of the silk fibroin. *J Biomed Mater Res. Sep 5;46(3):382-9.*
- [44] Culav, Elizabeth M., C. Heather Clark, and Mervyn J. Merrilees (1999) Connective tissues: matrix composition and its relevance to physical therapy. *Physical therapy* 79.3 308-319.
- [45] Unger, Ronald E., et al. (2007) Tissue-like self-assembly in cocultures of endothelial cells and osteoblasts and the formation of microcapillary-like structures on three-dimensional porous biomaterials. *Biomaterials* 28.27, 3965-3976.
- [46] Norma J. Greenfield (2006) Using circular dichroism spectra to estimate protein secondary structure. *Nat Protoc.* 1(6): 2876–2890.
- [47] J. Coates (2000) Interpretation of Infrared Spectra, A Practical Approach. *Encyclopedia of Analytical Chemistry*, pp. 1-23.
- [48] M. Gallignani and R. Brunetto (2004) Infrared detection in flow analysis - developments and trends (review). *Talanta*, vol. 64, pp. 1127-46.
- [49] M. Poliskie and J. O. Clevenger (2008) Fourier transform infrared (FTIR) spectroscopy for coating characterization and failure analysis. *Metal Finishing*, vol. 106, pp. 44-47.
- [50] Sandler, S. R., Karo, W. (1998) *Polymer Synthesis and Characterization*. Academic Press.
- [51] Differential Scanning Calorimetry: First and Second Order Transitions in Polymers. (Available: <http://www.colby.edu/chemistry/PChem/lab/DiffScanningCal.pdf>)
- [52] Differential Scanning Calorimetry (Introduction) [Online]. (Available: [http://www.uzaktanegitimplatformu.com/UEP/uep\\_ylisans/ey2/ey2\\_download/DSC%20Thermal2.pdf](http://www.uzaktanegitimplatformu.com/UEP/uep_ylisans/ey2/ey2_download/DSC%20Thermal2.pdf))
- [53] Junjie Zhang, Rui Duan, Lei Huang, Yujie Song, Joe M. Regenstein (2013) Characterisation of acid-soluble and pepsin-solubilised collagen from jellyfish (*Cyanea nozakii* Kishinouye). *Food Chemistry* 150, 22-26
- [54] J. P. Jacobs, C. M. Jones e J. P. Baille, (1970) Characteristics of a human diploid cell designated MRC-5. *Nature*, vol. 227, pp. 168-170.
- [55] C. Leibiger, N. Kosyakova, H. Mkrtchyan, M. Gleib, V. Trifonov e T. Liehr, (2013) First molecular cytogenetic high resolution characterization of the NIH 3T3 cell line by murine multicolor banding. *Journal of Histochemistry & Cytochemistry*, vol. 61, n. 4, pp. 306-312.
- [56] A. Nwaneshiudu, C. Kuschal, F. H. Sakamoto, R. R. Anderson, K. Schwarzenberger e R. C. Young, (2012) Introduction to confocal microscopy. *Journal of Investigative Dermatology*, vol. 132, n. 12.
- [57] Olympusfluoview, (Available: <http://www.olympusfluoview.com/theory/confocalintro.html>).
- [58] Goegan, P, Johnson, G, & Vincent, R. (1995) Effects of serum protein and colloid on the alamarBlue assay in cell cultures. *Toxicology in vitro: an international journal published in association with BIBRA* 9, 257–66.
- [59] abcam, [Online]. Available: [www.abcam.com](http://www.abcam.com).

- [60] Spandidos, A., Wang, X., Wang, H., Seed, B. (2010) PrimerBank: a resource of human and mouse PCR primer pairs for gene expression detection and quantification. *Nucleic Acids Research* 38, 792-799.
- [61] M. W. Pfaffl, (2001) A new mathematical model for relative quantification in real-time RT-PCR. *Nucleic acids research*, vol. 29, n. 9, p. e45.
- [62] L. technologies, (2012) Real-time qPCR handbook, Life technologies Corporation.
- [63] Gene Expression Workflow - Applied Biosystems [Online]. (Available: [http://www3.appliedbiosystems.com/cms/groups/portal/documents/generaldocuments/cms\\_075428.pdf](http://www3.appliedbiosystems.com/cms/groups/portal/documents/generaldocuments/cms_075428.pdf))
- [64] Fernanda Rodrigues Helmo, Juliana Reis Machado, Camila Souza de Oliveira Guimarães, Vicente de Paula Antunes Teixeira, Marlene Antônia dos Reis, Rosana Rosa Miranda Corrêa (2013) Fetal Wound Healing Biomarkers. *Disease markers* 35(6):939-44 .
- [65] Gabbiani G. (2003) The myofibroblast in wound healing and fibrocontractive diseases. , Jul;200(4):500-3.
- [66] Andrew Hsu, MD, and Thomas A. Mustoe, MD, FACS The principles of wound healing
- [67] Skierka, E., Sadowska, M., Karwowska, A. (2007) Optimization of condition for demineralization baltic cod (*Gadus morhua*) backbone. *Food Chem.*, 105, 215–218.
- [68] Norma J. Greenfield (2006) Using circular dichroism spectra to estimate protein secondary structure. *Nat Protoc.* 1(6): 2876–2890.
- [69] Plepis A.M.D., Goissis G., DasGupta D.K. (1996) Dielectric and pyroelectric characterization of anionic and native collagen. *Polym. Eng. Sci.*, 36, 2932-2938.
- [70] Kittiphattanabawon P., Benjakul S., Visessanguan W., Kishimura H. Shahidi F. (2010) Isolation and characterisation of collagen from the skin of brownbanded bamboo shark (*Chiloscyllium punctatum*). *Food Chem.* 119, 1519–1526.
- [71] Takeshi Nagai, Tomoe Ogawa, Takashi Nakamura, Tatsumi Ito, Hisaki Nakagawa, Kazuhiro Fujiki, Miki Nakao and Tomoki Yano (1999) Collagen of edible jellyfish exumbrella. *Journal of the Science of Food and Agriculture* 79, 855-858.
- [72] Haug 2004
- [73] Song E, Yeon Kim S, Chun T, Byun HJ, Lee YM (2005) Collagen scaffold derived from a marine source and their biocompatibility. 27(15):2951-61
- [74] Jeffrey RM, Martin LY. (2013) Bioengineered skin substitutes. *Sci Med* 4:6-15.
- [75] Aigner T, Stove J (2003) Collagens–major component of the physiological cartilage matrix, major target of cartilage degeneration, major tool in cartilage repair. *Adv Drug Del Rev*, 55:1569–1593.
- [76] Altman GH, Diaz F, Jakuba C, Calabro T, Horan RL, Chen J, Lu H, Richmond J, Kaplan DL (2003) Silk-based biomaterials. *Biomaterials.* 24:401–416.
- [77] Yang SF, Leong KF, Du ZH, Chua CK. (2001) The design of scaffolds for use in tissue engineering. Part 1. Traditional factors. *Tissue Eng* 7(6):679–89.
- [78] Chen C, Cao CB, Ma XL, Tang Y, Zhu HS. (2006) Preparation of non-woven mats from all-aqueous silk fibroin solution with electrospinning method. *Polymer*, 47:6322–7.
- [79] Um IC, Kweon HY, Park YH, Hudson S. (2001) Structure, characteristics and properties of the regenerated silk fibroin prepared from formic acid. *Int J BiolMacromol*, 29:91–7.
- [80] E. Bella. (2006) Apparato di co-elettrofilatura per la realizzazione di reti nanometriche con funzionalità biomediche. Università degli Studi di Trento, Tesi di Laurea Specialistica in Fisica e Tecnologie Biomediche.
- [81] Sohn SK, Strey HH, Gido SP. (2004) Phase behavior and hydration of silk fibroin. *Biomacromolecules*, 5:751–7.
- [82] Qiang Lu, Qingling Feng, KunHu, Fuzhai Cui. (2008) Preparation of three-dimensional fibroin/collagen scaffolds in various pH conditions. *Journal of Materials Science in Medicine.*